January 2020

Simulation Of Notch Driven Hydraulic Fracture In Open Hole Completion

Nejma Djabelkhir

SIMULATION OF NOTCH DRIVEN HYDRAULIC FRACTURE IN OPEN HOLE COMPLETION

by

Nejma Djabelkhir Tavakolian

Bachelor of Science and Technology, University of Science and Technology Houari Boumediene, Algiers, Algeria, 2000

Geological Engineer, University of Science and Technology Houari Boumediene, Algiers, Algeria, 2003

A Dissertation

Submitted to the Graduate Faculty

of the

University of North Dakota

In fulfillment of the requirements

for the degree of

Doctor of Philosophy

Grand Forks, North Dakota

August 2020

This thesis, submitted by Nejma Djabelkhir in partial fulfillment of the requirements for the Degree of PhD from the University of North Dakota, has been read by the Faculty Advisory Committee under whom the work has been done and is hereby approved.

Dr. Vamegh Rasouli

Dr. Branko Damjanac

Dr. Iraj Mamaghani

Dr. Minou Rabiei

Dr. Kegang Ling

Dr. Hui Pu

This dissertation is being submitted by the appointed advisory committee as having met all of the requirements of the School of Graduate Studies at the University of North Dakota and is hereby approved.

Christopher Nelson
Associate Dean of the Graduate School

Date

PERMISSION

Title Simulation of Notch Driven Hydraulic Fracture in Open Hole Completion

Department Petroleum Engineering

Degree Doctor of Philosophy

In presenting this thesis in partial fulfillment of the requirements for a graduate degree from the University of North Dakota, I agree that the library of this University shall make it freely available for inspection. I further agree that permission for extensive copying for scholarly purposes may be granted by the professor who supervised my thesis work or, in his absence, by the chairperson of the department or the dean of the Graduate School. It is understood that any copying or publication or other use of this thesis or part thereof for financial gain shall not be allowed without my written permission. It is also understood that due recognition shall be given to me and to the University of North Dakota in any scholarly use which may be made of any material in my thesis.

Nejma Djabelkhir
August 4, 2020

Table of Contents

Table of Figures

List of Tables

ACKNOWLEDGMENTS

I wish to express my sincere appreciation to my senior supervisor Dr. Vamegh Rasouli for all his helps and attentions during my PhD tenure as PhD student at the University of North Dakota. In particular, I would like to thank him for his support to my thesis topic and defense, providing me an exclusive opportunity to learn from his depth of knowledge in this field.

Provision of the XSite academic license through the Itasca IEP program was fundamental to conduct this research and highly appreciated. I would like to also thank Dr. Branko Damjanac for his continuous support and feedback on simulation models. I would also want to thank other members of my advisory committee members Dr. Minou Rabiei, Dr. Hui Pu, Kegang Ling and Dr. Iraj Mamaghani for their support. I would also like to thank my fellow classmates Nourelhouda Benouadah, Xueling Song for their helps. The financial support of the North Dakota Industrial Commission (NDIC) is highly appreciated.

Last but not the least, I would like to thank my husband Dr. Kouhyar Tavakolian and my parents-in-law for all their support at home and when I was busy with the final stage of drafting the thesis. I would also like to thank my parents and my brothers and sisters for their encouragements. I thank my friend Nassima Djelal and all my dear friends.

Dedicated to people who are missing in my life.

ABSTRACT

Hydrocarbon production from unconventional plays, including shale oil and gas, has begun in the USA since nearly two decades ago and experienced a rapid growth. Horizontal drilling and multi-stage hydraulic fracturing (HF) are the prime technologies in development and stimulation of unconventional reservoirs. Open hole (OH) and cased hole (CH) are the primary completion methods used in unconventional reservoirs. OH compared to cased hole (CH) completion is more desired as it requires less operation cost and time while it results in more production due to larger area of wellbore exposure to the formation. However, OH completion is susceptible to near wellbore issues such as wellbore stability, tortuosity and proppant screen out. Both completion methods have been practiced in field applications. This research is focused on studying the HF initiation and near wellbore propagation in OH condition. In OH fracturing, the natural fractures intersecting the wellbore wall are with different orientations and sizes and may be closed or open with different apertures. After fluid injection into the wellbore, these cracks will compete against each other to receive the fluid and act as the initiation point of fracture. Therefore, we may observe transverse fractures which are perpendicular to the wellbore axis, or axial (longitudinal) fractures parallel to the wellbore axis or a combination of both. The weakest fracture will be the initial point of fracture initiation and propagation. In this study we review different analytical models to determine which parameters affect fracture initiation and near wellbore propagation and which one may have the main impact. We use data from the Bakken shale formation in North Dakota for modelling and simulation. This knowledge will be used to design a small crack or fracture, which is known as notch, at the point of interest along the OH section, to dominate other existing fractures

and be the point of fracture initiation. We also use lattice numerical simulations, which is a particle based model to simulate a number of cases and compare the results with analytical solutions.

The results of this study indicated that stress anisotropy and notch orientation and dimension are the most important parameters that dominate the fracture initiation point and type of fractures propagating (i.e. transverse or axial). The next parameters include formation properties as well as fluid injection rate and viscosity. When the notch size is small, usually axial fractures are dominant, however, beyond a certain notch size, transverse notch will initiate and propagate. The notch size at the cross over point is a strong function of stress anisotropy and moves to the larger notch sizes when stress anisotropy reduces; to the extent that in isotropic stress condition regardless of the size of the notch, no transverse fracture will initiate. The simulation results showed how, in case of axial notch, the base length of the notch along the wellbore axis, plays an important role in fracture initiation pressure. The results indicated that the larger the notch size the lower the initiation pressure and easier for fracture to propagate. If the notch is not along the preferred plane of propagation, after moving away from near wellbore drilling induced zone, the fracture tends to reorient itself to align to the preferred direction. Simulation of multiple axial and transverse fractures and random fractures, similar to real field cases, showed that the initiation pressure increases as the number of fractures increases and that following the knowledge obtained from this study we can determine the most likely fractures that will serve as the fracture initiation point. This conclusion suggest that the near wellbore fractures should be picked up accurately using the image logs and other tools in order to analyze them using the workflow presented in this research to design the geometry of the notch that will dominate existing fractures for multi-stage HF operation.

CHAPTER 1

Open hole Fracturing Completion

1.1 Introduction

Hydrocarbon production from unconventional reservoirs requires stimulation techniques. In shale oil and gas plays, hydraulic fracturing (HF), or fracking operation, is the dominated stimulation technique that is currently practiced in the industry. In this method, a high pressure fluid with designed viscosity is injected into a horizontal wellbore to open a long bi-wing fracture of a few thousand feet. This fracture serves as the main path to direct the hydrocarbon to the wellbore, while the shattered zone around the fracture plane creates the drained zone or stimulated reservoir volume (SRV). Several parameters should be considered in the design of HF including in-situ stresses of the field, formation mechanical properties and fracturing fluid properties (Gandossi, 2013; Ling, Zeng 2013). Theoretically, HF initiates and propagates perpendicular to the direction of minimum in-situ stress, it is more straight plane in presence of large stress anisotropy and the stimulated reservoir volume (SRV) depends on elastic properties of the formation and the fluid injection rate and viscosity can change the initiation pressure significantly (Fallahzadeh et al, 2015; 2017; Serajian and Ghassemi, 2011; Jeffrey et al, 2010)

Broadly speaking, there are two main well completion techniques that commonly used in oil and gas industry: open hole (OH) and cased hole (CH) (Gottschling and Co, 2005). The benefits

of OH completion are its much larger area of exposure of the fluid to the formation, and that it is more cost effective. In CH completion, the fluid path is through small perforation tunnels drilled around the wellbore, so more pressure drops are expected so the operation is more expensive and difficult than OH completion, however, in many cases, to keep the wellbore integrity CH completion is the only applicable option.

In real field situation, there are several defects including natural fractures around the wellbore which play as the seed points to initiate the HF, in most cases they are oriented in directions different than ideal direction for fracture initiation and propagation. Similarly, in CH completion, drilling perforation tunnels in incorrect directions with respect to the in-situ stresses will results in complex fracture geometry, multiple fractures, and tortuosity near wellbore which creates severe operational and technical problems.

This study is focused on understanding the HF initiation and propagation in OH completion. The previous literature shows that in an OH wellbore both longitudinal (axial) and transverse fractures are observed. As depicted in Figure 1.1, the axial fracture propagates along the wellbore direction, whereas transverse fracture propagates perpendicular to the wellbore axis. Practically, transverse fracture is the desired type of fracture that is expected to create during HF operation. In this research, we discuss in details the conditions where axial and transverse fracture may create. We also, introduce the concept of creating a notch (small crack) around the wellbore to dominate transverse over axial fracture. The conditions where the notch will be effective are discussed and the analysis and discussions are supported by analytical models and numerical simulations. Ultimately, the goal is to propose creating notches with certain geometry and in defined directions in an OH section of the wellbore that dominates all existing natural fractures and defects and play as the main point of induced fracture initiation and propagation.

In this study, XSite, a newly developed software by Itasca group will be employed. This software is explicitly designed for simulation of hydraulic fractures. The simulator works based on the physics of the granular material.

In the following sections, a brief discussion regarding OH and CH completions will be presented with some highlights about each method. Then the objectives, research methodology and significance of this research study will be presented with an overview of the content of each Chapter of the thesis.

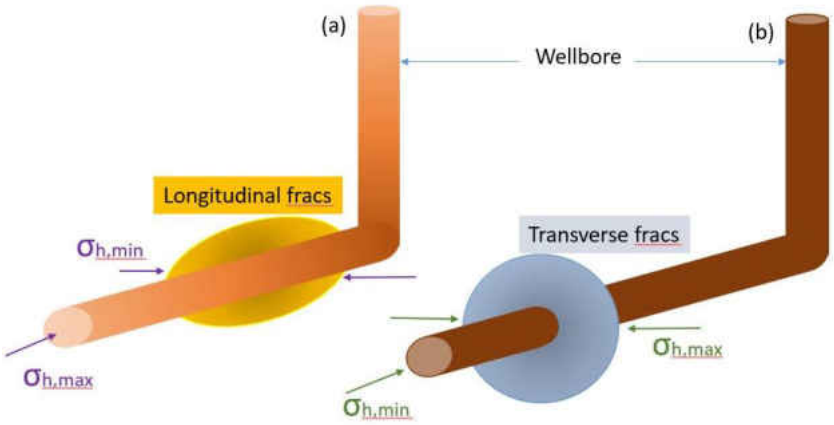

Figure 1.1: (a) longitudinal fracture (b) Transverse fracture. Horizontal wells in unconventional reservoir are often drilled in the direction of minimum stress.

1.2 OH versus CH Fracking Completion

Well-completion is a fundamental part of any hydrocarbon field development project. Well-completion represents a connection of hydrocarbon reservoir and surface facilities, which refers to the process of completing a well, so it is ready to produce hydrocarbons. For a comprehensive discussion on different types of reservoir completion one may refer to Bellarby (2009). Figure 1.2 presents the most commonly completion methods from simple to complex one based on the equipment used in the wellbore. The main objective of the design stage is to maximize the recovery from the well. Furthermore, a completion design is a combination of multiple disciplines, from

chemistry, mathematics, geology, hydraulics to material science, and practical hands-on wellsite experience Bellarby (2009). Well completion engineering plays a vital role in the process; it involves ensuring regular and safe production that should last for many years of the production life of oil and gas wells Economids (2000). For efficient production flow, it is essential to prepare the well for production by setting up the necessary equipment into the well to permit the safe and controlled flow hydrocarbons at the surface.

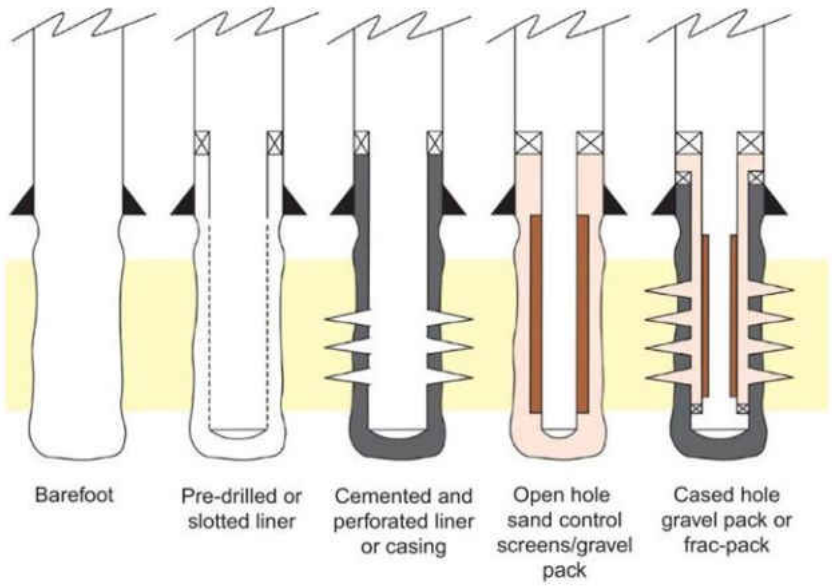

Figure 1.2: Reservoir completion methods. The figure shows different type of completions (from left to right) with a minimum of downhole equipment to the most completed one (Bellarby 2009).

One of the most crucial differences between OH versus CH completion is the cost of the personnel involved and the supplies needed in each procedure. Depending on the characteristics of the reservoir to be produced, one might be more favorable than the other. The analysis of physical properties and pore configuration are crucial for drilling and completion fluid design, as well as the selected treatment Renpu (2011). In OH completions, the casing is only required to run through the well to the top of the reservoir. Special fluids are utilized to prevent the well from collapsing, but this is a less costly procedure.

In CH completions, production casing is run through the entire length of the well, up to the various zones where hydrocarbons can be trapped. This type of completion implies significant charges to procure casings, cement, human resources, and equipment (such as Perforation guns) to stimulate production. There are two favored completion options while drilling a horizontal well. Primary, the flat section can be completed open-hole, or with slotted/perforated liner. Another completion system is cased/perforated liner requires cementing the production liner, and running multiple isolation systems to treat different sections of the wellbore effectively. According to the reservoir properties, and the oil field development-project specifications, the selection is made. Ultimately, the high completion costs or the lack of production due to ineffective stimulation make many reservoirs uneconomical to exploit (Al-Naimi et al 2008).

As mentioned before, fracking is a borehole stimulation performed on a well to increase production by improving the flow of hydrocarbons from the drainage area into the wellbore. An open hole fracking process presents an economical and viable alternative to cased-hole fracking in fields with multiple zones of poor reservoir quality and low pressure (Gottschling 2005). Most of the horizontal completions are drilled in the direction of the minimum stress in a low permeability reservoir that will affect the orientation of the induced fractures. Although the pressures play a significant role on guiding the fractures, the remote stresses favor the fractures to be transverse while the near-wellbore stress tends to favors the initiation of longitudinal or axial fractures as presented before in Figure 1.1.

1.2.1 Open Hole (OH) Fracking Completion

In an open hole well completion, the production casing is just set above the pay zone, while the entire deepens bottom of the pay zone is left uncased, as depicted in Figure 1.3, the completion starts after the reservoir section has been drilled and the drill string is pulled out Bellarby (2009).

To take full advantage of the formation in a lateral well, operators companies use an open-hole fracking technique as more pay zone being exposed along the length of wellbore (Ellis, Kniffin, and Harkrider, 2007; Renpu, 2011). However, it is not always the case because of the instability of the wellbore and fluid entry Ellis et al (2007) . Different OH completion methods include bar foot completion, pre-drilled and pre-slotted liners, stand-alone screens, gravel packs and open-hole expandable screens Bellarby (2009).

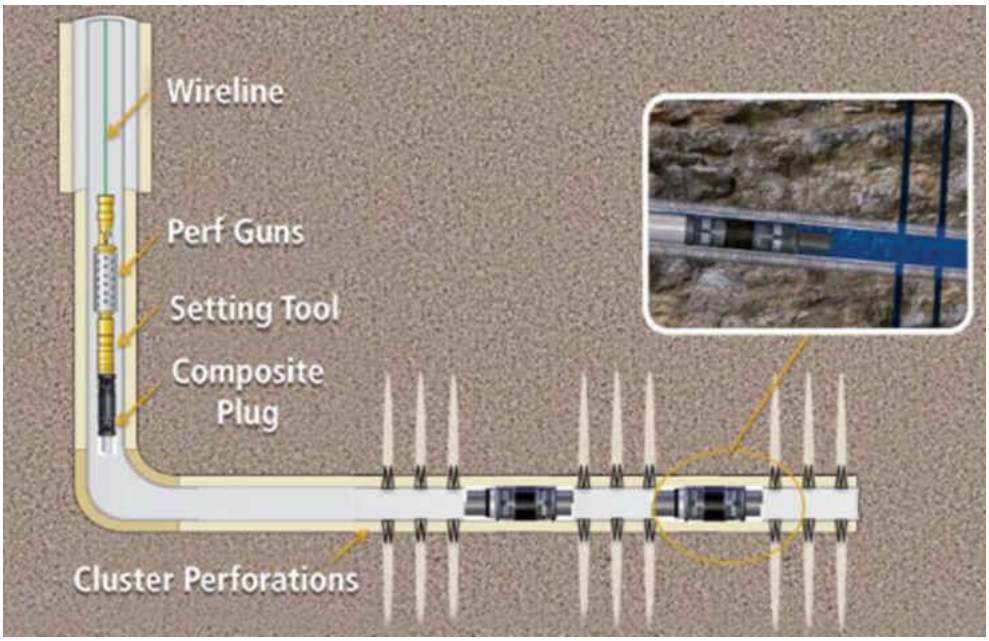

Figure 1.3: Plug and Perf completion system (Bagci et al 2017).

To access the targeted formation, and make the best connection with the reservoir, it is imperative to a follow a certain footprint. To effectively stimulate the formation, a correct depth should be always well controlled (Gottschling 2005). As described below, an open-hole fracking operation relies on notching first day and fracking on a second (Gottschling 2005; Knowlton, 1990):

1- Run a string of tubing with an air notch tool on bottom and make sure that the logging tools were able to reach the bottom of the tubing. Figure 1.4 shows an example of hydraulic notching

tool cutting a notch as it is rotated while a high pressure stream of abrasive-containing liquid is jetted through small orifices,

2- Steel line measurement is performed by lowering a weight on the end of the steel line inside the tubing,

3- The total pipe length is determined; this is a critical measurement as it is the length that will be used in the correlation of the gamma ray,

4- Position the notches in all zones by matching the top and bottom of the formation and determine the depth of the notch tool using Gamma ray, Sonic and Caliper,

5- Frac-procedure commence. When the needed frac pipe is in the well, a steel line measurement (SLM) is taking of the pipe.

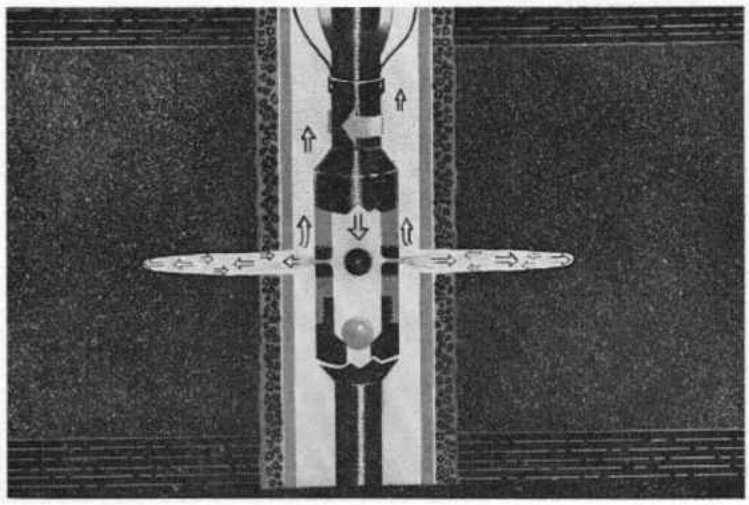

Figure 1.4: The hydraulic notching tool cuts a notch as it is rotated while a high pressure stream of abrasive-containing liquid is jetted through small orifices (Huitt 1960).

OH completion's advantages include maximum exposure to pay zone, less pressure drawdown during flow, no formation damage occurs due to cementing and perforation. Inability to plug off water or gas zones and stimulate the separate zones within the productive zones and requirement for frequent well-bore clean out are examples of shortcomings of this completion

method. A brief overview of different OH completion methods will be presented in the next Chapter.

1.2.2 Cased Hole(CH) Fracking Completion

Cased hole completion consists of casing and cementing and perforation subsequently. The first step is that the casing/liner has to be cemented, then comes the mud displacement and wellbore clean-out Bellarby (2009). The hole is drilled through the target formation(s), and production casing is run cemented in the hole. Hydraulic fracturing is conducted in short sections called stages along the lateral section of the wellbore and starts at the end of the wellbore (toe) and progresses towards the beginning (hill). The operation includes the following typical steps:

1- A perforating gun is lowered into a targeted position within the horizontal portion of the well.
2- An electrical current is sent down the well to set off a small explosive charge. This shoots tiny holes through the well casing and out a short, controlled distance into the shale formation.
3- The holes created by the "perf" gun serve two purposes. They provide path for the fracturing fluid to enter the formation and subsequently allows natural gas to enter the wellbore.

Advantages of CH completion include: excessive gas and water production can be controlled more easily, adaptable to multiple completion techniques, can be easily deepened and control most sand. Some of the shortcomings of this method include cost of casing cement and perforating for long zones, well productivity is less that productivity of open hole completion, and no adaptable to special drilling techniques to minimize formation damage.

1.3 Objectives

As explained above, creating a proper notch is of significant importance in OH completion to ensure that the fracture initiation and propagation is performed optimally. Therefore, the overall

goal of this study is to investigate how to enhance the openhole fracturing technique by cutting a notch in the wellbore wall to serve as a weak point where the hydraulic fracture initiates. The detailed objectives of this work can be summarized as followings:

1. Comprehensive review of existing literature on the impact of the notch geometry on fracture initiation and propagation. This includes analytical models, lab experimental studies, numerical simulations and field observations.
2. Under what conditions axial and transverse fractures will be created and how the notch can dominate transverse fractures. Also, what is the impact of fluid viscosity and injection rate as well as pressurization rate on initiation pressure.
3. Determine the impact of in-situ field stresses on the type of fractures (axial vs transverse) around the wellbore in a notched OH wellbore.
4. The applications and limitations of analytical models in estimation of fracture initiation pressure in presence of a notch emanating from a cylindrical borehole will be discussed. This will be extended to star fractures, where more than one bi-wing notch it edging from the wellbore.
5. Capabilities and unique features of lattice simulations for HF simulations and studying the effect of notch on fracture initiation and propagation. XSite software, which is a particle based numerical simulator and works on the basis of distinct element method (DEM), will be implemented in this study.
6. Conduct numerical simulations using published lab data as well as field scales and compare the results with analytical models to identify the impact of the notch on fracture pressures. This will be extended to presence of multi cracks emanating from the borehole.

7. Recommend notch geometry and orientation in an OH lateral wellbore with existing natural fractures to dominate fracture initiation in desired spot and direction.

1.4 Methodology

The methodology that will be used to achieve the above objectives comprises of data inventory, analytical solutions and numerical simulations. These are briefly explained below.

1. In order to perform calibrated numerical simulations, we collect sets of lab data from the literature. Similarly, field scale data will be gathered for the same purpose. While the simulations will be based on Bakken formation, we use data from other fields for comparison purposes.
2. Numerical simulations will be run using XSite software to estimation fracture initiation pressure in OH completion and in presence of notches with different length and orientations. The impact in-situ stresses and formation properties will be studied. Sensitivity analysis of various parameters will be done to determine the competition between axial versus transverse fractures and the impact of the notch size and orientation on this.
3. Different analytical models will be introduced to predict the fracture initiation in a borehole with a crack emanating from its edge. The impact of notch size and orientation on generation of axial and transverse fracture will be discussed and the effect of fluid viscosity and injection rate and pressurization rate will be studied. The limitations and range of applications of each model will be discussed.
4. The results of analytical models and numerical simulations will be compared to draw some practical applications in terms of determining the best notch geometry and orientation in an OH completion for desired HF results.

1.5 Significance

The results of this research study will present multifold novelties including the followings:

1. This research project helps to address the gaps between analytical solutions and numerical simulations and elaborate potential solutions.
2. Unique features of the XSite software, and lattice numerical simulations, as will be presented in this study, is one of the first attempt to study the impact of notches on OH completion HF.
3. The outcome of this project will help to drill notches at specific points along the lateral section of an OH within each fracking stage in order to optimize HF initiation and propagation.
4. The results of this study can also be applied partially in CH completion where the fracturing fluid injection through a perforation may penetrate into natural fractures behind the cement sheet. Also, the length of the perforation may also be designed in the same approach that is discussed for the notch in this study.
5. Practical recommendations and suggestions that are proposed in this study can improve the operation of OH HF which in turn can be of significant financial benefits for the companies.

1.6 Thesis Structure

This thesis consists of five chapters.

Chapter 1 provides the background to the project and a very brief explanation of the basics of hydraulic fracturing in open-hole versus cased-hole, emphasizing on the techniques used in open-hole fracking. It also contains the objectives of this study, the methodology used and the significance of this research.

In Chapter 2 a brief review of the literature regarding the OH completion methods will be presented. Also, a summary of past studies related to the lab work, numerical simulations and

analytical models to estimate initiation pressure of HF from an OH with a notch and multi notches will be given.

Chapter 3 presents a brief overview of the background and theory of lattice simulation used in this study and the features and modelling using the XSite software. Constitutive lattice formulation and simulation features are also summarized.

Chapter 4 comprises of different analytical models that study the impact of the notch size and orientations on HF initiation pressure and stress intensity factor. These models integrate the impact of different parameters including net pressure on the notch surface, rock elastic properties and pressurization rate. The range of applications and limitations of these models will be discussed.

Chapter 5 presents the results of the numerical simulations. The simulations consider the effects of notch orientation and dimension and the impact of different parameters in initiation pressure from an OH. Also, in this Chapter the results are compared with analytical models presented in the preceding Chapter and conclusions are made.

In Chapter 6 a summary of the findings from this study will be presented along with some recommendations and future studies that can be carried out.

1.7 Summary

This Chapter introduced the OH and CH completion and the advantages and shortcomings of each method. It was highlighted that in OH completion, creating a notch with proper size and orientation is necessary to ensure that the HF initiates and propagate in desirable direction. Also, it was explained that field in-situ stresses as well as injecting fluid properties and formation characteristics will impact the effectiveness of the notch. The notch also can dominate the generation of axial versus transverse fractures in OH. Also, in this Chapter, a summary of the

main objectives of this research, the methodology which will be implemented, distinguished aspects of this study and the structure of this thesis were presented.

In the next Chapter, a review of the literature will be presented to give a background to the OH completion methods and the models that are used for estimation of HF pressure in notched wellbores.

CHAPTER 2

Review of Literature: Near Wellbore Fracturing in Open Hole Completion

2.1 Introduction

In the previous Chapter the advantages of the OH completion over CH completion were briefly mentioned. While CH completion is perhaps a more frequently used technique due to the additional wellbore stability and flexibility in production, whenever possible, the operators prefer to complete the well OH to benefit from the extra exposure to the formation and more production.

As one may expect, in OH completion, the type of near wellbore issues is different than CH completion and with respect to the HF operation may include the dominance of fracture initiation point along the horizontal section and change of fracture initiation and breakdown pressure due to the existence of the natural fractures around the wellbore, fracture tortuosity and screen outs (Belyadi, H et al, 2019). In multi-stage HF in OH as well as CH completion, the stress shadow effect is another design parameter that needs to be considered to properly estimate fracture dimensions.

The use of a notch in OH completion will assist in better design of the HF treatment. This was briefly explained in the preceding Chapter and will be discussed in further details in this and next Chapters. The design of the notch (e.g. dimension and orientation) with respect to the wellbore

direction and the orientation of principal stresses has a significant impact on the effectiveness of the notch.

In this Chapter, we present a brief overview of the past research and studies on the impact of the notch on HF initiation and propagation. We classify these studies into analytical models, experimental studies, numerical simulations and field practices.

2.2 Analytical Models

The impact of an existing crack or notch on fracture initiation and propagation in medium with different geometry has been the subject of studies in different science and engineering disciplines. These methods, in general, include the effect of the notch by modifying the critical stress intensity factor based on the shape of the notch and its position with respect to the structure.

The concept of weight function initially introduced by Bueckner (1970) has been extensively used in future work. According to this theory, as quoted by Rice (1972) "the stress intensity factor is expressed as a sum of work-like products between applied forces and values of the weight function at their points of application". Rice (1972) used this theory to determine the intensity factor for a crack in a remotely uniform stress field subject to an arbitrary traction distribution on the faces of a crack.

Glinka (1996) presented the weight functions to calculate the stress intensity factors around cracks with different shapes in a thick cylinder subjected to complex stress fields. He provided the approximation of the weight functions with different orders.

Dunn and Suwito (1997) studied the fracture initiation at sharp notches. The geometry of the corner that they considered in their studies is shown in Figure 2.1 (left). They determined the magnitude of the stress intensity K_I^n for notched mode I three-point flexure specimens (see Figure 2.1, right) using a combination of Williams (1952) asymptotic method, dimensional

considerations, and detailed finite element analysis. They showed that K_I^n is a function of the geometry of the structure and the loading.

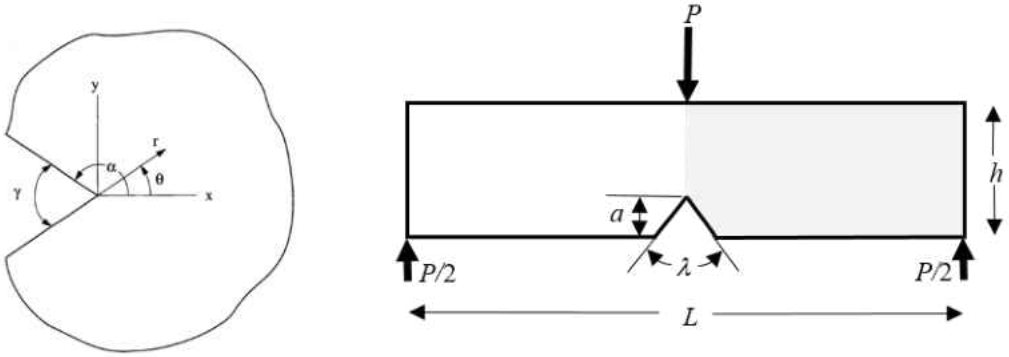

Figure 2.1: Geometry of the corner used to determine the fracture initiation pressure (left) and the geometry of notched three-point flexure specimen used to extract the critical stress intensity (After Dunn and Suwito (1997).

The critical stress intensity factor (K_I^n) was calculated as:

$$K_I^n = \sigma^0 h^{1-\lambda} f\left(\frac{a}{h}\right) = \left(\frac{3PL}{2bh^2}\right) h^{1-\lambda} f\left(\frac{a}{h}\right) \tag{2.1}$$

where, based on the parameters shown in Figure 2.1, and that λ-1 is the elastic singularity, they proposed the following polynomial fit for f(a/h) when $0.5 \leq f(a/h) \leq 0.7$:

$$f\left(\frac{a}{h}\right) = c_1\left(\frac{a}{h}\right) + c_2\left(\frac{a}{h}\right)^2 + c_3\left(\frac{a}{h}\right)^3 + c_4\left(\frac{a}{h}\right)^4 + c_5\left(\frac{a}{h}\right)^5 \tag{2.2}$$

The results of their experiments on notched polymethyl methacrylate (PMMA) three-point flexure specimens with notch angles of 60°, 90°, and 120° demonstrated the feasibility of using a critical value of K_I^n to correlate fracture initiation.

In a similar attempt, Leguillon and Yosibash (2003), presented a criterion to predict crack onset at a sharp notch in homogeneous brittle materials. Their experiments on a stiffer material (Alumina/Zirconia) showed that it is less sensitive to small notch tip radii than that of PMMA.

With specific application in Hydraulic fracturing, Rummel (1987) used the weighting function approach to estimate the critical borehole pressure at unstable crack extension. The intensity of the

stress field in the vicinity of the crack tips can be formulated based on the principle of superposition of stress intensity factors (K_I) from each loading source. In his 2D modelling, he considered the magnitude of the two horizontal stresses, borehole pressure and the pressure inside the crack to estimate the total intensity factor of the system. This method allows evaluating the impact of each parameter on fracture initiation. Figure 22 depicts the concept of the superposition of loading sources. A detailed discussion about this model will be presented in Chapter 4 using the data from Bakken formation in North Dakota.

Charlez (1997) used the weighting function to calculate the HF initiation pressure in presence of a crack from the edge of a circular opening as a function of average magnitude of the stresses, differential stresses, fluid pressure and pore pressure. In particular, he considered the pressurization rate in his equations. In fast pressurization, he stated that the crack pressure will be equal to the pore pressure, whereas, in slow pressurization, it becomes the same as the wellbore pressure. Similar results reported by Detournay and Carbonell (1997). Further discussion of this model will be presented in Chapter 4.

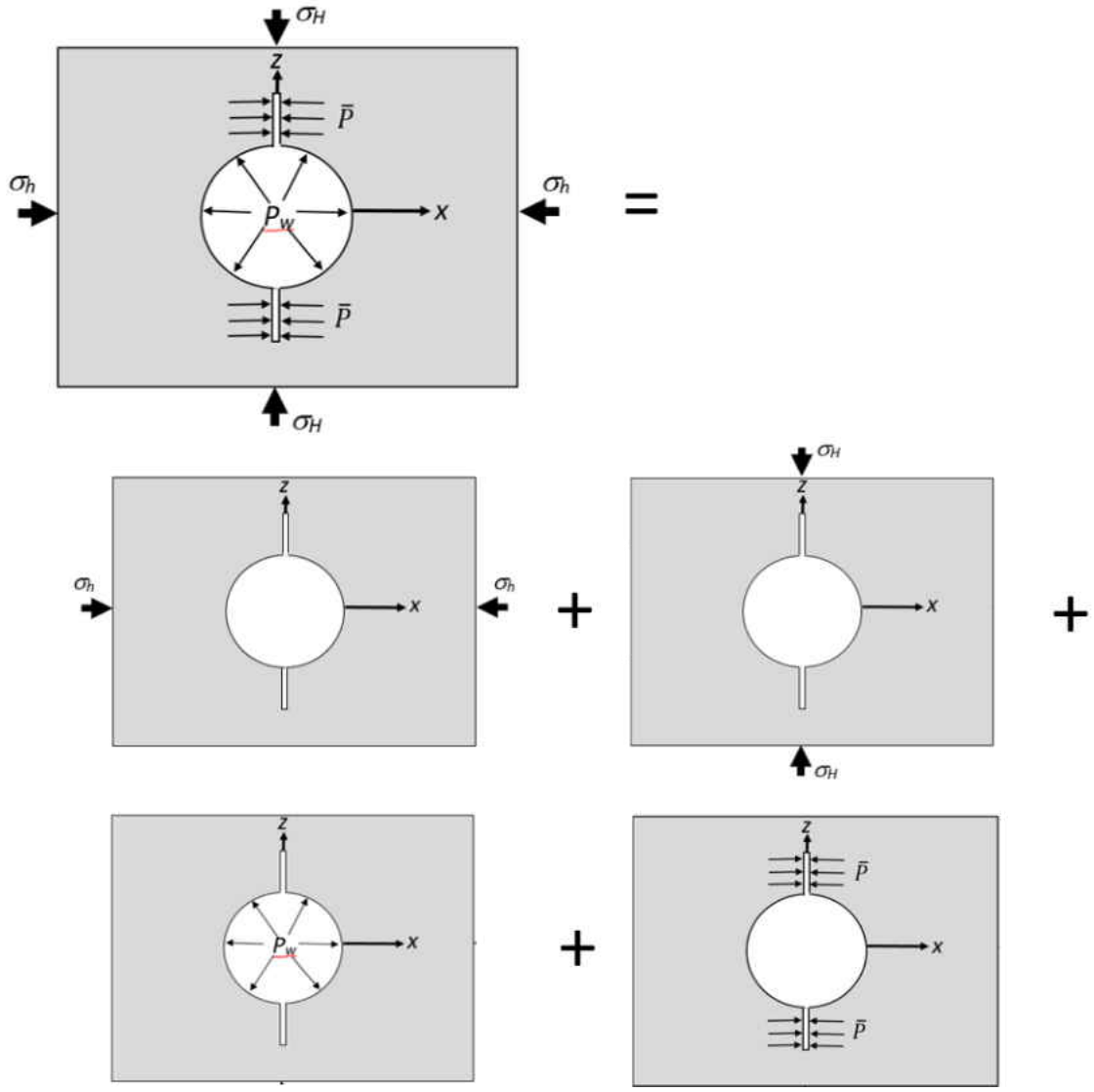

Figure 2.2: Superposition of four loading sources to determine total system intensity factor (after Rummel, 1987)

A very applicable analytical model to the applications within the context of this research was proposed by Nilson and Proffer (1984). They investigated the fracture initiation from a pre-existing crack emanating from a wall of a cylindrical excavation. Using the weight functions, they calculated the stress intensity and opening displacements for planar (transverse) or axisymmetric (axial or longitudinal) fractures emanating from a cylindrical or spherical hole in an elastic medium. They showed how their solutions reduce to known exact solutions when the notch size becomes very short and to the penny-shaped or Griffith fracture in case of very long fracture. They

proposed the solutions for both wedge-shaped and disc-shaped fractures and also for more than one axial fracture emanating from a circular borehole. Their proposed generalized integral formulas present a fast, simple, and reasonably accurate method for solving a wide range of engineering problems, and specific to this study, hydraulic fracturing applications, where borehole pressurization, stress magnitude and anisotropy and fracture length is important parameters.

Lecampion et al (2013) further investigated the model proposed by Nilson and Proffer (1984) and calculated the fracture initiation from a horizontal borehole along the direction of min horizontal stress in a normal stress regime with different notch sizes for both axial and transverse fractures. They used the data corresponding to four different fields (Barnett, Marcellus, Haynseville, and Undisclosed). The results of scaled fracture initiation pressures as a function of the normalized initial notch size (divided by wellbore radius) for both axial and transverse fractures are presented in Figure 23. The state of stresses is also presented in these Figures for each field. The results are presented for the case of slow pressurization rate where transverse fractures can be created. From the results of this Figure, it is seen that in case of isotropic stresses (i.e. Barnett) regardless of the notch size, the axial fracture is always dominating and requires less pressure than transverse fracture to create. Otherwise, transverse fracture can be created if the notch size is larger than a critical value (γ_0^*). The lower the stress anisotropy, the larger the γ_0^*, i.e. the cross over from axial to transverse fracture. It is also seen that the Hubbert-Willis (H-W) initiation pressure for the case of fast pressurization and Haimson-Fairhurst (H-F) initiation pressure corresponding to slow pressurization are the upper and lower limits of the pressures in the proposed model by Lecampion et al (2013). In Chapter 4 we present the details of this model and the results for the case of Bakken formation. The results will be further compared with the corresponding numerical simulation models in Chapter 5.

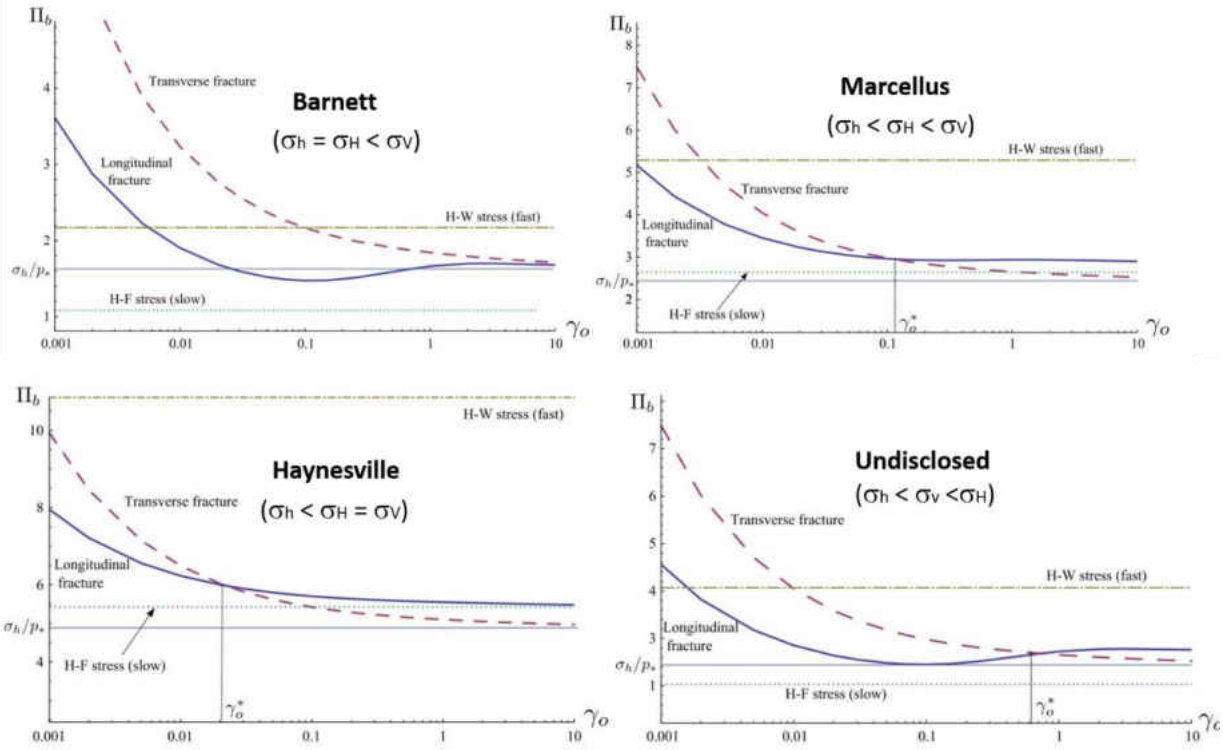

Figure 2.3: Fracture initiation pressure as a function of the initial defect size for both axial and transverse notch for the case of slow pressurization (Lecampion et al, 2013).

2.3 Experimental Studies

In a different attempt by Weijers et al (1994) they conducted series of experimental tests to investigate the possible reasons for high fracture initiation pressure in the wellbore drilled with high azimuth with respect to the preferred fracture plane in the Dan Field. In their scale lab experiments they observed changes in the initiation pressure as a function of fracture geometry. Figure 2.4 presents the images of a two rock block tested in the lab where wellbore was drilled perpendicular to the preferred fracture plane (left) and at 45° with respect to the preferred fracture plane. In the first case both axial and transverse fractures are observed, whereas in the latter case multiple fractures in addition to fracture reorientation are visible. This suggested that the change of breakdown pressure in the field cannot be only related to the stresses.

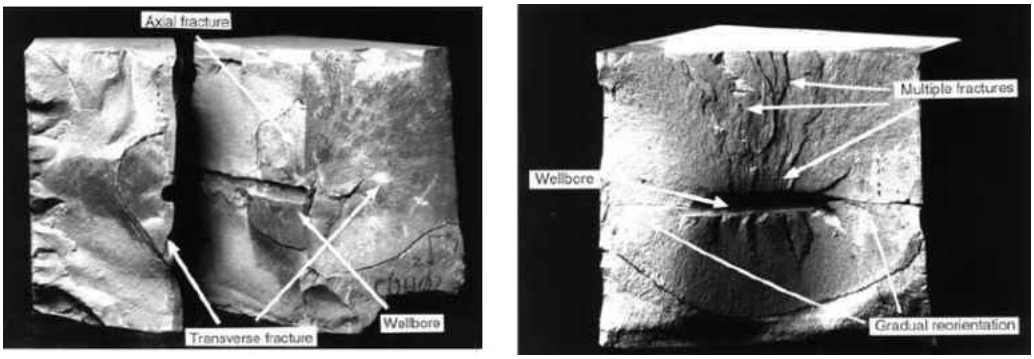

Figure 2.4: Development of different fracture geometries in a wellbore drilled parallel (left) and at 45° with respect to the preferred fracture plane (right) Weijers et al (1994).

The results of the studies by Weijers et al (1994) also showed that transverse fractures initiate at low flow rate and viscosity in presence of high horizontal stress contrast, whereas the axial fractures initiate at high flow rate and viscosity while the fracture reorient gradually and multiple fractures form. The multiple fractures are more created when the wellbore is at an oblique orientation with respect to the preferred fracture plane. Figure 2.5 shows schematically the formation of different type of fractures as a function of the maximum pressure versus the product of the flow rate and viscosity (or pressurization rate). As mentioned, at high values of pressurization rate multiple fractures are more likely to be observed.

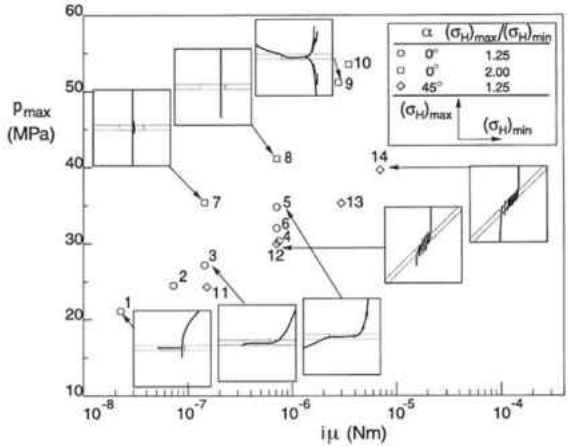

Figure 2.5: Different type of fracture geometries are observed depending on the product of the flow rate and viscosity and the maximum pressure (Weijers et al 1994).

In an extensive series of lab testing to simulate the in-situ hydraulic fracturing experiments conducted at the Mont Terri underground research laboratory in Switzerland, Nakagawa et al (2016) conducted polyaxial HF tests on 3"×3"×6" to 2.5"×2.5"×6" rectangular samples natural (shale) and analogue rock samples (soda-lime glass) with preexisting cracks and layers.

As an important finding of their studies with respect to this work was that the use of a pre-notch will reduce the breakdown pressure. This will avoid the abrupt fracture growth due to the sudden release of strain energy in both fluids in the system and the solid around the borehole. The stabilized fracture growth is important when it is intended to capture the growth of the fracture and visualize its interaction with existing natural fractures.

Nakagawa et al (2016) also conducted HF/visualization experiments, using 100% glycerol containing 1%wt sulfur-rhodamine B as the fracturing fluid at slow injection rate of 0.425 μL/min and fast injection rate of 8.50 μL/min, (20 times than slow rate). The tests were done on intact rock (i.e. no fractures) as well as weak and strong rocks. Figure 2.6 represents the pressure versus fluid volume plots. The results show that, in general, the breakdown pressure (i.e. the peak of the curves) is higher in the fast injection rate than that of slow injection rate. In slow injection rate, the strong block (prepared at 650°C) behaves similarly to the intact rock. Figure 2.7 is the post HF visualization enhanced by fluorescence. From this Figure it is also observed that the strong block at slow injection rate results in similar well defined planar fracture geometry to that of the intact rock. Interestingly, this is the same fracture geometry that is produced for the weak block at slow injection rate, whereas, at fast injection rate, dendritic fracture network are produced in the weak block. This observation is further confirmed by looking at Figure 2.8 where the hydraulic fracturing responses of glass samples containing fracture networks with similar fracture properties, subjected to either slow or fast injection of fracturing fluid are presented. In fast injection, the

fracture front is free of fluid and creates a well-defined, flat hydraulic fractures. In contrast, in slow injection the preexisting cracks are filled with the injecting fluid and there is no clear sign of HF. The reason for these observations, as also reported by other researchers is that in fast injection, the fluid does not have adequate time to fill in the preexisting cracks, so the fluid will not load the fractures as opposed to slow injection rate.

The difference in slow versus fast injection is schematically shown in Figure 2.9. The rapid pressure drop along the fracture in case of fast injection results in a wedge effect, which creates a vacuum or vapor filled zone behind the leading edge of the fracture. The low fluid pressure in this zone cannot activate the potentially preexisting cracks, hence, the induced fracture will continue its preferred propagation direction and has more chance to cross the interfaces, as compared to the low injection case (Nakagawa et al, 2016).

The results of the analytical models and numerical simulation that will be presented in Chapters 4 and 5, respectively, are in agreement with the above findings.

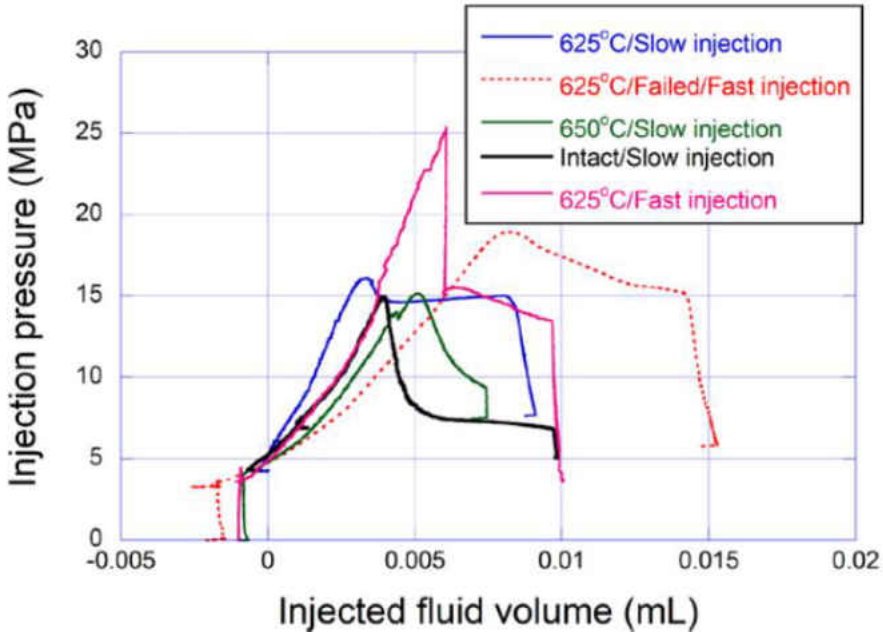

Figure 2.6: Pressure-Volume plot in HF experiments at slow and fast injection rates (Nakagawa et al, 2016).

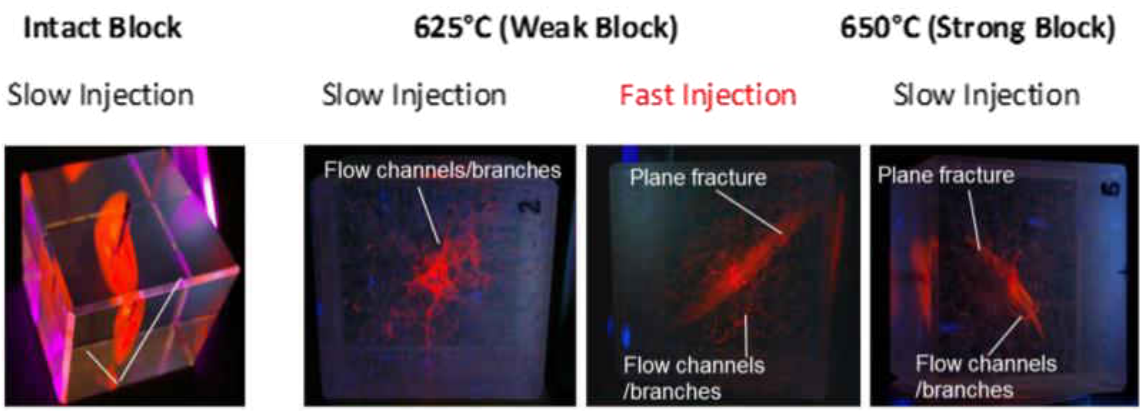

Figure 2.7: HF visualization enhanced by fluorescence induced by long-wavelength UV light (Nakagawa et al, 2016).

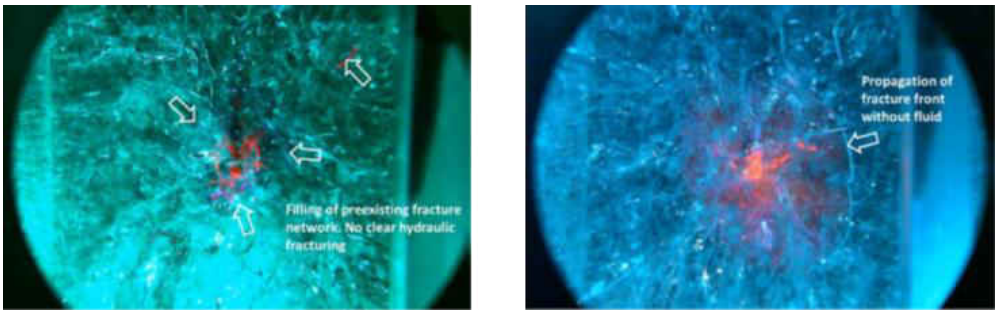

Figure 2.8: HF if weak blocks with slow (left) and fast (right) injection rate (Nakagawa et al, 2016).

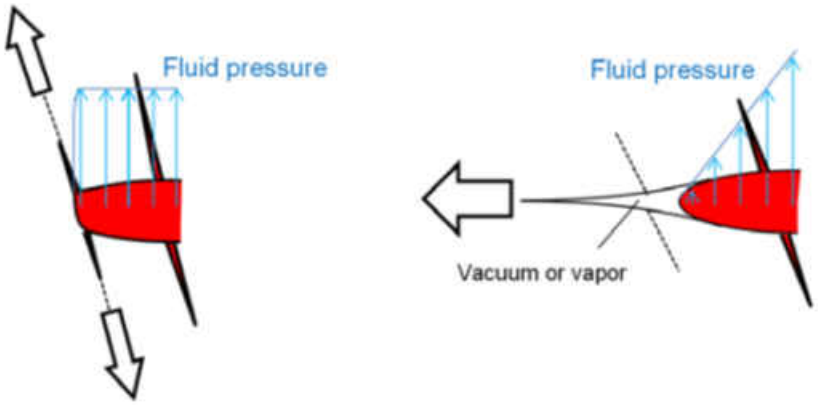

Figure 2.9: Fracturing by slow (left) versus fast (right) injection (Nakagawa et al, 2016).

Schwartzkopff (2017) conducted experiments to investigate the breakdown pressures and fracture propagation surfaces of a pressurized circular thin notch emanating from a circular

borehole, subjected to external confining stresses. Figure 2.10 shows the prototype mould of the 75° pre-existing circular notch before and after it is placed inside the sample.

Figure 2.10: Prototype mould of the 75° pre-existing circular notch (left) and prototype specimen cut in half along the axis of the borehole, the 75° pre-existing circular notch appears at the bottom of the borehole section (Schwartzkopff, 2017).

Under the shear stress conditions that they studied, their results showed that the breakdown pressures can be estimated using only the resultant normal stress on the plane of the notch. They also mapped the propagation surfaces from the experiments and compared to numerical predictions based on the maximum tangential stress criterion and observed a close agreement. Their results also confirmed that the propagation of arbitrarily orientated notches will eventually realign to be perpendicular to the minor principal stress direction.

Figure 2.11 represents the experimental model set up that Chen et al (2018) used to investigate the effect of the notch geometry of fracture initiation pressure. They performed true triaxial HF tests on 30 cm cubical mortar samples. From the test results presented in Figure 2.12, they observed that fracture initiation pressure decreased as the notch length and injection rate increased. However, the initiation pressure decreased as the notch angle decreases. The fracture showed to propagate perpendicular to the direction of minimum stress.

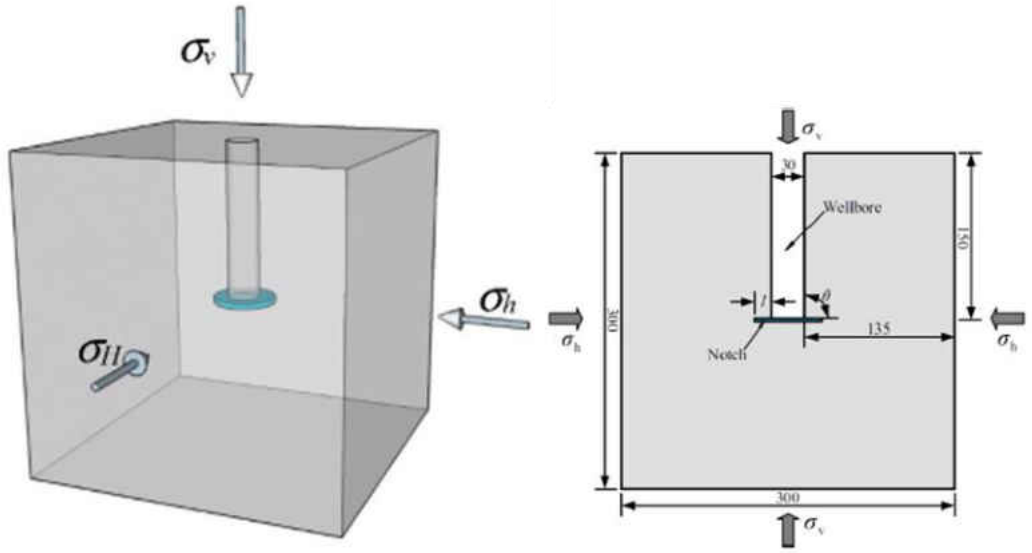

Figure 2.11: Model set up used by Chen et al (2018) to run HF experiments to study the effect of the notch geometry on initiation pressure.

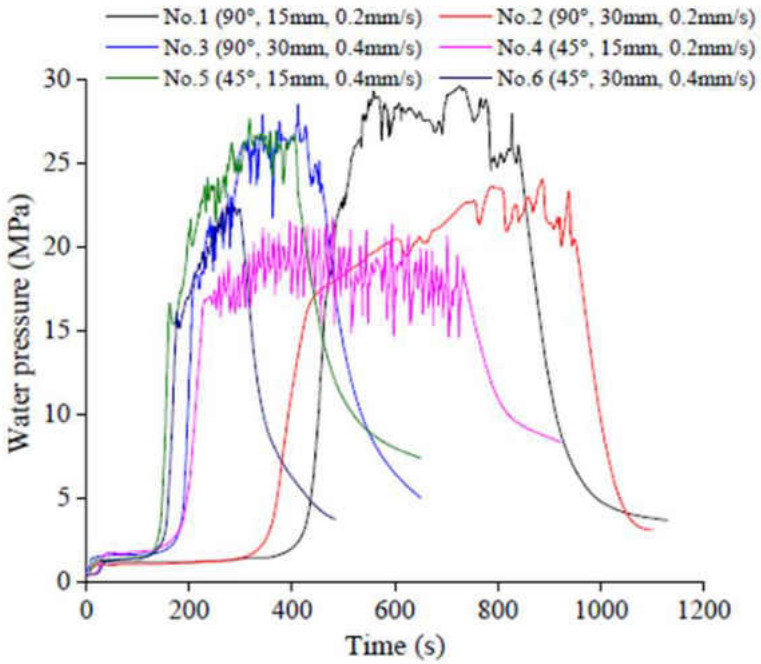

Figure 2.12: Experimental results of notched HF tests by Chen et al (2018). Notches with different length and angle were used and the effect of the injection rate was also considered.

2.4 Numerical Simulations

Aidagulov et al (2015) developed a 3D model to predict the position, orientation and pressure at which a fracture initiates from a notched open hole (see Figure 2.13, left). The right image of The lab test data from Chang et al (2014) was used in this study to validate the model results. This lab set up is shown in Figure 2.13 (right). Stresses are analyzed using the brittle fracture criteria and resolved with boundary element method (BEM). Their studies showed that the conventional maximum tensile stress (MTS) criterion cannot reproduce the observed trend in initiation pressure and fracture orientation. Therefore, they proposed the nonlocal modification of the MTS criterion based on the stress averaging technique (SAMTS) to predict the initiation of fracture at the borehole or notch wall. The concept is presented schematically in Figure 2.14. The proposed model predicted well the initiation pressure in a uniaxially stressed dry boreholes tested in the lab and could capture the borehole size effect. In further analysis of simulating experimental data, their model was able to predict the position and orientation of the initiated fracture. As a limitation of the method, Aidagulov et al (2015) mentioned that it overestimates the absolute pressure.

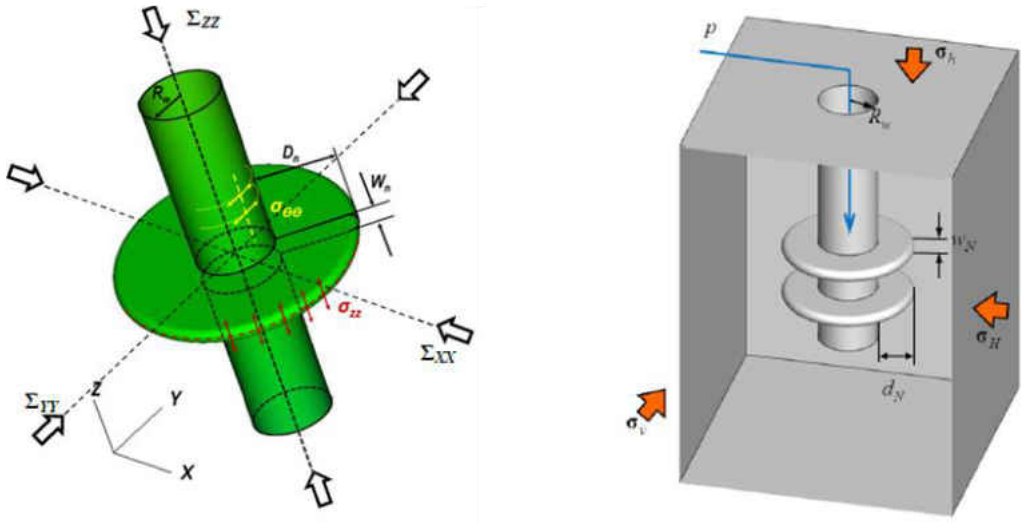

Figure 2.13: Model geometry of an open hole with a transverse circular notch (left) and the schematic of the lab testing block used for numerical simulations by Aidagulov et al (2015).

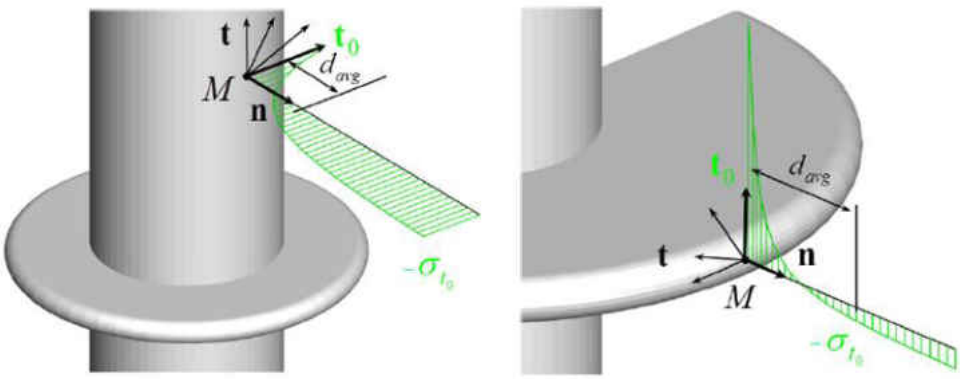

Figure 2.14: The stress averaging technique (SAMTS) to predict the initiation of fracture at the borehole (left) or notch wall (right) proposed by Aidagulov et al (2015).

In addition to lab experimental studies carried out by Nakagawa et al (2016), as mentioned in Sub-section 2.3, they also implemented LBNL's hybrid TOUGH-RBSN (RBSN=Rigid-Body-Spring-Network) numerical Code to solve the dynamic fracture propagation in response to fluid injection. Upscaling of the lab to field data was also conducted. One of the simulations that they carried out was to investigate the effect of a preexisting notch on HF initiation pressure. In order for this, in the RBSN model as presented in Figure 2.15 (left), the mechanical resistance in tension was completely removed for those lattice elements that were considered as initial notches. Also, the permeability and the porosity were initially increased like when they are mechanically activated for hydraulic fracturing. The simulation was done with a compressibility of (4.6×10^{-9} Pa^{-1}). As the results of Figure 2.15 (right) show, the breakdown pressure is less for the model with notch, meaning that it is easier to propagate a fracture from an initial crack. The existence of the notch will allow some of the fluid to be stored inside the crack, instead of the entire fluid being stored in the injection system. Therefore, as explained earlier, the fracture propagation is more gradual and less abrupt.

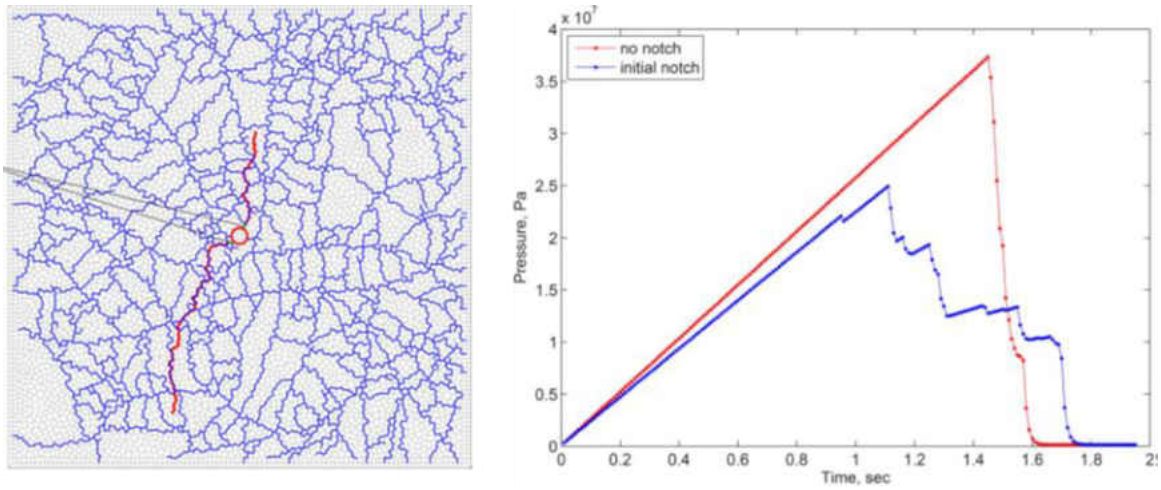

Figure 2.15: RBSN model for a HF with notch (left) and the pressure evolution for models with and without notches (Nakagawa et al, 2016).

Song and Rahman (2018) used the 3D J-integral (as opposed to the stress intensity factor, crack tip opening displacement or energy release rate) to evaluate crack geometry, stress field and stability state of fracture tip for fluid driven fractures. As stated by Song and Rahman (2018) "J-integral is a path integral along the contour starting from any point on bottom surface of the crack and ending in top surface". The value of J-integral is equal to the energy release rate during crack extension, which is independent on its integration path. The path-independence characteristics of the J-integral has become a powerful tool for studying different types of loading, material laws and field problems, in both linear elastic and elastoplastic conditions.

Lhomme (2005) investigate the fracture initiation of HF in a permeable sandstone with the objective of understanding the possibility of forcing the location of the fracture initiation to occur from the open hole section. He developed his model based on a transverse fracture by extracting a set of scalings for a radial fracture driven by a viscos fluid in a permeable elastic-brittle material assuming the compressibility effect induced by the compliance of the injection system. He also conducted laboratory experiments to validate the results. Some of the lab observations could not be justified with the developed model which shows the complexity of rock properties.

Hussain and Murthy (2019) presented solutions to mixed mode (I/II) notch stress intensity factors of sharp V-notches using point substitution displacement technique

Martinez et al. (2019) used the extended finite element method (XFEM) to simulate the effect of the notch angle on HF initiation in both 2D and 3D. Figure 2.16 depicts the model geometry they used. The notch angle is considered from the σ_x, which is the minimum confining stress. As the results of Figure 2.17 demonstrates, the larger the notch angle, the less the breakdown pressure. They also reported that the fracture propagation starts from the notch tip and then deviates to become perpendicular to the minimum confining stress direction, a conclusion which is expected. In addition, Martinez et al. (2019) stated that the horizontal stress anisotropy is the dominant factor affecting the HF propagation path.

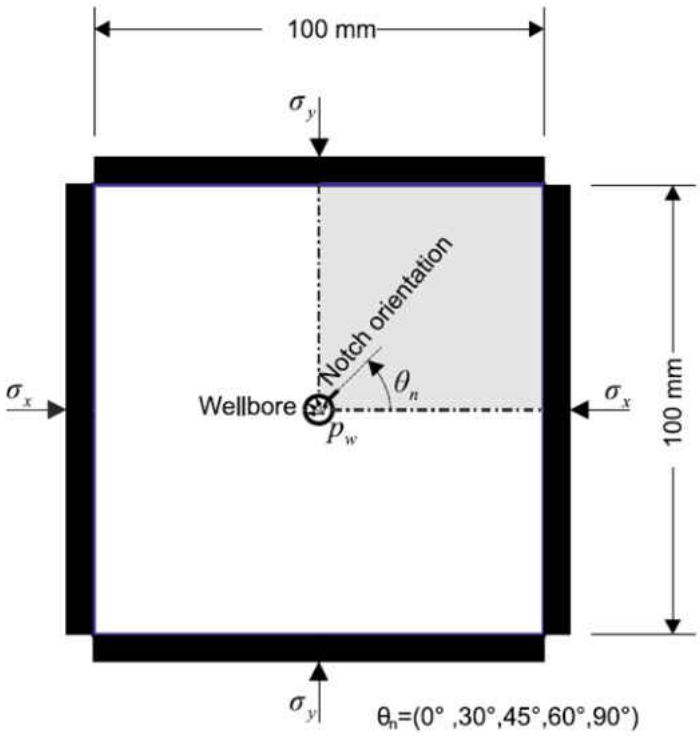

Figure 2.16: The model geometry used to simulate the effect of notch angle on HF pressures (Martinez et al, 2019).

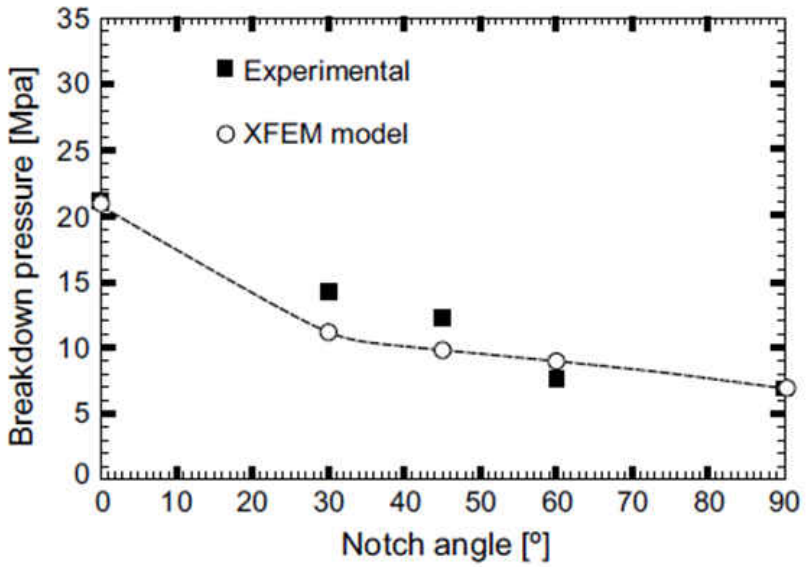

Figure 2.17: HF Breakdown pressure as a function of the notch angles (Martinez et al, 2019).

Most of the numerical simulations, for the sake of simplicity and processing time, consider a predefined fracture plane perpendicular to the direction of minimum stress. However, it is evident that, depending on state of stresses and rock inhomogeneity, the fracture may follow an irregular and non -planar path. In addition, to more realistically simulate the formations that we encounter in oil and gas industry, the use of continuum models where the rock is considered as one medium is not appropriate. In this study, as we will discuss in the next Chapter, a particle based numerical model based on lattice simulation will be used to simulate the near wellbore hydraulic fracturing initiation and propagation pressure. We will present the results in Chapter 5 and compare the results with analytical models of Chapter 4. The advantages of the lattice numerical simulations will be discussed and presented in Chapter 5.

2.5 Field Practices

Not many field scale observations are reported to show the impact of the notch on HF treatment. In in-mine hydraulic fracturing it is intended to create parallel cracks oriented across the axis of

the wellbore. In-seam boreholes with this type of fracture system can be used for different applications including coal bed methane production, sealing of degassing boreholes and controlled collapse of the roof (Patutin & Serdyukov, 2017). In order to create a fracture in a preferred direction from the wellbore wall, Patutin and Serdyukov (2017) used an indenter impression located between two inflatable packers. During indentation fracturing, the crack is propagated due to the injection of high pressure fluid. Figure 2.18 shows the view of the designed indenter to create a transverse fracture.

Figure 2.18: The designed indenter to create fracture in a desired direction: in transportation mode (left) and in operation (right) (Patutin and Serdyukov 2017).

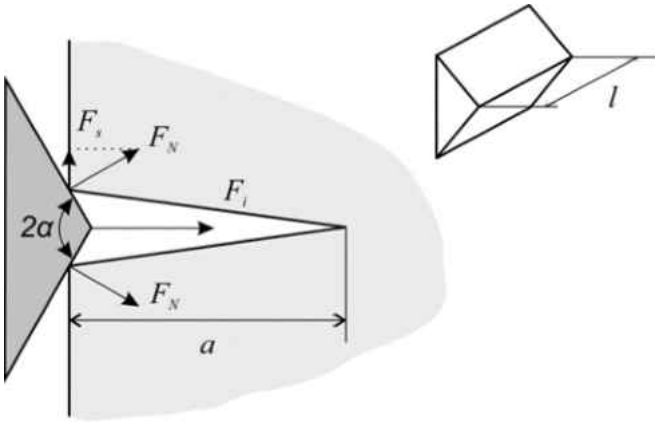

Figure 2.19: The interaction forces between the indenter and the opening crack (Patutin and Serdyukov, 2017)

Assuming a wedge shape indenter pushing the wellbore wall with force F_i to open the edges of an existing crack with depth a, the stress intensity factor is calculated as (see Figure 2.19):

$$K_I = 0.8256\frac{F_s}{l}\sqrt{\frac{\pi}{a}} \tag{2.3}$$

$$K = -1.1215\sigma\sqrt{\pi a} \tag{2.4}$$

$$F_s = \frac{F_i}{2\tan(\alpha)} \tag{2.5}$$

In above equations the stress intensity factor from the compression stress on the infinity is l is the length of the wedge-shaped indenter's cutting edge, α is the wedge-shaped indenter angle.

If $K_I + K = 0$ the length of the crack that is opened by the indenter can be estimated as:

$$a = \frac{0.3681\,F_i}{\sigma l\tan(\alpha)} \tag{2.6}$$

The above equation shows that the use of an indenter with a smaller wedge angle increases the crack length. Patutin and Serdyukov (2017) also noted that when the crack is extended due to the implementation of an indenter: $K_I + K = K_{IC}$. For the sandstone this value is $0.59 \cdot 106$ N/m$^{3/2}$ based on averaged test results, and:

$$a = \frac{0.4128\,F_i}{l\tan(\alpha)}\sqrt{\frac{\pi}{a'}} - 1.1215\sigma\sqrt{\pi a'} = K_{IC} \tag{2.7}$$

Here, a' is the length of the crack that is formed in the rock mass by indenter impression. In practice, several indenters need to be used on the fracture plane to increase the effectiveness of the oriented HF (Patutin and Serdyukov, 2017).

Figure 2.20 shows the fracture initiation pressure in a normal stress regime, as a function of wellbore deviation and orientation with respect to the maximum horizontal stress (σ_H) as presented by Abbas et al (2009). From this Figure it is seen that minimum breakdown pressure occurs for a vertical wellbore, hence they proposed that regardless of the direction of the wellbore, drilling small vertical hole along an open hole section, a fracture will initiate from the vertical hole, and therefore, there is no need to employ mechanical isolation for the fracture initiation. The

application of the notch is indeed along with the same idea, however, the notch will create a fracture all around the wellbore wall, whereas, the vertical borehole is directing the fluid in one direction, so its application requires an adequate knowledge of the in-situ stresses.

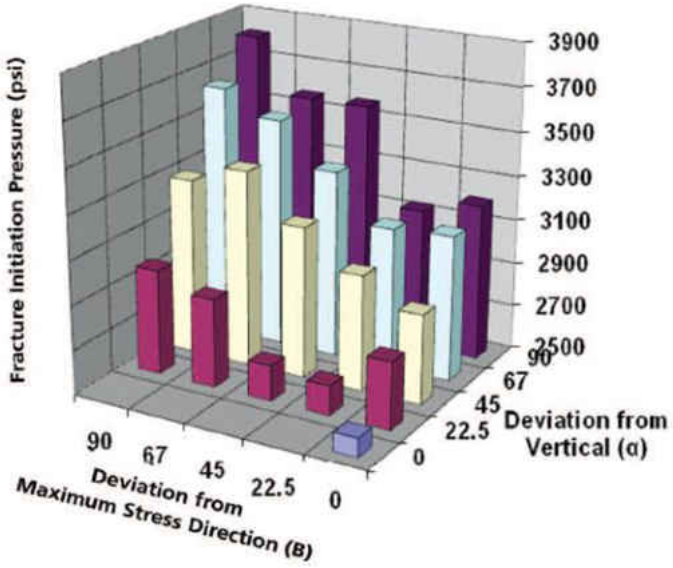

Figure 2.20: Fracture initiation pressure as a function of wellbore deviation and direction with respect to the direction of σ_H (Abbas et al, 2009).

Abbas et al (2009) proposed a jetting tool (see Figure 2.21) to create the single vertical hole for oriented fracturing. The tool was designed to provide diameter, length and a required orientation to bypass the stress induced zone around the wellbore as well as being aligned in the direction which requires the least pressure to initiate the HF. They demonstrated the application of the jetting tool in two field scale case studies and observed promising results. As shown in Figure 2.21, the tool enters the wellbore with the jetting side faced down (top Figure), and as it leaves the well, the jetting side is indicated by the white line on top (bottom Figure).

Figure 2.21: The jetting tool proposed by Abbas et al (2009) to create a vertical hole to facilitate fracture initiation.

2.6 Summary

This Chapter presented a summary of different analytical models, experimental testing, numerical simulations and some field scale practices to investigate the HF in open hole completion and in specific to understand the impact of an initial crack (notch) on initiation and propagation pressure. The importance of the notch in terms of reducing the initiation pressure and resulting in a less abrupt fracture propagation was one of the outcome from all these studies. Also, the results of these studies demonstrate that the stress anisotropy is a key parameter in forming either axial or transverse fracture from a notch. The size and direction of the notch with respect to the in-situ stresses should be considered in order to create the desired fracture. The impact of injection rate and fluid viscosity on the type of generated fractures was another important conclusion from these studies. In conclusion, these studies provide strong evidence, that by designing a proper notch geometry, it may be possible to control the location of fracture initiation from open hole section of the wellbore, reduce the initiation pressure and facilitate the fracture to propagate in the preferred plane of propagation earlier to avoid near wellbore issues such as tortuosity and screen out. This is of significant importance, especially in multi stage HF operations and required further studies. We study this topic through some analytical models that are resented in Chapter 4 and

numerical simulations in Chapter 5. In the next Chapter, a brief overview of the lattice numerical simulation, which is the method we use in this study using the XSite software will be presented.

CHAPTER 3

Lattice Formulation and XSite Software

3.1 Introduction

In this Chapter, first a brief overview of the lattice simulation, which is a type of discrete element method (DEM) is presented. XSite software, developed by Itasca group works based on lattice for hydraulic fracturing (HF) simulations. An overview of the XSite software and its feature will be presented in the second part of this Chapter with some examples to of open-hole (OH) completion HF simulations, which will be developed in further details in Chapter 5 as the main topic of this research study. For detailed review of lattice formulation and XSite software features, the readers can refer to the XSite description of formulation (2011), and HF Simulator User Guide (2013). A brief summary from these references are presented in this Chapter.

3.2 Lattice Formulation

The numerical simulation program of XSite is based on the Synthetic Rock Mass (SRM) and Lattice methods. The SRM is a simulation technique that was developed based on the distinct element method (DEM), the SRM is accounted to be more efficient than DEM, it is used to describe the mechanical behavior of a rock mass in three dimensions, this approach is used to represent the rock mass characteristic by using the bonded-particle model (BPM), which include

an assembly of circular or spherical particles bonded to each other. Therefore, the BPM offers a great solution for the simulation of hydraulic fracturing (Damjanac and Cundall, 2016) and gives a good approximation of mechanical behavior of a brittle rock (Potyondy and Cundall, 2004).

Lattice simulation, which is grain-based numerical model, is a simplification of the BPM in which the finite-sized particles and contacts are replaced by nodes and springs as shown in Figure 3.1. The lattice is a modified version of the smooth joint model (SJM) which is a group of circular/spherical particles. The lattice simulation model is computationally more efficient than SJM, the simulated three dimensional model is represented by a random number of discrete mass (nodes) connected by springs.

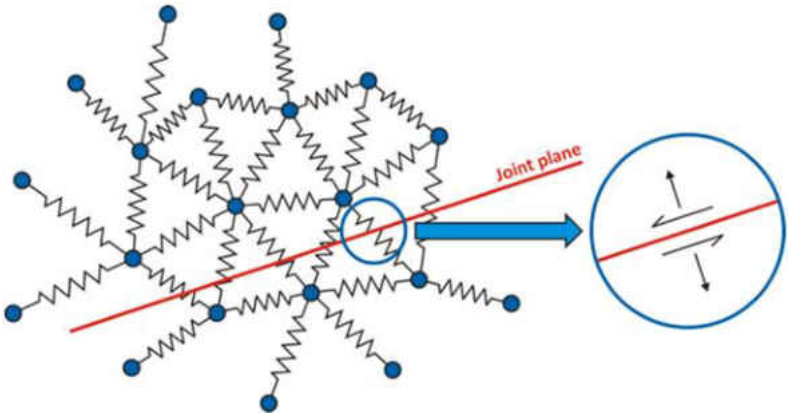

Figure 3.1: Schematic model of a lattice array. Nodes and springs (Cundall, 2011)

3.2.1 Mechanical Model

The lattice is a group of nodes connected by a non-linear spring, it applies random distribution of lattices and springs with microscale mechanical properties. The lattice uses the same concept of PFC (Particle Flow Code) PFC3D, a simplification of the DEM (Discrete Element Model) which is considered as a discontinuum method. The XSite software, which uses the lattice formulation, is based on a time step algorithm, and treat rock as an assembly of bonded particles that follow a combination of a force displacement law and law of motion during the calculation. The numerical

formulation of the code is provided by Damjanac et al (2011). The computational model is an explicit numerical method, and the formulations are based on dependent variable. The codes follow a non-linear behavior, efficient to model some features such as fracture, slip and joints. The injected fluid can follow either a Newtonian law or a power law and can contain proppant (characterized as grand particles with specific size and dimension) and the code allows a single fluid and single phase.

a) Lattice Model

The law of lattice motion uses the central difference equations 3.1 and (3.2 below during the simulation, to calculate the translational degrees of freedom. The Angular Velocity of nodes are calculated using equation 3.3:

$$\dot{u}_i^{(t+\Delta t/2)} = \dot{u}_i^{(t-\Delta t/2)} + \Sigma F_i^{(t)}\, \Delta t/m \tag{3.1}$$

$$\dot{u}_i^{(t+\Delta t)} = \dot{u}_i^{(t)} + \dot{u}_i^{(t+\Delta t/2)}\, \Delta t \tag{3.2}$$

$$\omega_i^{(t+\Delta t/2)} = \omega_i^{(t-\Delta t/2)} + \frac{\Sigma M_i^{(t)}}{I}\, \Delta t \tag{3.3}$$

In the above equations, $\dot{u}_i^{(t)}$ and $u_i^{(t)}$ are the velocity and position (respectively) of component *i* (*i* =1,3) at time t, $\sum F_i$ is the sum of all force-components *i* acting on the node of mass *m*, with time step Δt. The angular velocities are represented by ω_i , of component *i* (*i* =1,3) at time *t*.

Then, the forces (normal and Shear) acting on springs are updated and calculated using equations 3.4 and 3.5 where *N* and *S* are the normal Shear forces, respectively, taking into account spring normal k^N and shear stiffness k^s, the conditioning is set automatically if a force is larger than the spring strength, then a micro crack is created (Damjanac et al, 2016)

$$F^N \longleftarrow F^N + \dot{u}_i^N\, k^N\, \Delta t \tag{3.4}$$

$$F_i^s \longleftarrow F_i^s + \dot{u}_i^s\, k^s\, \Delta t \tag{3.5}$$

b) Condition for Fracture Propagation

In XSite, the resolution of a model is a very important parameter to choose correctly and is sensitive to a size of that model and cannot be chosen arbitrary. This might represent an issue for a large model. As explained by Cundall (2011) for mode 1 fracture, the fracture toughness is proportional to $\sigma_T\sqrt{R}$, where R is the resolution and σ_T is the tensile strength. To overcome this issue, a J integral formula was implemented in XSite which allows to calculate the rate of the released energy during fracture extension

In order to calculate the spring failure, a stress intensity factor has to be compared to rock toughness and can be derived from domain expression of J-Integral in 3D as:

$$J = \frac{1}{R}\int_v \left[\left(\sigma_{ij}u_{j,k} - W\delta_{ki}\right)q_{,i}n_k - F_i\,u_{i,j}\,qn_j\right]dV - \frac{1}{R}\int_s T_j\,u_{j,k}qn_k dS \tag{3.6}$$

Here, V is a domain that includes a point, P, of the crack front, $2R$ is the length of the crack front included in V, W is strain energy density, and q is a sufficiently smooth function in V that is unity at P and vanishes on the contour of V. According to Damjanac et al (2011), function qn_i can be interpreted as imposing a unit translation at P in the n_i – direction while the material points on the contour of V remain fixed. As such, the domain method for evaluating J can be interpreted as the deLorenzi virtual crack-extension technique. For 3D application, a domain, V, of spherical shape with radius R is considered.

The discrete Form of the domain expression for J-Integral is represented as:

$$\begin{aligned} J = \frac{1}{R}\sum_{nd}\big[&(\sigma_{11}^{nd}\,V^{nd})U_1 + (\sigma_{12}^{nd}\,V^{nd})U_2 + (\sigma_{13}^{nd}\,V^{nd})U_3 - (W^{nd}V^{nd})n_1\big]q_{,1}^{nd} \\ &+ \left[\left(\sigma_{21}^{nd}\,V^{nd}\right)U_1 + \left(\sigma_{22}^{nd}\,V^{nd}\right)U_2 + \left(\sigma_{23}^{nd}\,V^{nd}\right)U_3 - \left(W^{nd}V^{nd}\right)n_2\right]q_{,2}^{nd} \\ &+ \big[(\sigma_{31}^{nd}\,V^{nd})U_1 + (\sigma_{32}^{nd}\,V^{nd})U_2 + (\sigma_{33}^{nd}\,V^{nd})U_3 - (W^{nd}V^{nd})n_3\big]q_{,3}^{nd} \end{aligned} \tag{3.7}$$

where the summation is taken on lattice nodes with the centre included in the (spherical) domain of integration, U_i^{nd} is the gradient of displacement component *i* in direction *n*, and V^{nd} is nominal node volume.

The stress intensity factor is defined as:

$$K_i = \sqrt{JE} \tag{3.8}$$

In this equation, *J* is the *J* integral and *E* is the rock's Young's modulus. The following conditions has to be taking into consideration when calculating the stress intensity factor (Damjanac & et al 2016), where K_I is the local stress intensity factor and K_{IC} is the local fracture toughness.

- If $K_I \ll K_{IC}$, Spring tensile strength is the criterion for fracture propagation.
- If K_I is close to K_{IC}, use $K_I \geq K_{IC}$, the local fracture toughness will be the criteria.

3.2.2 Fluid Flow Model

The fluid flow motions in XSite are treated in different way. First, when the simulation starts in the model input, the fluid is created in the joints, this is called "flow Joints." Second, new fluid nodes are generated, after the microcracks are created due to the springs breakage, known as "Matrix Fluid." It is important to note that the fluid circulates between the fractures (joints) and the matrix.

a) Flow in Joints

The fluid flow in joints is simulated using the fluid elements (fluid nodes) as shown in Figure 3.2, that are connected by pipes, those pipes can be located either in the centre of a broken spring or pre-existing joints, representing a conduit to the fluid flow. The pressure of the fluid is found within the fluid element. The flow rate between nodes through the pipe is calculated using the blurbification theory below (Qiu et al. 2019):

$$q = \beta k_r \frac{a^3}{12\mu} [p^A - p^B + \rho_w g(z^A - z^B] \quad (3.9)$$

In this equation, a is the hydraulic aperture, μ is viscosity of the fluid, and p^A and p^B fluid pressures at nodes "A" and "B", respectively. z^A and z^A are elevations of nodes "A" and "B", ρ_w is fluid density, and g is the acceleration due to gravity. k_r is the relative permeability, which is a function of saturation, and becomes 1 when the pipe is saturated. β is a dimensionless calibrated parameter.

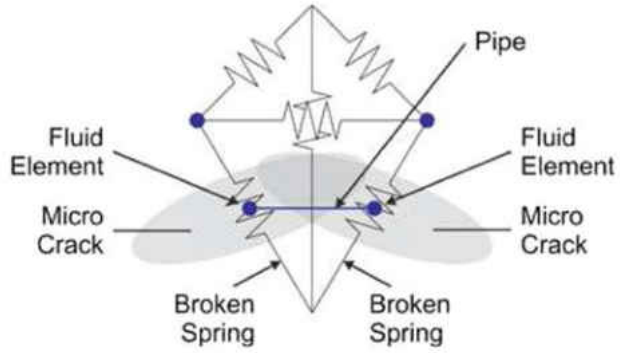

Figure 3.2: Correlation between the 3D particle model and corresponding pipe network (Damjanac, Detournay, and Cundall 2016)

The pressure increment delta P increases and it is solved as below:

$$\Delta P = \frac{Q}{V} K_f \Delta t_f \quad (3.10)$$

Here, Q is the sum of flow rate from the pipes connected to the fluid element, V is the volume of the fluid element, K_f is the apparent fluid element bulk modulus, and Δt_f is the flow time step (Damjanac et al, 2016).

b) Matrix Flow

The matrix flow which is the permeability in the model is in fact the leak-off into the intact rock. There are different variables to be considered in the matrix flow. The locations of these variables are shown in Figure 3.4. The blue circles represent lattice nodes, the red dots which represent the pressures are located in the centre of the springs.

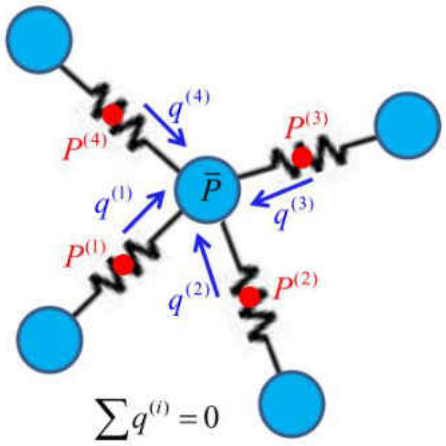

Figure 3.3: Location of variables in the matrix flow scheme (Damjanac et all 2011)

Scanning effect takes place for quality check of the calculated pressure taking into consideration the flow rate, conductivity and node pressures using the lattice data structure. $\bar{P}$ represents the pressure at each node is calculated as (η_i is the conductivity):

$$\bar{P} = \sum_{i=1,N} \eta P^{(i)} / \sum_{i=1,N} \eta_i \tag{3.11}$$

3.2.3 Hydro-Mechanical Coupling

The mechanical process and fluid flow are essential in HF. The coupling fluid mechanical for fracture propagation is implemented in XSite using the codes that were suggested by Peter Cundall. It is more efficient than the one actually run in the software as it allows faster computational time. Two aspects are now contributing in the simulation, the rock compressibility and a stable time step. In fact, the longer fluid time steps is now permitted as the apparent fluid bulk modulus is very small comparing to fluid bulk modulus considered as "relaxation parameter' of the model. The fluid bulk modulus property is related to the compressibility of the Hydraulic fluid and the stiffness of the lattice model. Another parameter that is crucial in the simulation process is the permeability of the fracture. In XSite this parameter is based upon the initial fracture aperture and deformation of the model (computed from the fluid pressure). The fluid pressure impacts the strength of the

model and the deformation of the model that impact the fluid pressures that can be determined even with undrained state.

3.3 Building a HF Model in XSite

In this section the steps to build and run a HF model in XSite software are presented. For the details of XSite software the reader should refer to the HF Simulator User Guide (2013), as here the main features of the software related to the simulations of this research are reviewed.

3.3.1 Rock and Fluid Properties, and In-Situ Stresses

XSite allows constructing a rectangular prism as the initial model of the rock. The length, height and width can be determined by the user, and these can be all equal. A reference point is defined, from which all future measurements are done. Detailed rock and fluid properties can be entered manually by the user. Figures 3.5 and 3.6 show an example of the rock and fluid properties menu, respectively. The data in these two Tables correspond to the Bakken formation in North Dakota, Williston Basin. Both metric and imperial units can be selected. As it is seen from the right panel of Figure 3.5, the software considers anisotropic rock properties, in particular for shale formations. Rock anisotropy has not been considered in this study. Fracture toughness and fluid viscosity are the two important rock and fluid properties with respect to the HF simulations. In Bakken these values considered as 2 MPa.m$^{0.5}$ and 0.002 pa.s (2cp), respectively.

The in-situ stresses are applied as three principal stress components of vertical, minimum and maximum horizontal stresses (σ_v, σ_h , σ_H). The orientation of these stresses can be defined in such a way to mimic normal (σ_v>σ_H>σ_h), strike-slip (σ_H>σ_v>σ_h) and reverse/thrust fault (σ_H>σ_h>σ_v) stress regimes. Figure 3.7 shows the panel where the magnitude and directions of the three principal in-situ stresses can be entered. As it is seen at the bottom of Figure 3.7, the only boundary

condition that is considered in XSite is fixed or roller boundaries. For smaller models where large deformation reaches the boundaries, it can cause a significant change in in-situ stresses at the boundaries and a stress based boundary condition may be more appropriate. This is not automatically observed and applied in the XSite. A numerical trick that has been proposed and also used in this study is the implementation of the Soft boundaries. The Soft boundaries are soft material (e.g. 10 to 100 times lower stiffness than the rock Young's modulus) that are built all around the model to simulate stress based boundary. This material absorbs the deformation while maintaining relatively constant stress.

Figure 3.8 shows an example of sketch model in XSite representing a 1.5m×2.5m×2.5m rock block including 0.125m soft boundary (100 times less Young's modulus than that of the formation) placed around all 6 faces.

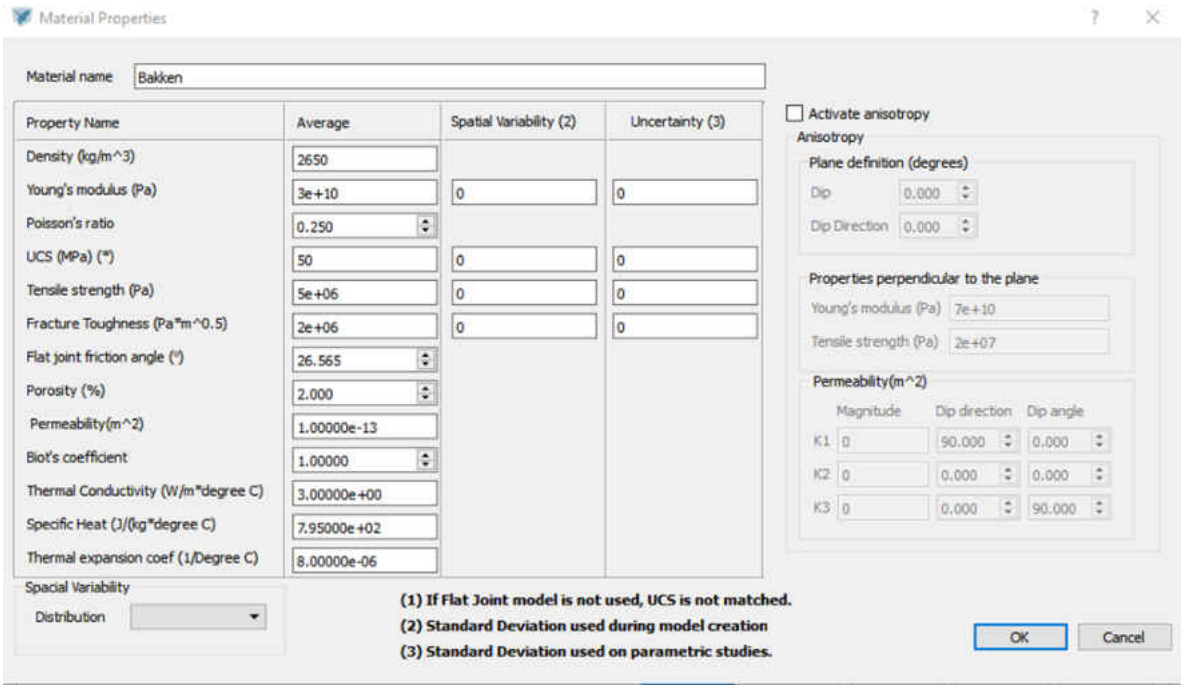

Figure 3.4: An example of XSite Material Properties window. Input data corresponds to Bakken formation.

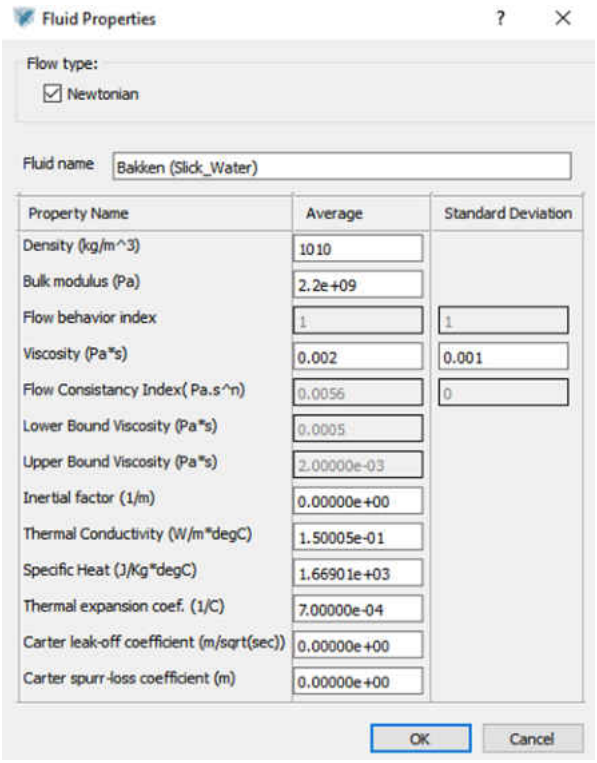

Figure 3.5: An example of XSite Fluid Properties window. Input data corresponds to Bakken formation.

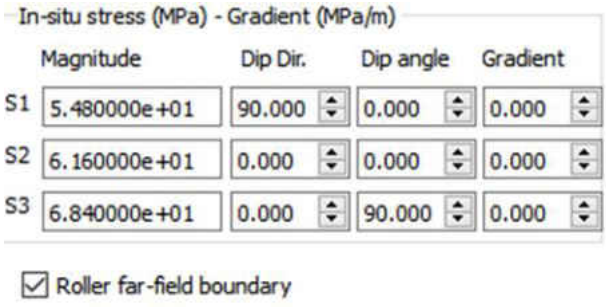

Figure 3.6: An example of XSite in-situ stress window. Input data corresponds to Bakken formation.

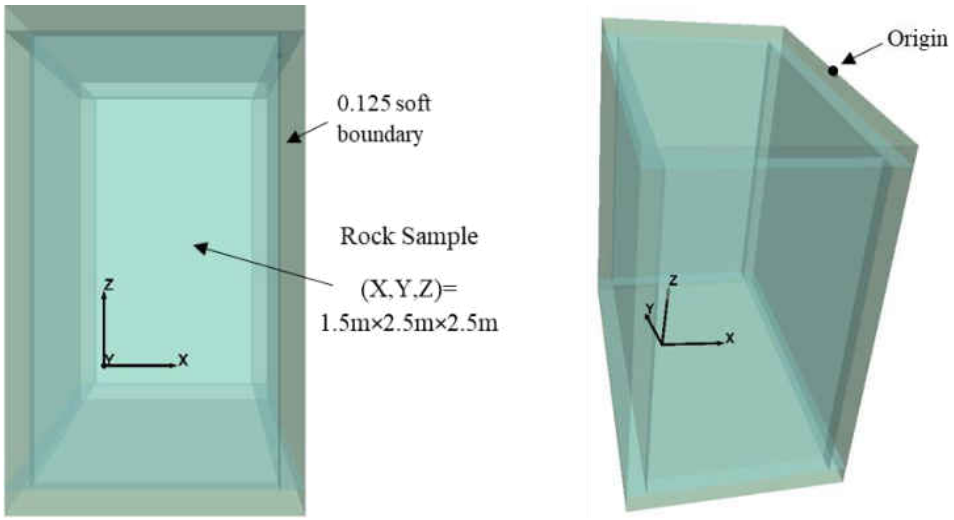

Figure 3.7: An example of rock geometry with Soft boundary in XSite

3.3.2 Borehole Construction and Fluid Injection

There are three ways of fluid injection in XSite for the purpose of HF simulations. These include injection via a cluster from a borehole section, injection through an open-hole (OH) section and injection via perforation tunnels in cased-hole (CH) completion. For demonstration purposes we consider a 0.7m horizontal wellbore section with radius of 0.11m (i.e. 8.5in borehole diameter) drilled in the rock geometry of Figure 3.7 along X direction, here the direction of minimum horizontal stress (σ_h). The rock and fluid properties as well as stresses magnitude are based on the data presented in Figures 3.5 to 3.7, also listed in Table 4.1 in Chapter 4. Figure 3.8 (top) shows the borehole menu in XSite with two separate panels. Clicking on the "Add" button of the upper panel allows to enter fluid injection schedule in one or multiple stages (see Figure 3.8, bottom left). Clicking on the "Add" button on the lower panel, as shown in Figure 3.8 (bottom right) enables adding one wellbore section at a time with the trajectory and radius of the wellbore. Combination of borehole, OH completion and perforations can be chosen and wellbore trajectory, while it is straight line, can be vertical, deviated or horizontal. As it is seen in this Figure, we consider an OH completion in this example. The Cluster panel at the lower panel of Figure 3.8 (top) is activated

when borehole type is selected. It is important that that each stage of fluid injection is correctly assigned to the corresponding segment so the software recognizes where the fluid injection should start from.

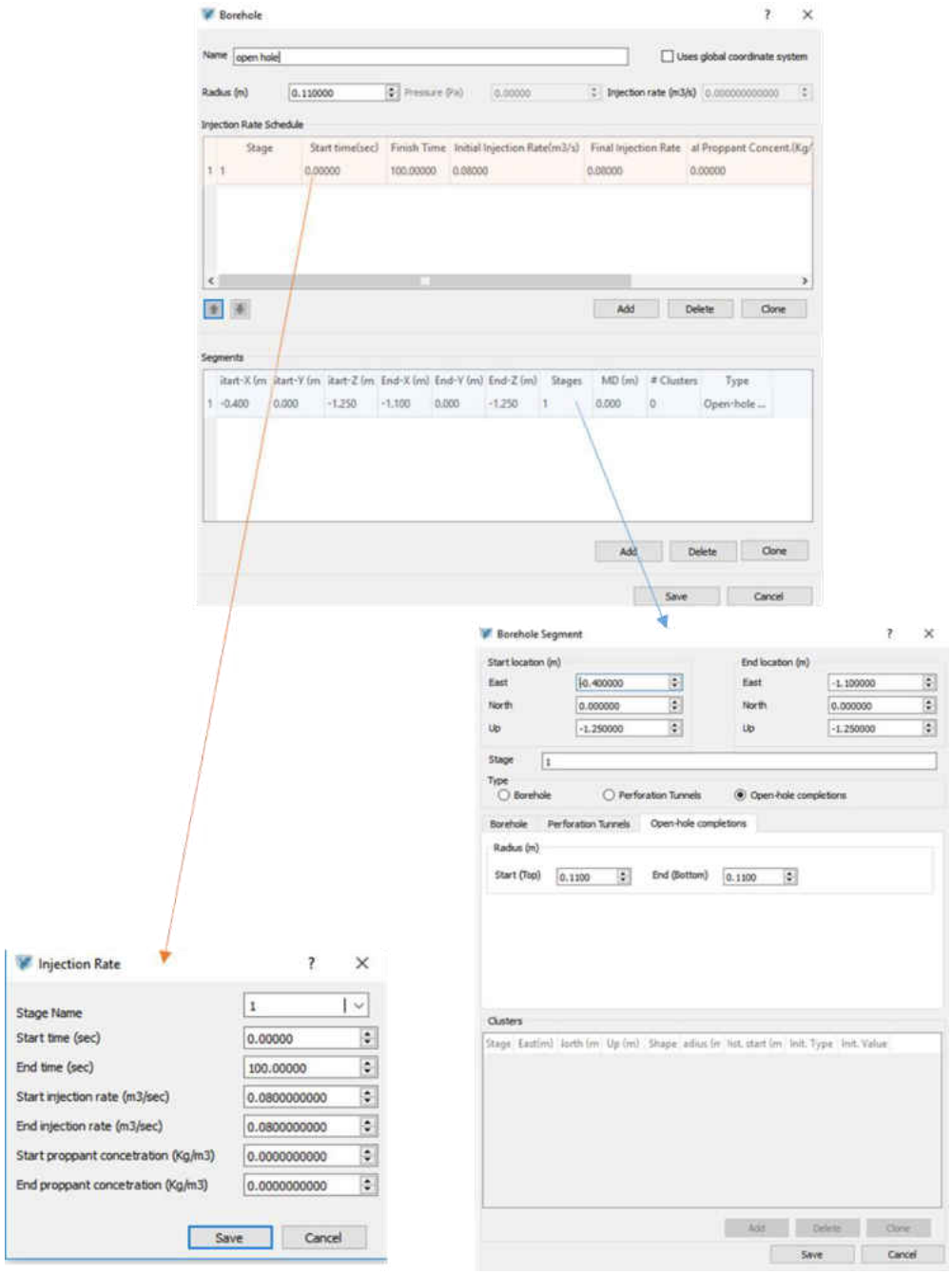

Figure 3.8: Borehole panel in XSite (top) to enter fluid pumping (low left) andborehole trajectory and geometry and radius (bottom right). The OH completion is chosen in this example with cluster section being inactivated

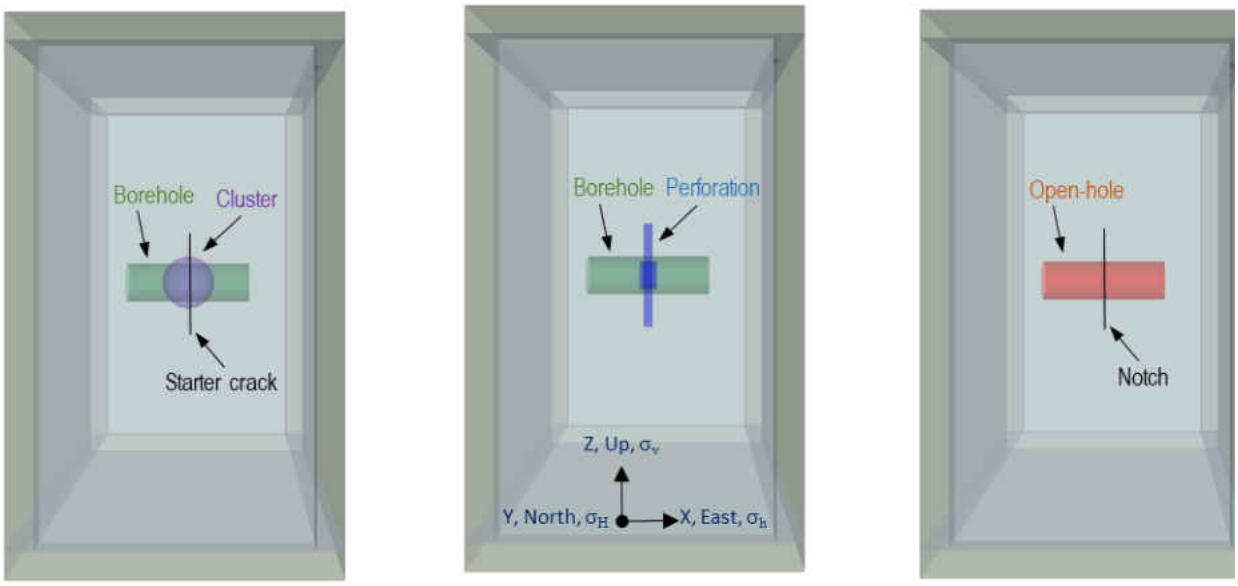

Figure 3.9: Different options for fluid injection in XSite, via a borehole and cluster (left), perforations (middle) and OH completion (right).

Figure 3.9 shows schematically the three options for the fluid injection in XSite. In case of injection through the cluster, a spherical (more common) or cylindrical shape cluster is placed at the point where the injection is intended to begin from the borehole (see Figure 3.9, left). The size of the cluster is slightly larger than the wellbore radius (here, cluster radius was chosen as 0.15m). The cluster is the point of the fluid injection. In order to facilitate the fracture to initiate, a very weak starter crack (either rectangular or circular shape) is placed in the middle of the cluster oriented along the preferred plane of propagation, i.e. perpendicular to σ_h. The size of the starter crack is slightly larger than the cluster diameter (here we used a circular fracture with radius of 0.3m) with a very small opening (aperture) of in the order of 1×10^{-5}m. Figure 3.10 shows the joint set panel in XSite where several parameters associated with the starter crack can be defined by the user. The same panel is used to introduce any natural fracture planes in the model with various orientation, stiffness, spacing, aperture mechanical properties (i.e. Tensile strength, friction angle, cohesion and dilation angle). The use of the cluster injection is more

meaningful for field scale HF simulations, where the size of the fracture is much larger than the areas of fluid injection inside the fracture stage, hence, assuming point injection is a good assumption. One can install casing and cement in this type of injection.

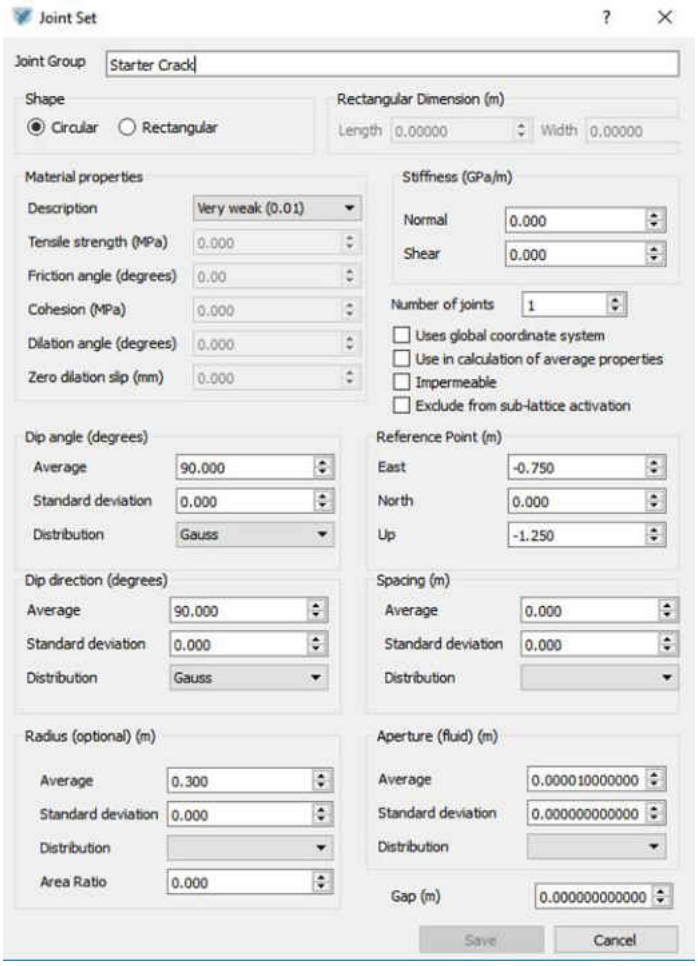

Figure 3.10: Joint Set panel in XSite to enter the parameters of natural fractures

The second option for fluid injection is for the cased holes and through perforation tunnels (Figure 3.9, middle). In this case two boreholes are constructed. The outer borehole represents the borehole and the inner one with smaller size represents the casing. the perforation tunnel is installed in the middle of the inner borehole. The space between the two boreholes are cemented. Perforations in different orientations can be considered with different length and diameter. In Figure 3.9 the radius of the outer and inner boreholes set to 0.11m and 0.09m (corresponding to

an 8.5" wellbore with 7" casing). Two perforations are installed in the middle of the model in this example with in the upper and lower side of the wellbore with diameter of 0.0254m (1 in) and a length of 0.3m.

The third option for fluid injection in XSite is through the OH completion (see Figure 3.9, right). In this case, instead of borehole, we choose the OH completion feature to install a wellbore section. In this case, the fluid is injected through the entire OH section area once the fluid mode is activated. Here, in order to facilitate the fracture initiation, we install an initial crack oriented along the preferred fracture propagation direction, i.e. in this example, perpendicular to the direction of σ_h. The size of this initial crack, also known as notch, will have a great impact on fracture initiation. This is the main topic of this research which will be discussed in details in the next two Chapters. Also, similar to the first case, we assume an aperture of 1×10^{-5}m for this initial crack. The OH completion is suitable for the cases where the near wellbore HF is simulated and the objective is to study the fracture initiation and short propagation around the wellbore.

3.3.3 Resolution

The resolution of the model is perhaps the most important parameter in simulation. It is defined as the average lattice node spacing. The smaller the lattice resolution, the more accurate the modelling will be but at the expense of a larger processing time. The number of nodes across a given model dimension should be considered before setting the resolution. For example, if approximately 50 nodes across a 500-m block are required, then the resolution should be set to 1000 cm. The model run time is very sensitive function of the resolution, particularly if the uniform resolution is used throughout the model. Roughly, the simulation time is inversely proportional to the resolution power of five. This sensitivity can be reduced if variable resolution

As stated in the HF Simulator User Guide (2013) "The apparent fracture toughness of the lattice will be a function of the spring tensile strength (calibrated to the macroscopic strength of the material) and the current resolution. Thus, if the spring tensile strength is calibrated to macroscopic tensile strength of the material, the fracture toughness can be matched by adjusting the resolution. For relatively small resolutions (of the order of 1 cm or smaller), the lattice toughness will be of the order of 1 MPa×$m^{0.5}$, which is typical or rocks. However, if the resolutions are greater (e.g., of the order of 1 m or greater, as usually necessary for simulation of the problems on the time and length scales of interest for field operations), the default lattice setup will overestimate the realistic rock toughness and will not match the specified fracture toughness. The fracture toughness will be matched if Store Spring Forces is checked (in Reset Lattice menu) after initialization of stresses (forces) in the model."

In general, the resolution for the domain next to an OH section should be 10 times less than the borehole diameter. For cluster injection, as the near wellbore fracture analysis is not the main focus and fracture propagation at large scale is taken into consideration, the resolution is compared with respect to the model size. As a rule of thumb, for a 1m model size we need to consider at least 50 nodes, i.e. 2cm resolution. For more accurate results, the resolution of 1cm may be considered, while it increases the running time exponentially larger.

a) Domain Resolution

In order to optimize the discretization, one may use different resolutions at different locations of the model. Usually, finer resolutions are used closer to the injection point or important features in the model and coarser resolutions towards the boundaries. Rectangular, cylindrical and triangular resolution domain geometries are available in XSite. We will use domain resolution in Chapter 5 for OH HF simulations.

In this study, for the case of transverse fracture we consider three resolution domains as shown in Figure 3.11. The cylindrical domain around the axis of the wellbore has length of L=2m and diameter of D=0.20m with a resolution of 2.2cm. This will ensure that growth of any axial fracture, if it occurs due to the small notch size, will be propagated in a high resolution zone. The second cylindrical domain with length of L=0.85m and diameter of D=0.25m is in perpendicular to the wellbore axis, along the direction that the fracture is expected to propagate. This domain has a high resolution of 2.2cm. The third cylindrical domain with length of L=0.88m and diameter of D=2.15m has a resolution of 4.4cm and the remaining of the model was assigned a resolution of 8.8cm using the resolution feature under the "Solution" Tab. The transition from one to the second domain has a ratio of 2 for resolution to ensure the stability of the model and accuracy of the results.

For conveniences, throughout this research study, we refer to the scaled length of the notch as $\gamma = L_n / a$. Here L_n is the length of the notch, that for a circular transverse fracture is equivalent to its radius and a is the wellbore radius (see Figure 3.11).

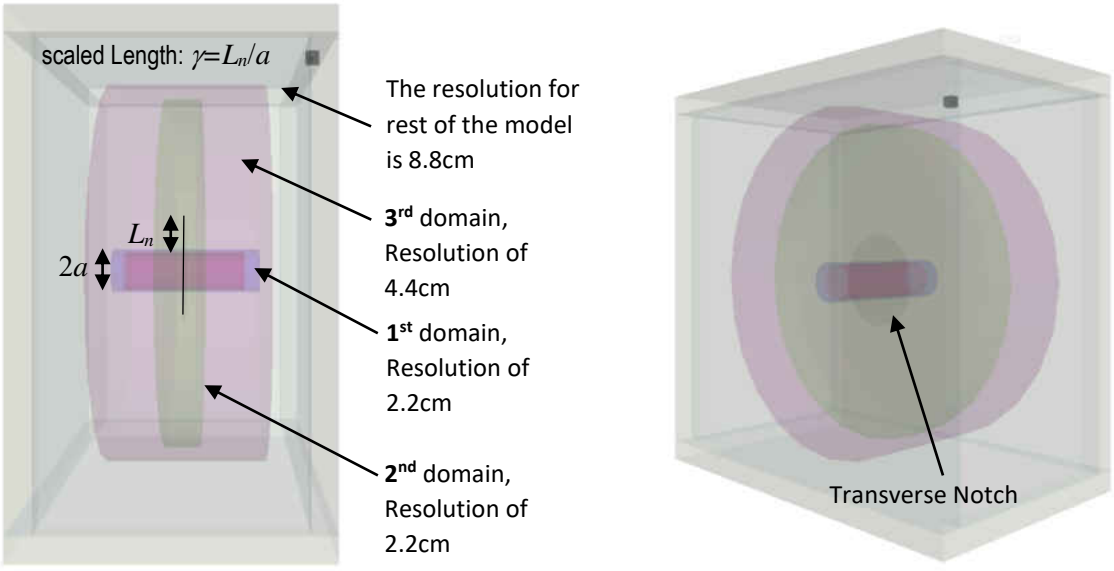

Figure 3.11: Resolution domains for a transverse fracture model

In case of an axial fracture, as the fracture extension is along the wellbore axis, in order to use the same model geometry, but at the same time maximize the length available to the fracture to grow, we changed the orientation of the wellbore along the Y (North) direction, as opposed to the case of transverse fracture (see Figure 3.9). Here the wellbore length is 2m. In this case, the direction of σ_h and σ_H was swapped so the min horizontal stress is perpendicular to the wellbore axis. Figure 3.12 (left) shows the model geometry for an axial fracture with a rectangular shape notch. In this Figure L_n is the length of the notch in one side of the wellbore, a is wellbore radius and L_b is the base length. Similar to the transverse notch we define the scaled length as $\gamma = L_n / a$.

The notch aperture is 1×10^{-5}m. As it is seen from this Figure, in case of an axial notch, in addition to the notch length (L_n) going inside the formation, the fracture has a length along the wellbore axis. Here, L_b =0.5m. We name this the notch base length (L_b) and investigate the impact of that on fracture initiation pressure in Chapter 5. Two rectangular resolution domains were considered in this example (see Figure 3.12 (middle and right). The inner domain has an equal length and width of L=W=2.1m and thickness of T=0.3m with a resolution of 2.2cm. The same dimensions for the outer domain are L=W=2.3m and thickness of T=0.5m with a resolution of 4.4cm. The rest of the model has a resolution of 8.8cm which was set through the "Solution" Tab.

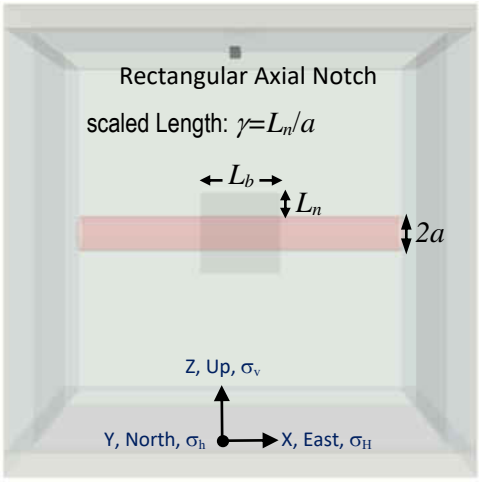

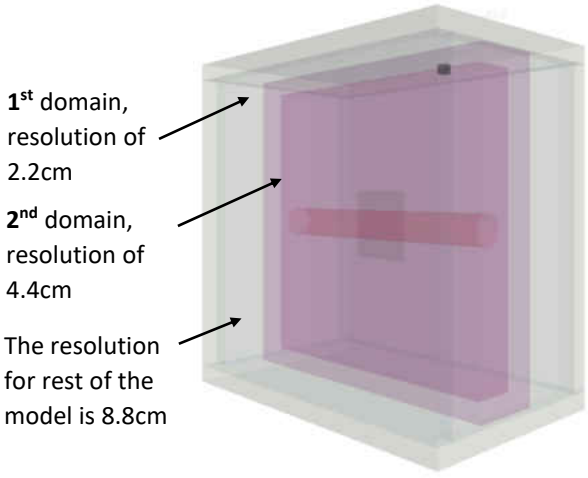

Figure 3.12: Model geometry of an axial notch and fracture (left) and the resolution domains

b) Nested Resolution

This feature can be used to optimize model discretization by building a graded resolution transition from the finest resolution (typically in a domain that includes the injection points in the center of the model) to the coarser resolutions towards the model boundaries. User should avoid sudden jumps in resolution (e.g., the ratio of resolutions between the adjacent domains greater than two) Nesting resolution can be applied only to rectangular closed-volume domains.

3.3.4 Solution

In order to run a HF model in XSite, usually, three main steps are to be taken. Firstly, the borehole is excavated. During this step, the model is not subjected to either mechanical (i.e. effect of in-situ stresses) or fluid flow (injection of fracturing fluid). This is followed by the equilibrium step, where the in-situ stresses are applied to the model. This step needs to continue until the entire model reaches the equilibrium. This may be checked by looking at the contours of the velocity: the model usually reaches equilibrium when the velocity vectors go below 1×10^{-6}m/s. the final stage is the hydromechanical phase, where, under the effect of in-situ stresses the fluid pumping starts. The Batch simulation panel (see an example of it in Figure 3.13) is used to set up the three solution steps and then execute the model. The panel shows the time corresponding to each step and the bottom section of the panel in Figure 3.13 reports a summary of the model status and any possible errors.

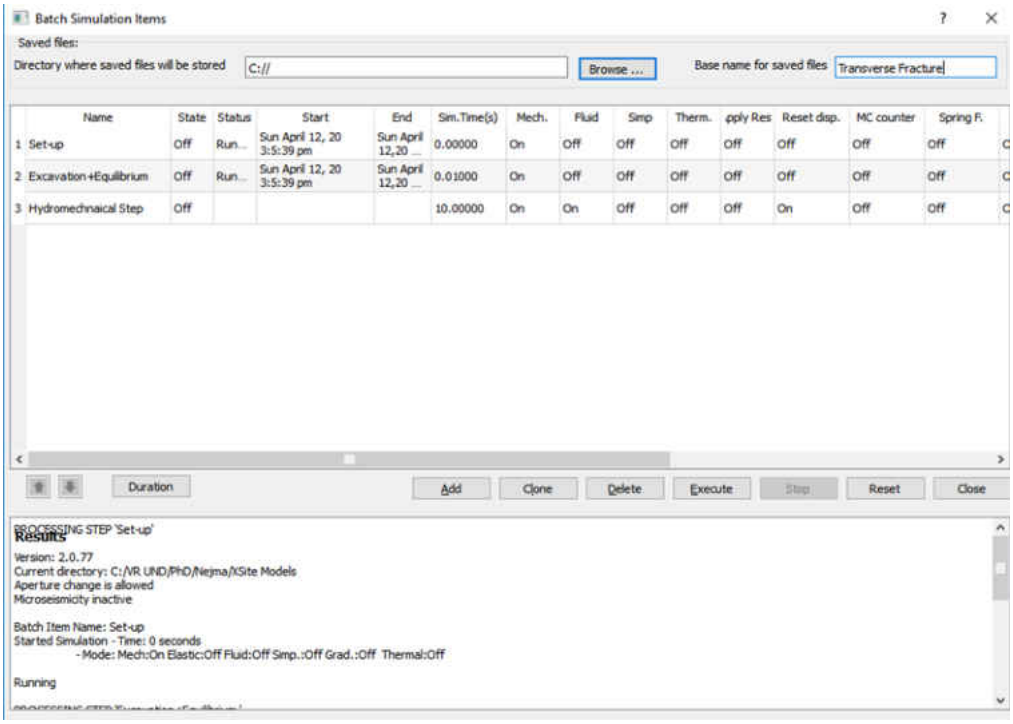

Figure 3.13: Batch Simulation panel in XSite to set up the three main stages and execute the model

3.4 Simulation Examples

To demonstrate some applications of the XSite for HF simulations, here a few examples are presented.

3.4.1 Injection Rate Effect on Fracture Pressures

For demonstration purposes, using the data corresponding to the Bakken formation (see Table 4.1, Chapter 4) and model geometry of Figure 3.11, we performed HF simulations in OH completion.

To investigate the effect of injection rate change of fracture pressures, a transverse notch model with length of L_n=0.066m, or scaled length of γ=0.066/0.11= 0.6 considered for simulation purposes. Detailed simulations will be presented in Chapter 5. Figure 3.14 shows the fracture apertures corresponding to injection rates of Q=0.06m^3/sec (top) and 0.08m^3/sec. Figure 3.15 presents the plot of fracture pressure and crack numbers versus time.

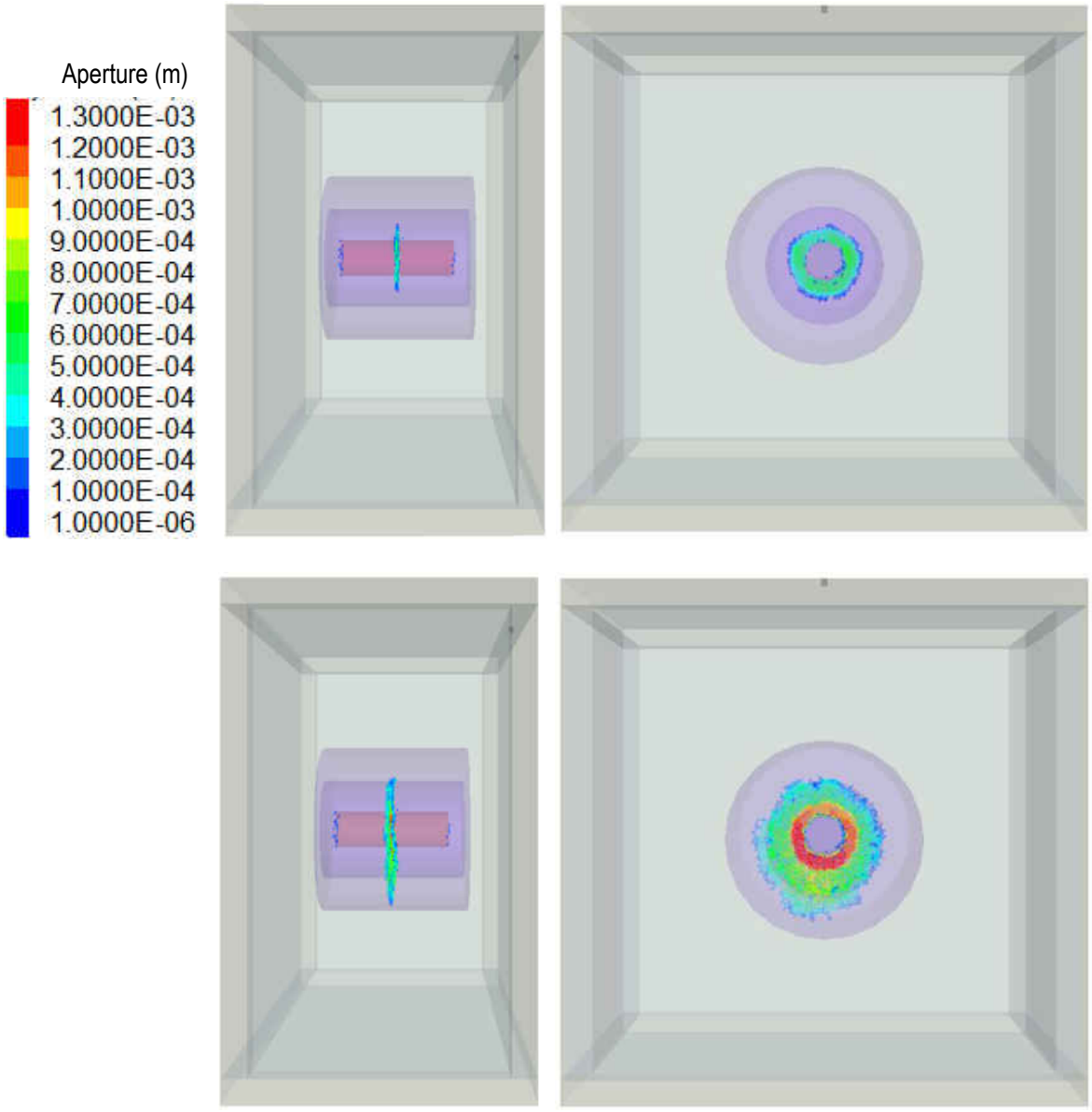

Figure 3.14: Fracture apertures corresponding to injection rate of Q=0.06m3/sec (top) and Q=0.08m3/sec (bottom) over simulation time of t=0.sec

As the injection rate continues, the pipes which connect lattices are broken and create cracks. We define the fracture initiation pressure (FIP) as the pressure corresponding to the time when all pipes are broken around the notch perimeter. From Figure 3.15 it is seen that as the flow rate increases, the time to reach the FIP reduces and the FIP tends to increase. It is also interesting that at the beginning of the simulation the fracture grows more symmetrically with circular shape, whereas at longer time it becomes more asymmetric and non-circular. This is most likely due to the fact that at the early propagation time the fracture propagates in viscosity dominated regime where the fluid viscosity controls the fracture geometry. However, at longer time, the fracture propagation regime changes to transition and then toughness dominated regime with toughness becoming the main controlling parameter of fracture geometry.

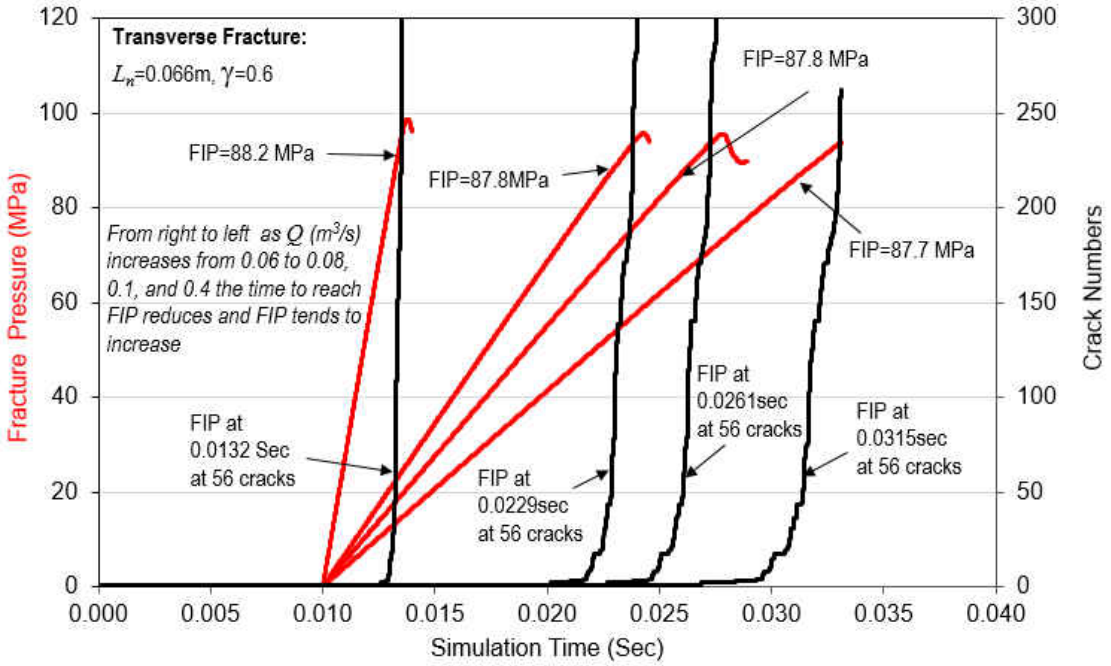

Figure 3.15: Fracture pressure and crack numbers versus time for different injection rates

3.4.2 Fluid viscosity Effect on Fracture Pressures

To investigate the effect of fluid viscosity on fracture pressure, we run three models with the same flow rate as before but viscosities of 0.002pas.sec, 0.02pas.sec and 0.2pas.sec, respectively. The plot of pressure and crack numbers versus time are shown in Figure 3.16. it is seen that as viscosity increases the fracture initiation pressure increases and also the time to reach the FIP becomes larger. This conclusion is in agreement with what we expect as higher viscosities require more energy for the fluid to be pumped and it increases the fracture pressure.

The above results indicate the capabilities of the lattice simulation in taking into account the effect of different parameters influencing the HF pressure. In Chapter 5 several examples of simulations of HF will be presented.

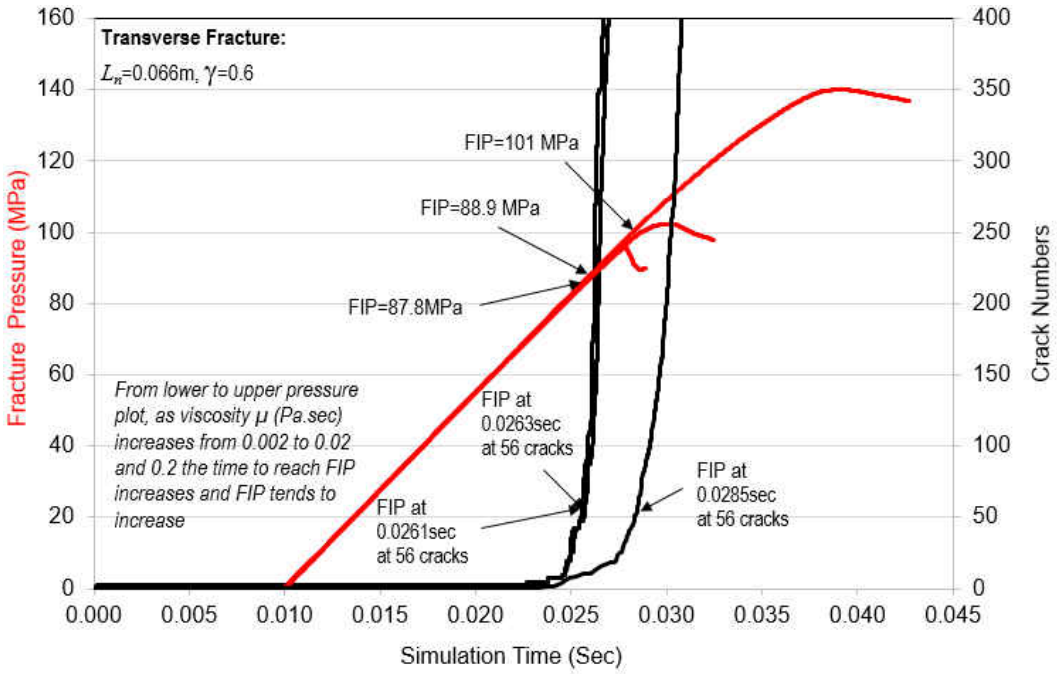

Figure 3.16: Fracture pressure and crack numbers versus time for different fluid viscosities

3.5 Summary

A summary of formulations used in lattice numerical simulation were presented in this Chapter. Also, the features of the XSite software which uses this particle based simulation were introduced. The capabilities of lattice simulation in coupling the fluid and stress in hydraulic fracturing modelling makes it unique for applications if this study and this is presented in detail in Chapter 5.

CHAPTER 4

Analytical Models

4.1 Introduction

As mentioned in the previous Chapters, OH hydraulic fracturing offers several advantages over CH completion. The challenge, however, is that the fracture initiation and propagation in long OH sections are dominantly controlled by the existing natural fractures around the wellbore. Therefore, in real applications, the mechanics of hydraulic fracturing is considered as propagation of an existing crack with a given geometry and direction from the wellbore wall.

In this Chapter, firstly a brief review of the classical Kirsch models to estimate the fracture pressure around a circular borehole will be given. This is based on the assumption of isotropic elastic rock. Then, the theory of critical borehole pressure at unstable crack extension proposed by Rummel (1987) will be presented which calculates the initiation pressure based on superposition of the stress intensity functions associated with the stresses, wellbore pressure and the pressure inside the crack. The analytical model presented by Charlez (1997) which integrates the effect of pressurization rate on fracture initiation from a borehole with a bi-wing notch will be discussed. This will be followed by the analytical model of Nilson and Proffer (1984) which includes the competition between axial and transverse fracture initiation due to the notch geometry and the shape of the cavity.

4.2 Stress Perturbation around a Wellbore

In Petroleum geomechanics, it is common to consider the vertical or overburden stress (σ_v), minimum horizontal stress (σ_h) and maximum horizontal stress (σ_H) as the three principal stresses, which are also known as far field or in-situ stresses. The common industry approach to determine the magnitude of these stresses is based on construction of the Mechanical Earth Model (MEM). The vertical stress is simply an integration of the density times the thickness of different layers. The density log is the main input to estimate the vertical stress profile. Knowing that the horizontal stresses are functions of the vertical stress and the rock elastic properties (in simple isotropic medium these are the Young's modulus and Poisson's ratio), the MEM workflow builds the continuous logs of rock elastic and strength properties along the wellbore trajectory based on their relationship with the physical properties of the formations which are obtained from petrophysical logs. These input are used to build the profile of the horizontal stresses through the well know poro-elastic equations. The details of the MEM workflow can be found from several literatures (e.g. Rasouli et al 2011)

Due to drilling operation, the in-situ stresses around the wellbore are altered. Figure 4.1 shows the drilling induced stresses in a cylindrical coordinate system at a point with distance r from the wellbore center and angle φ with respect to the maximum far field horizontal stress (σ_H). The induced stresses are the vertical stresses (σ_{zz}), radial stresses (σ_{rr}), tangential or hoop stresses ($\sigma_{\theta\theta}$) and the shear stresses ($\sigma_{r\theta}$). Figure 4.1 shows cross section of a vertical wellbore with vertical stress being perpendicular to the plane.

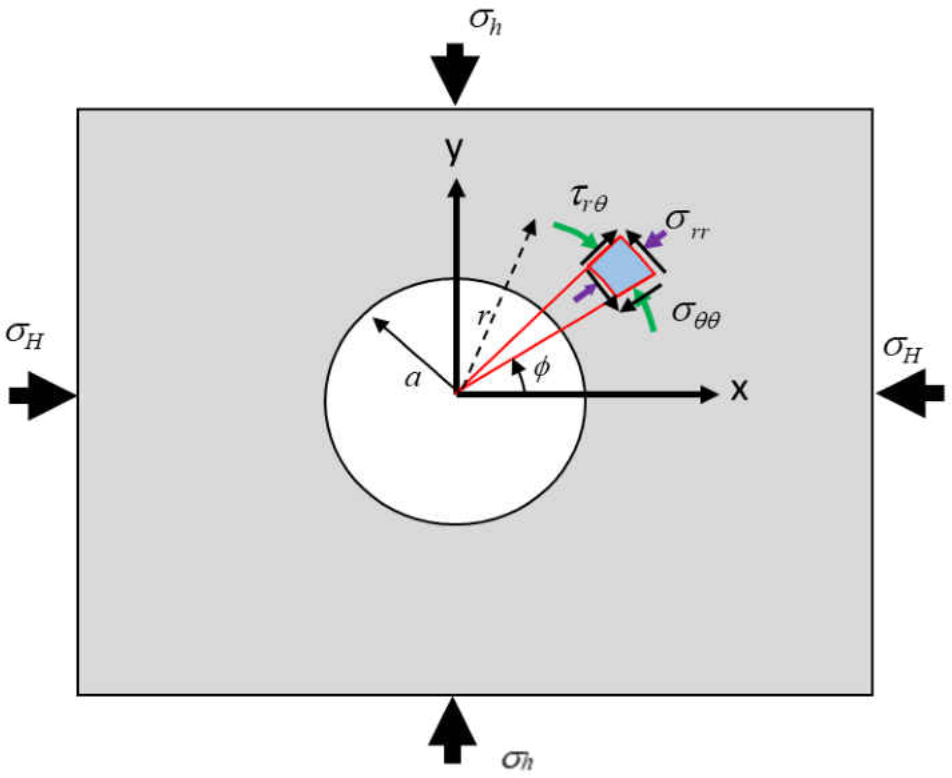

Figure 4.1: Plan view of a vertical wellbore with in-situ and drilling induced stresses.

Assuming homogeneous and isotropic elastic rock, the induced stresses can be estimated from Kirsch's equations:

$$\sigma_{rr} = \frac{1}{2}(\sigma_H + \sigma_h)\left(1 - \frac{a^2}{r^2}\right) + \frac{1}{2}(\sigma_H - \sigma_h)\left(1 - \frac{4a^2}{r^2} + \frac{3a^4}{r^4}\right)\cos 2\varphi + \frac{a^2}{r^2}P_b \quad (4.1)$$

$$\sigma_{\theta\theta} = \frac{1}{2}(\sigma_H + \sigma_h)\left(1 + \frac{a^2}{r^2}\right) - \frac{1}{2}(\sigma_H - \sigma_h)\left(1 + \frac{3a^4}{r^4}\right)\cos 2\varphi - \frac{a^2}{r^2}P_b \quad (4.2)$$

$$\sigma_{zz} = \sigma_v - 2v(\sigma_H - \sigma_h)\frac{a^2}{r^2}\cos 2\varphi \quad (4.3)$$

$$\sigma_{r\theta} = \frac{1}{2}(\sigma_H - \sigma_h)\left(1 + \frac{2a^2}{r^2} - \frac{3a^4}{r^4}\right)\sin 2\varphi \quad (4.4)$$

In the above equations, P_b is the wellbore pressure and all stresses are assumed to be the total stresses, so for calculation purposes they should be changed to effective stresses (i.e. total stress minus the pore pressure, P_p).

In the context of this research, hydraulic fracturing operations are commonly performed in horizontal wellbores drilled in the direction of σ_h, which is the most stable direction in case of

normal ($\sigma_v>\sigma_H>\sigma_h$) or strike-slip stress regime ($\sigma_H>\sigma_v>\sigma_h$). In this case, as shown in Figure 4.2, the two far field stresses acting on the wellbore wall are σ_v and σ_H. In case of normal stress regime, if axial (longitudinal) fractures develop around the wellbore, it will be along σ_v direction (perpendicular to the least tangential stress, $\sigma_{\theta\theta}$, i.e. on the top and bottom of the wellbore, along z direction), as depicted in Figure 4.3. In this Figure, $\bar{P}$ is the average pressure inside the crack. In this case, the drilling induced stresses around the wellbore are obtained from the Kirsch's equations by replacing $\sigma_v=\sigma_h$, $\sigma_H=\sigma_v$ and $\sigma_h=\sigma_H$ in equations 4.1 to 4.4, for the case of normal stress regime which results in:

$$\sigma_{rr} = \frac{1}{2}(\sigma_v + \sigma_H)\left(1 - \frac{a^2}{r^2}\right) + \frac{1}{2}(\sigma_v - \sigma_H)\left(1 - \frac{4a^2}{r^2} + \frac{3a^4}{r^4}\right)\cos 2\varphi + \frac{a^2}{r^2}P_b \tag{4.5}$$

$$\sigma_{\theta\theta} = \frac{1}{2}(\sigma_v + \sigma_H)\left(1 + \frac{a^2}{r^2}\right) - \frac{1}{2}(\sigma_v - \sigma_H)\left(1 + \frac{3a^4}{r^4}\right)\cos 2\varphi - \frac{a^2}{r^2}P_b \tag{4.6}$$

$$\sigma_{yy} = \sigma_h - 2v(\sigma_v - \sigma_H)\frac{a^2}{r^2}\cos 2\varphi \tag{4.7}$$

$$\sigma_{r\theta} = \frac{1}{2}(\sigma_v - \sigma_H)\left(1 + \frac{2a^2}{r^2} - \frac{3a^4}{r^4}\right)\sin 2\varphi \tag{4.8}$$

Similarly, in case of strike-slip stress regime, if axial (longitudinal) fractures develop around the wellbore, it will be along σ_H direction (perpendicular to the least tangential stress, $\sigma_{\theta\theta}$, i.e. on the sides of the wellbore along x direction), as shown in Figure 4.3.

In both cases of normal and strike-slip stress regimes, the transverse fractures develop orthogonal to the wellbore axis, perpendicular to the y direction or against σ_{yy}. The conditions where either transverse or axial fractures are more favorable to initiate and propagate from the wellbore wall will be discussed later in this Chapter.

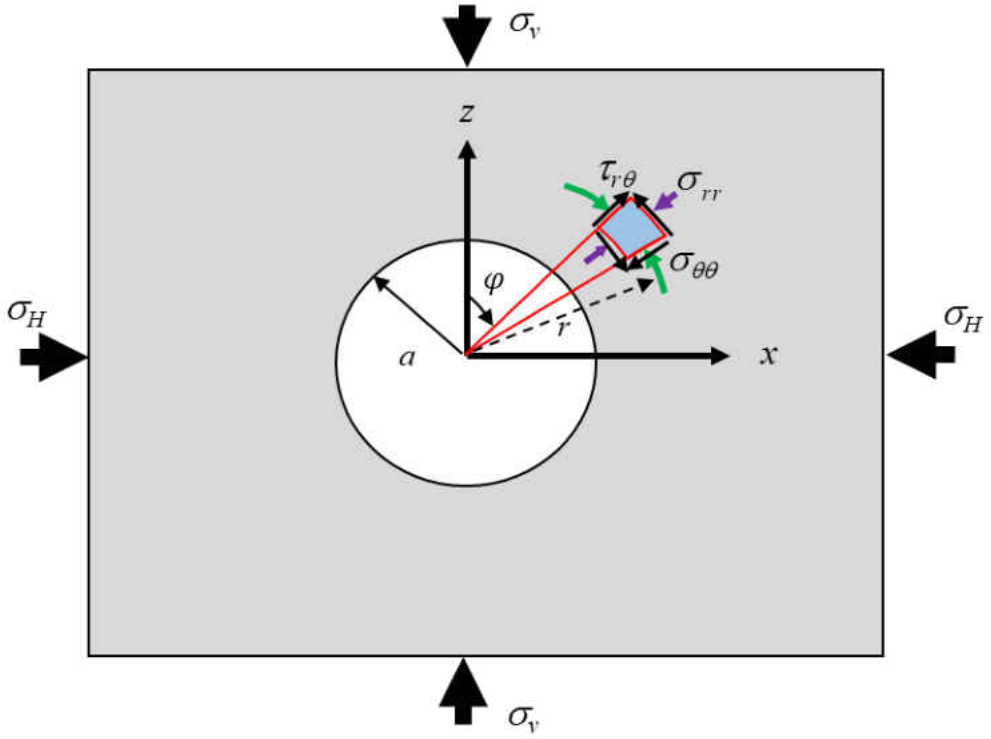

Figure 4.2: Plan view of a horizontal wellbore drilled parallel to σ_h direction with in-situ and drilling induced stresses.

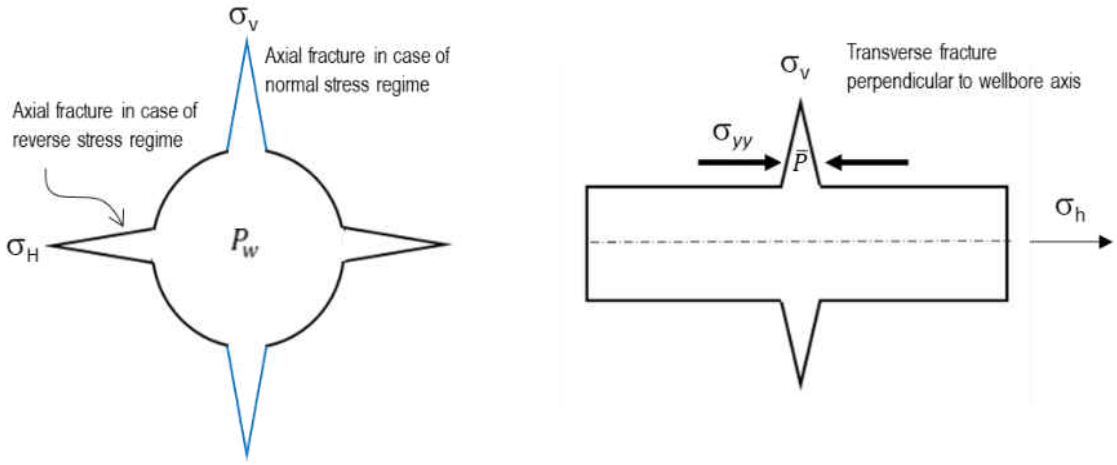

Figure 4.3: Axial (left) and transverse fractures (right) around a horizontal wellbore.

Figure 4.4 shows the plot of the vertical, radial and tangential stresses as a function of the distance from the wellbore wall. The input data are taken from Table 4.1 which corresponds to typical parameters of Bakken Shale formation in North Dakota, USA. We use this data throughout

this thesis for consistency purposes. From Table 4.1, it is seen that the magnitude of the stress anisotropy (i.e. σ_H-σ_h) is not significant, so in some examples in this Chapter we also use larger stress anisotropy to demonstrate the initiation pressure changes due to a large stress anisotropy.

Table 4.1: Bakken Shale Formation mechanical properties and in-situ stresses

Property		**Unit**	**Value**
Density	ρ	Kg/m^3	2650
Young's Modulus	E	GPa	30
		Mpsi	4.3511
Uniaxial Compressive Strength	UCS	MPa	50
		psi	7,251
Tensile Strength	To	MPa	5
		psi	725
Toughness	K_{IC}	Mpa.m^0.5	2.0
		psi.in^0.5	1820.1
Friction Angle	ϕ	degree	30
Poisson's ratio	v	-	0.25
Porosity	$\emptyset$	%	2
Permeability	K	Darcy	0.1
Minimum Horizontal Stress	σ_h	MPa	54.8
		psi	7950
Maximum Horizontal Stress	σ_H	MPa	61.6
		psi	8,930
Vertical Stress	σ_v	MPa	68.4
		psi	9,920
Pore Pressure	P_p	MPa	30
		psi	4,350
Wellbore Pressure	P_b	MPa	30
		psi	4,350
Fluid Viscosity	μ	Pa.s	0.002
Flow Rate	Q	m^3/s	0.08
		bbl/m	30
Borehole Radius	a	inch	4.375
		m	0.11

Figure 4.4 (left) shows the stresses corresponding to φ=0° or along the direction of σ_v (remember that φ is the angle from maximum stress direction, which in this case is σ_v), whereas Figure 4.4 (right) represents the stresses corresponding to φ =90°, or along σ_H direction.

From Figure 4.4, it is seen that the radial stress is minimum at the wellbore wall and is equivalent in all different directions around the wellbore but increases as moving away from the wellbore wall. It ultimately reaches the value of σ_v along φ=0° and σ_H along φ=90° at far distance from the wellbore, i.e. getting back to the far field stresses. This distance, appears to be approximately 4 times the radius of the wellbore. On the other hand, the tangential stresses ($\sigma_{\varphi\varphi}$) are maximum at the wellbore wall but they are different in different directions. It is the largest at φ=90° (parallel to σ_v direction) and the least along φ=0° (parallel to σ_H direction). The tangential stresses reduce as moving further away from the wellbore wall and at far distance they reach σ_H and σ_v along φ=0° and φ=90°, respectively.

It is interesting to note that based on this simplified model, the induced stresses are independent of the wellbore radius, while, in real field cases, as the size of the wellbore is increased, due to the higher potential for existence of the micro cracks and different type of defects around the wellbore the rock becomes less strong and the induced stresses around the wellbore will be different.

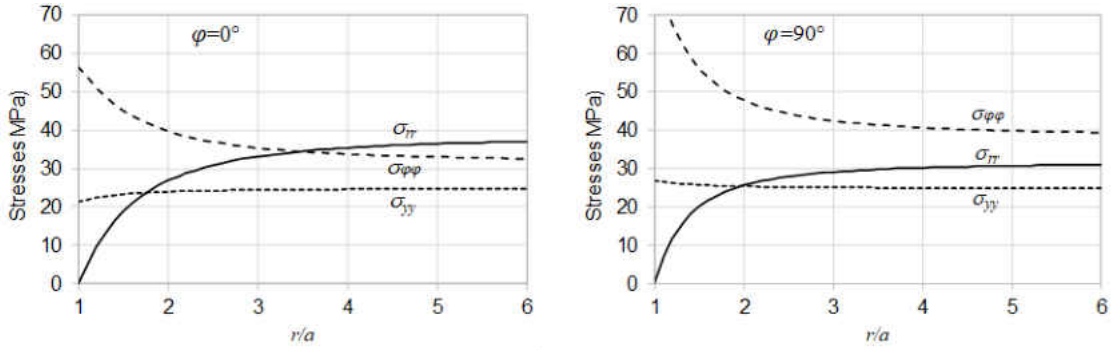

Figure 4.4: Distribution of drilling induced stresses around a horizontal wellbore drilled along $\boldsymbol{\sigma_h}$ direction based on Kirsch's equations.

One interesting case to consider is the distribution of stresses around the wellbore, i.e. replacing *r=a* in equations 4.5 to 4.8. In this case, the induced stresses around the wellbore wall will simplify to the followings:

$$\sigma_{rr} = P_b \tag{4.9}$$

$$\sigma_{\theta\theta} = (\sigma_v + \sigma_H) - 2(\sigma_v - \sigma_H)\cos 2\varphi - P_b \tag{4.10}$$

$$\sigma_{yy} = \sigma_h - 2v(\sigma_v - \sigma_H)\cos 2\varphi \tag{4.11}$$

$$\sigma_{r\theta} = 0 \tag{4.12}$$

The above equations indicate that around the wellbore the radial stress is the wellbore pressure (or mud pressure) and it is applying the same pressure in different directions. The shear stress is zero but the tangential stress is direction dependent. For the two directions along σ_v (i.e. $\varphi = 0°$) and σ_H (i.e. $\varphi = 90°$), equation 4.10 will be simplified as:

$$\varphi = 0° \Rightarrow \quad \sigma_{\theta\theta} = 3\sigma_H - \sigma_v - P_b \tag{4.13}$$

$$\varphi = 90° \Rightarrow \quad \sigma_{\theta\theta} = 3\sigma_v - \sigma_H - P_b \tag{4.14}$$

Equations 4.13 and 4.14 imply that the maximum tangential compression stress around the wellbore will occur along σ_H direction whereas along the σ_v direction, or in general, perpendicular to the least stress direction, the wellbore wall is under the minimum amount of compressional stress. From the point of view of this work, this means that the axial hydraulic fracture will initiate perpendicular to the σ_H direction, assuming adequate wellbore pressure is pumped.

Assuming $K = \frac{\sigma_H}{\sigma_v}$, equation 4.10 can be rewritten as:

$$\frac{\sigma_{\theta\theta}}{\sigma_v} = (1 + K) - 2(1 - K)\ \cos 2\varphi - \frac{P_b}{\sigma_v} \tag{4.15}$$

where,

$$\varphi = 0° \Rightarrow \quad \frac{\sigma_{\theta\theta}}{\sigma_v} = 3K - 1 - \frac{P_b}{\sigma_v} \tag{4.16}$$

$$\varphi = 90° \Rightarrow \frac{\sigma_{\theta\theta}}{\sigma_v} = 3 - K - \frac{P_b}{\sigma_v} \tag{4.17}$$

Figure 4.5 presents the plot of $\frac{\sigma_{\theta\theta}}{\sigma_v}$ versus K for two different directions of $\varphi = 0°$ and $\varphi = 90°$, respectively. It is seen that when stresses are isotropic around the wellbore (K=1.0) tangential stresses are as twice as σ_v, in all directions. For K=0, corresponding to the maximum stress anisotropy, the tangential stress is compressional and as big as three times the σ_v at $\varphi = 90°$, whereas it is tensional and equal to -σ_v at $\varphi = 0°$. This Figure also shows that for K<0.33, the tangential stresses become tensional along $\varphi = 0°$.

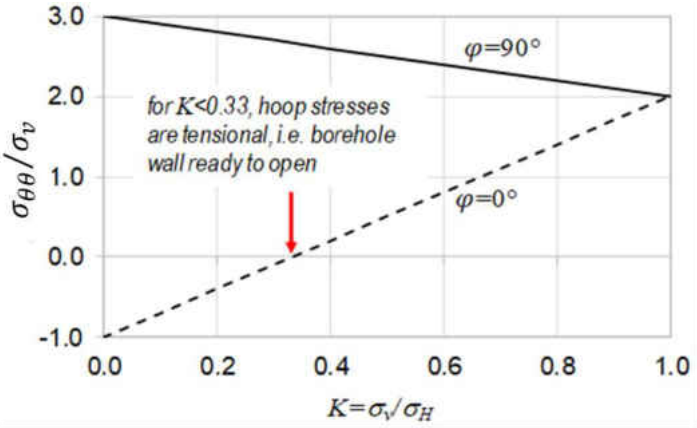

Figure 4.5: Variation of tangential stresses around the wellbore wall as a function of stress anisotropy.

To initiate hydraulic fracture, the fluid pressure inside the wellbore should overcome the tangential stress along $\varphi = 0°$ plus the tensile strength (T_0) of the formation. The tensile strength of the rocks is commonly considered as 10% of the Uniaxial Compressive Strength (UCS). The fracture breakdown pressure, or critical borehole pressure is expressed as (Detournay and Carbonell, 1997):

$$P_c = 3\sigma_H - \sigma_v + T_0 - P_p \tag{4.18}$$

The above equation is known as Hubbert-Willis (H-W) expression, which is applicable to impermeable rocks. Later on, it will be discussed that this equation corresponds to the fast pressurization into a wellbore with an infinitely small length crack edging from the wellbore wall.

In this situation the wellbore fluid cannot penetrate into the crack, hence its pressure will be equivalent to the pore pressure.

Considering permeable rock, the above equation is modified as the Haimson-Fairhurst (H-F) expression (Detournay and Carbonell, 1997):

$$P_c = \frac{3\sigma_H - \sigma_v + T_0 - 2\eta P_p}{2(1-\eta)} \tag{4.19}$$

In the above equation, η is a poro-elastic constant varying between 0 and 0.5 and this constant controls the stress induced by the pore fluids.

One paradox coming from equations 4.18 and 4.19 is that if we replace $\eta = 0$ (i.e. ignoring the fluid pressure effect in the pores, or considering a dry rock) in equation 4.19, it leads to:

$$P_c = \frac{1}{2}(3\sigma_H - \sigma_v + T_0), \tag{4.20}$$

instead of converging to equation 4.18 for an impermeable rock. This means that the breakdown pressure based on H-F criterion could be as low as half the H-W value. It will be discussed later that this equation corresponds to slow pressurization into a wellbore with infinitely small crack edging from the wellbore wall. In this case, the crack pressure is equal to wellbore pressure, hence pore pressure does not have any contribution to the total critical pressure P_c.

Another discrepancy related to the above breakdown pressures is the fact that these pressures correspond to the peak of pressure-time curve, however, based on the non-linearity that is observed before the peak point, it appears that the fracture initiates before reaching to this peak point. So, it is important to distinguish between fracture initiation and breakdown pressures (Detournay and Carbonell, 1997).

In the next section, it will be discussed that in real field cases, there are always defects such as natural fractures around the wellbore which act as the initiation point for hydraulic fracture, so

the initiation and propagation of an induced fracture should be considered based on the fracture mechanics, which is different that the classic mechanics explained above for the hydraulic fracture.

The above information provides some insight into how the stresses are distributed around the wellbore after drilling, however, in practice, cares should be taken when using these equations as they are based on the assumption of isotropic and elastic rocks, which are not observed in real field applications.

4.3 Axial Crack Edging from a Horizontal Wellbore

In this section the theoretical model proposed by Rummel (1987) based on the superposition of the stress intensity factors of different parameters affecting the initiation pressure of a borehole with a bi-wing axial crack is presented.

Figure 4.6 depicts the same circular borehole shown in Figure 4.2 with an addition of a crack with half-length *c* on each side of the wellbore. The borehole is assumed to be in an infinite plate. Normal stress regime is assumed. To simplify the problem, we assume that the crack is perpendicular to σ_H direction, i.e. along $\varphi = 0°$. This is perpendicular to the least resistant stress direction and most favorable direction for the fracture to open comparing to all other directions. The borehole is pressurized and the fluid can penetrate into the crack. In this section, we adopt the approach presented by Rummel (1987) to estimate the critical borehole pressure at unstable crack extension.

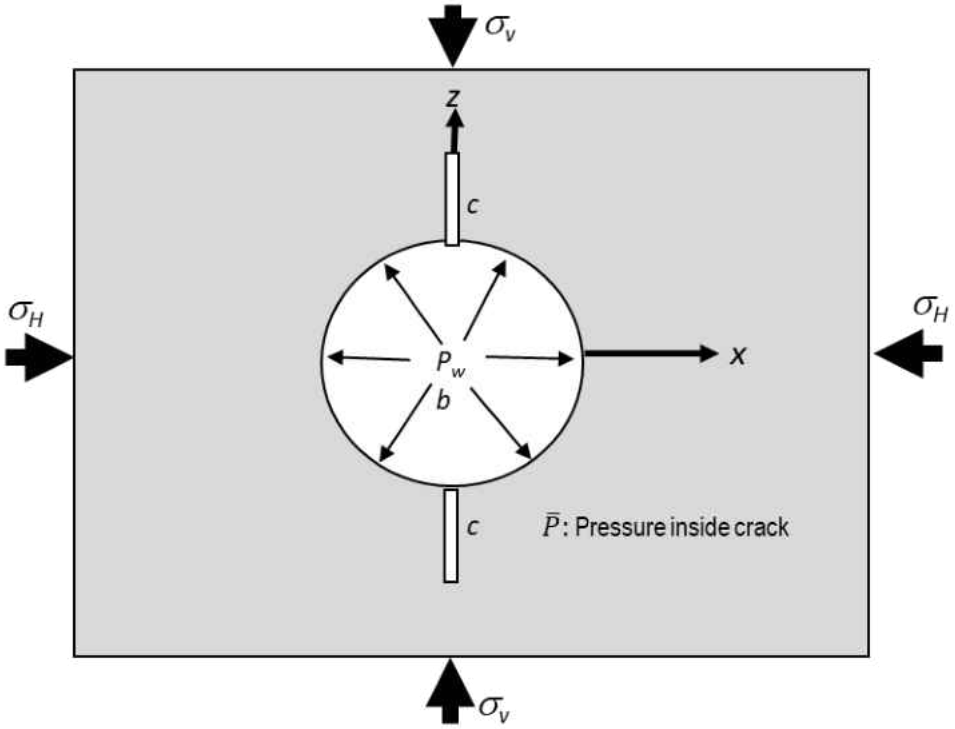

Figure 4.6: Fracture mechanics model for crack growth in a pressurized circular borehole.

The intensity of the stress field in the vicinity of the crack tips can be formulated based on the principle of superposition of stress intensity factors (K_I) from each loading source:

$$K_I(\sigma_v,\ \sigma_H,\ P_b, \bar{P}) = K_I(\sigma_v) + K_I(\sigma_H) + K_I(P_b) + K_I(\bar{P}) \tag{4.21}$$

Rummel (1987) formulated the values of each of the above intensity factors as:

$$K_I(\sigma_v) = -\sigma_v\sqrt{a}f(b) \tag{4.22}$$

$$K_I(\sigma_H) = -\sigma_H\sqrt{a}g(b) \tag{4.23}$$

$$K_I(P_b) = P_b\sqrt{a}\ h_b(b) \tag{4.24}$$

$$K_I(\bar{P}) = \bar{P}\sqrt{a}\ h_c(b) \tag{4.25}$$

where,

$$b = 1 + \frac{c}{a} \tag{4.26}$$

$$f(b) = -2\sqrt{\frac{(b^2-1)}{\pi b^7}} \tag{4.27}$$

$$g(b) = \sqrt{\pi b}\left(1 - \frac{2}{\pi}\sin^{-1}\frac{1}{b}\right) + 2(b^2+1)\sqrt{\frac{(b^2-1)}{\pi b^7}} \tag{4.28}$$

$$h_b(b) = 1.3\frac{b-1}{1+b^{3/2}} + 7.8\frac{[\sin(b-1)/2]}{2b^{5/2}-1.7} \tag{4.29}$$

h_c is defined based on the assumption of pressure distribution in the crack. For example, for constant pressure inside the crack:

$$\bar{P}(x) = \bar{P} \tag{4.30}$$

$$h_{c1} = \sqrt{\pi b}\left(1 - \frac{2}{\pi}\sin^{-1}\frac{1}{b}\right) \tag{4.31}$$

Figure 4.7 shows the plot of functions $f(b)$, $g(b)$, h_b, h_c (for constant pressure case) versus b (crack size normalized by borehole radius).

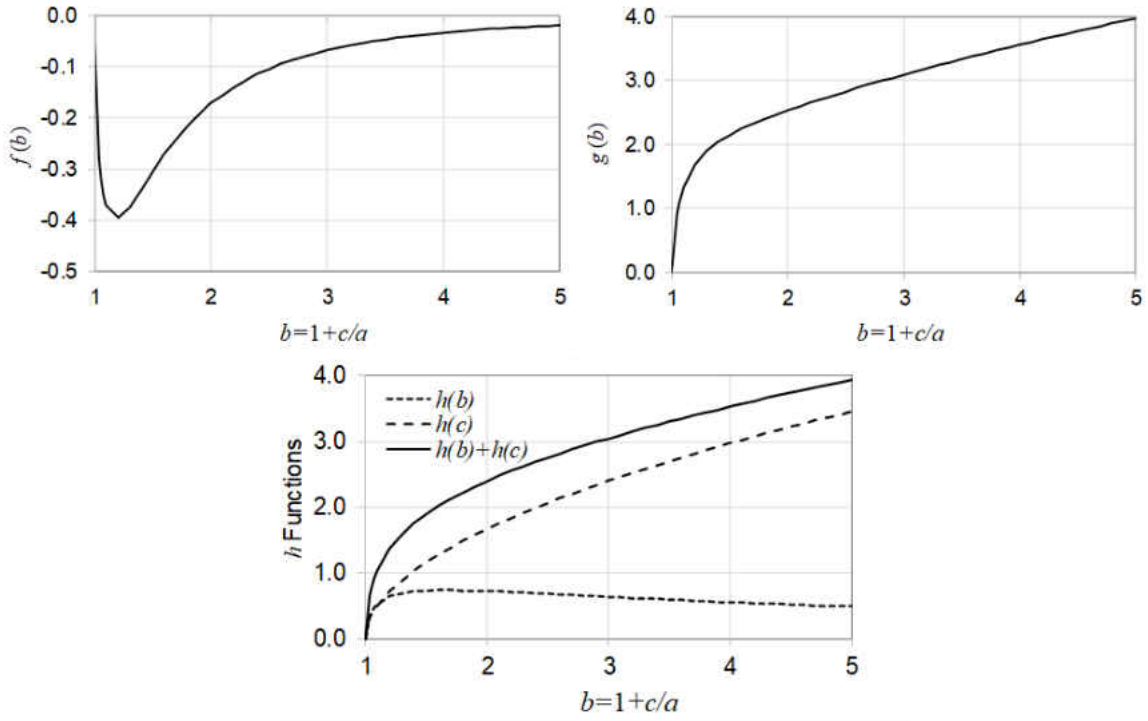

Figure 4.7: Functions $f(b)$, $g(b)$, h_b, h_c (for constant pressure case) versus b.

The critical borehole pressure at unstable crack extension is defined according to the superposition of the stress intensity functions. This, considering the three intensity factors associated with σ_v, σ_H and P_b will be expressed as:

$$P_c = \frac{1}{h_b+h_c}\left(\frac{K_{IC}}{\sqrt{a}} + \sigma_v f + \sigma_H g\right) \tag{4.32}$$

In the above equation, K_{IC} is the rock's fracture toughness for model I crack growth (opening mode).

Comparing the first term in the above equation:

$$P_\infty = \frac{1}{h_b+h_c}\left(\frac{K_{IC}}{\sqrt{a}}\right) \tag{4.33}$$

with classical fracture mechanics equation 4.18, it suggests that P_∞ represents the hydraulic fracturing tensile strength of the rock measured under zero far field stresses. It is also known as cohesive stress. It is evident that P_∞ is a function of the wellbore size (a), i.e. it is scale dependent, a property that is not captured in classical fracture mechanics.

In case of crack length becoming very short, b=1, f=0, g=0, h_b=0, h_c=0, hence to open the crack at the borehole wall, the wellbore pressure must exceed the value of P_∞, which in this case tends to infinity (see equation 4.32). This indicates why opening a fracture in lab experimental set up where the drilled borehole is free of any noticeable defects may not be possible without creating a notch. Similarly, this also justifies the reason for development of axial (longitudinal) fractures in horizontal wellbores when there are no effective natural fractures around the wellbore. This is the core idea of this project, where cutting cracks (notches) around the open hole section of the horizontal wellbores are proposed to act as the fracture initiation points. Design of the size and geometry of these notches and the impact of injecting fluid characteristics on the effectiveness of the notch will be discussed in details through numerical simulations with reference to the lab experimental data in the next Chapter.

From equation 4.32 the fracture coefficients associated with σ_v, σ_H and $P_b = P_\infty$ can be defined as:

$$k_{\sigma_v} = \frac{f}{h_b+h_c} \qquad k_{\sigma_H} = \frac{g}{h_b+h_c} \qquad k_{\infty} = \frac{1}{h_b+h_c} \tag{4.34}$$

And the pressures corresponding to each of these loading source can be calculated as:

$$P_{c(\sigma_v)} = k_{\sigma_v}\sigma_v \qquad P_{c(\sigma_H)} = k_{\sigma_H}\sigma_H \qquad P_{c(\infty)} = k_{\infty}\frac{K_{IC}}{\sqrt{a}} \tag{4.35}$$

Here, K_{IC} is the toughness of the formation.

The above coefficients determine the contribution of each of the far field stresses as well as the cohesive force on hydraulic fracture breakdown pressure.

Using Bakken data from Table 4.1, the intensity factors and critical pressures corresponding to different loading sources were calculated and the results are presented in Figure 4.8. It is to be noted that these results correspond to $\varphi = 0°$, i.e. along σ_v direction, which is the most favorable direction for fracture initiation and propagation. From this Figure, it is observed that as the crack size is increased the impact of the $K_{I(\sigma v)}$ is reduced while $K_{I(\sigma H)}$ is increased to some extent and then reduces. In terms of critical pressures, it is seen that at very small crack size (i.e. b tends to unity) σ_v has the largest contribution, which is due to the fact that the crack is primarily under the compression by this induced stress component. However, as the crack size becomes larger, the effect of σ_H becomes greater while σ_v presents less contribution to the total borehole pressure at crack extension. It is also interesting to see that the borehole pressure P_b or P_∞ presents a large increase when the crack size reduces and tends to zero. This, in fact, indicates the large borehole pressure required to open the wellbore wall in absence of any crack and indeed, the necessity for cutting a notch in order to assist the fracture propagation in lab experiments. Therefore, as Figure 4.8 (bottom) shows, the total borehole pressure at unstable crack extension is extremely large in absence of crack, however, it experiences a sharp drop as soon as the crack is introduced to the wellbore wall and then increased to some extent before it plateaus. From Figure 4.8, unstable crack

growth (i.e. critical pressure reduces as crack length increases) is observed for crack lengths of less than 10% of wellbore radius (i.e. c=0.1a or b=1.1). The critical pressure then increases but reaches a plateau for crack lengths of larger than wellbore diameter (i.e. c=2a or b=3). While lower critical pressures associate with smaller crack sizes than wellbore diameter, in practice, the small crack length may not be sufficiently long to bypass the disturbed stress zone around the wellbore due to the drilling operation, hence, they do not present an effective entry to propagate the fracture. This is a key point in the design of the notch geometry for OH hydraulic fracturing design that will be considered in the next Chapter.

It is also to be noted that in the current discussion, the impact of pressurization rate (i.e. the product of viscosity of the injecting fluid and flow rate) is not taken into consideration on fracture breakdown pressure. This effect will be discussed in detail in the next Section.

Figure 4.9 presents the fracture coefficients corresponding to maximum and minimum horizontal stresses. Similar to the conclusions obtained from Figure 4.8, it is seen that the impact of σ_v reduces and σ_H increases, respectively as the crack size increases and these coefficients plateau for crack sizes larger than wellbore diameter (i.e. b>3). The interesting point is that these coefficients converge to the values of 3 and -1, respectively, in absence of crack (i.e. stress concentration around a borehole without a crack), which is presented by classical fracture mechanics (see equation 4.13). Also, from Figure 4.9 it is seen that as crack size becomes very small, hydraulic fracturing tensile strength tends to a very large number needing high pressure to open the rock around the wellbore.

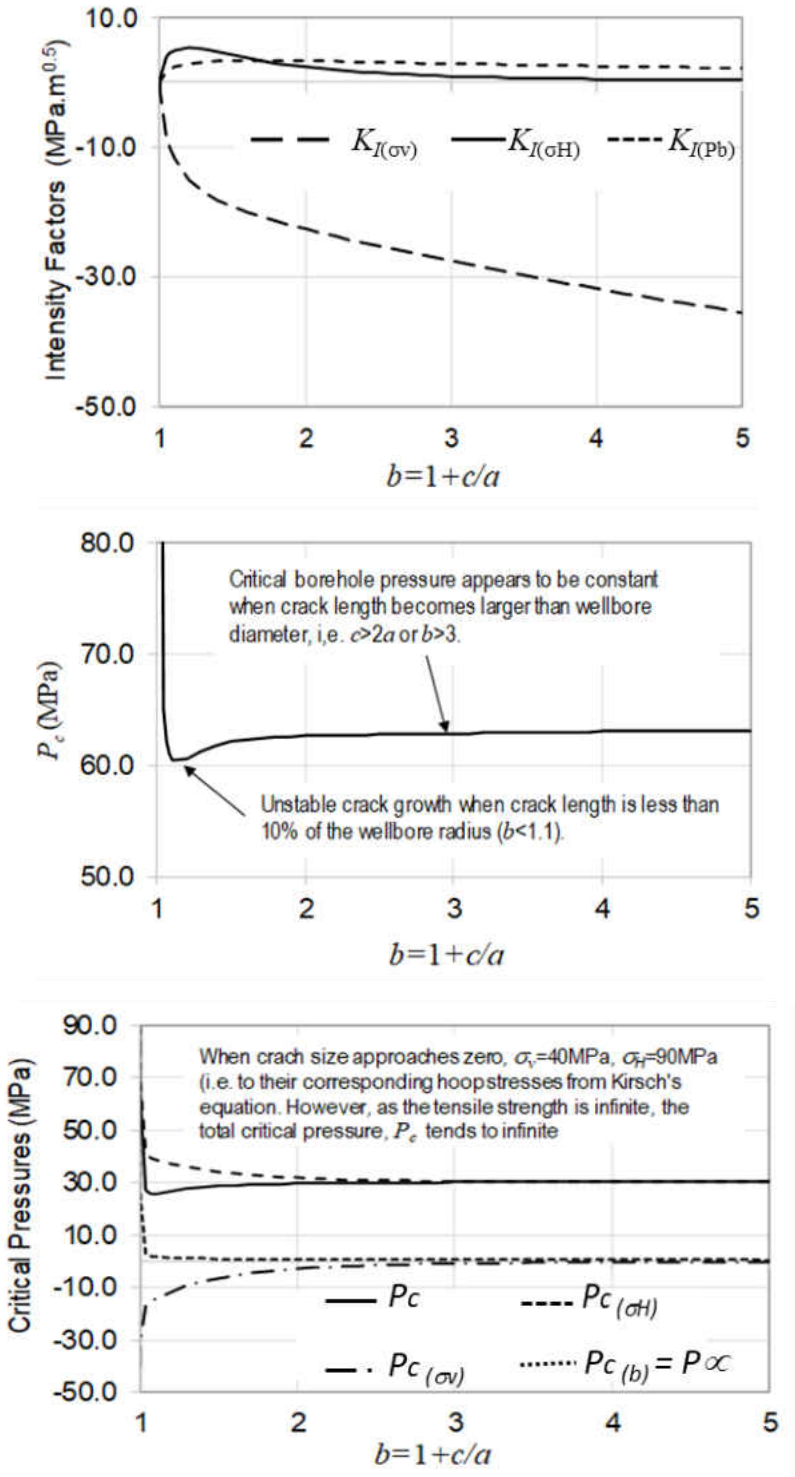

Figure 4.8: Intensity factors (top) and borehole pressures (middle) at unstable crack extension values for different loading sources as a function of crack length at the wellbore wall. The bottom figure shows the total pressure, P_c.

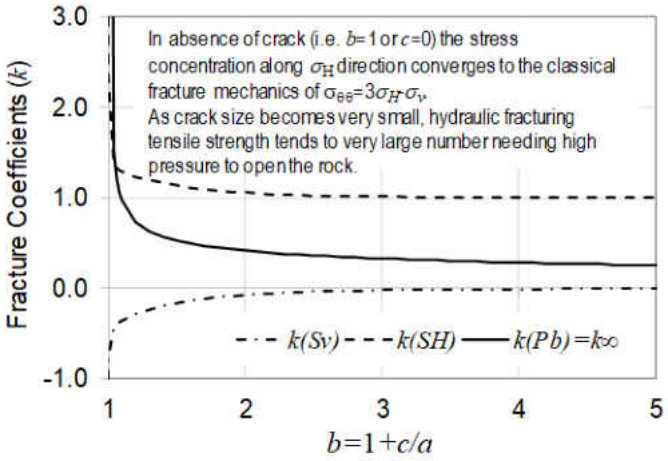

Figure 4.9: Fracture coefficients corresponding to different loading sources.

Figure 4.10 shows the results of hydraulic fracturing tensile strength (see equation 4.33) as a function of wellbore radius (a) and the crack size. As mentioned before, P_∞ is scale dependent and as the results of Figure 4.10 shows, it reduces as wellbore size becomes larger. Again, it appears that this impact is less pronounced for crack sizes larger than wellbore diameter. However, in absence of crack, theoretically, a very large amount of pressure is needed to open the wellbore wall in tension, similar to the conclusions made from Figure 4.9. This result is in good agreement with hydraulic fracturing lab experiments where the drilled borehole is free of any defects and without cutting a notch it is not possible to initiate hydraulic fracture.

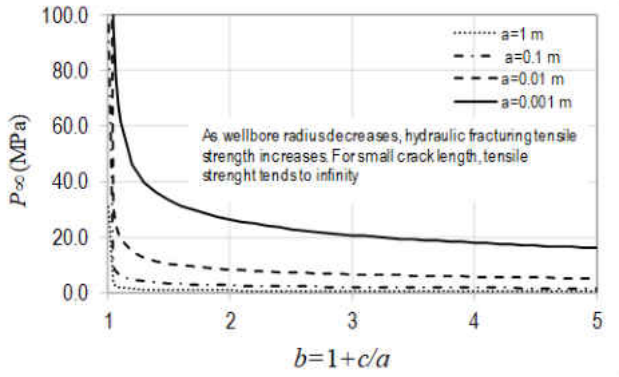

Figure 4.10: Hydraulic fracturing tensile strength as a function of wellbore size.

4.4 Wellbore Pressurization Rate

The discussion presented in the previous sections did not consider the effect of the pressurization rate on breakdown pressure. Pressurization rate is the product of injecting fluid viscosity and flow rate (μQ). It is important to understand the impact of this parameter on hydraulic fracturing breakdown pressure, as in field applications, the viscosity and the flow rate are the only controllable design parameters. Also, in the lab experiments, in order to run hydraulic fracturing tests comparable to field scales, as will be discussed in Section 4.5, much smaller fluid viscosity should be injected at very low pumping rate. As it is evident, the pressurization rate is an important parameter in operation of hydraulic fracturing tests.

As the objective of this study is to investigate the impact of pre-existing crack or notch on fracture initiation and propagation, we consider the wellbore geometry shown in Figure 4.6 with an axial crack length of c edging at a wellbore with radius a. Here, in addition to the wellbore pressure (P_b) and the average pressure in the crack ($\bar{P}$), we include the pore pressure (P_p) effect, due to the fluid pressure inside the pores, or also known as the reservoir pressure.

Before increasing pressure inside the wellbore, it can be assumed that the average crack pressure is the same as pore pressure. If pressure increases in the wellbore slowly (i.e. pseudo-static injection rate), the pressure drop in the crack can be ignored and the crack pressure continuously remains equal to the wellbore pressure. This is known as slow pressurization rate. On the other hand, if the pressurization rate is infinitely high, the pressure drop in the crack becomes infinite, and during the initiation process, the crack pressure is equal to the reservoir pressure (Charlez, 1997).

Pressurization rate can be formulated as dimensionless parameter (f):

$$f = \frac{\bar{P} - P_p}{P_b - P_p} \tag{4.36}$$

For high pressurization rates, f=0 whereas f=1 for low pressurization rates. At equilibrium (i.e. when K_I=K_{Ic}), the pressure required to propagate an existing crack at the wellbore wall will be:

$$P_c\left[\frac{c}{a},f\right]=\alpha_1\left(\frac{c}{a},f\right)\frac{K_{IC}}{\sqrt{a}}+\alpha_2\left(\frac{c}{a},f\right)\frac{\sigma_v+\sigma_H}{2}-\alpha_3\left(\frac{c}{a},f\right)\frac{\sigma_v-\sigma_H}{2}-\alpha_4\left(\frac{c}{a},f\right)P_p \tag{4.37}$$

In the above equation, coefficients α_1, α_2, α_3 and α_4 are functions of both crack length (c/a) and the pressurization rate (f). These functions define the contribution of four independent terms on fracture breakdown pressure: the material toughness (α_1), the average and deviatoric parts of the geostatic stress tensor (α_2 and α_3, respectively), and the pore pressure (α_4). This equation shows that the rock toughness and average of stresses increase the critical pressure to propagate a crack, whereas, the deviatoric stress and pore pressure have a negative impact. Detournay & Carbonell (1997) provided solutions for these functions. Figure 4.11 shows the change of these dimensionless functions with respect to the crack length for the two cases of fast (f=0) and slow (f=1) pressurization rates, respectively.

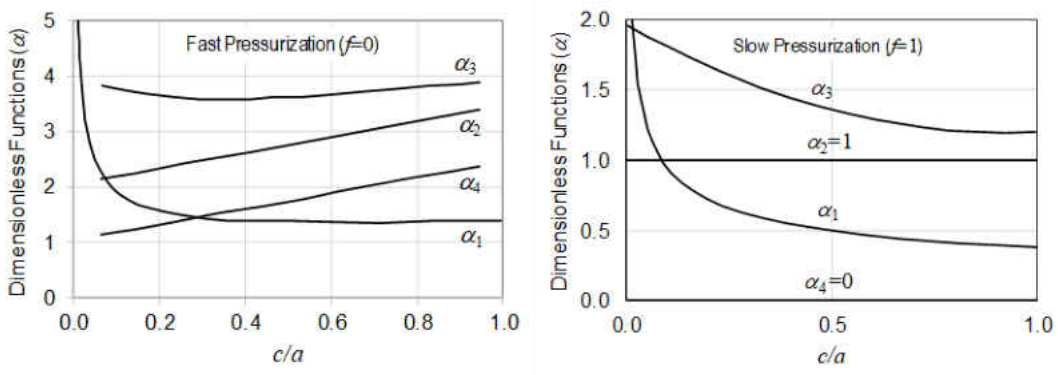

Figure 4.11: Dimensionless functions for the case of rapid (left) and slow (right) pressurization rates (after Charlez, 1997).

For the case of very small crack length (i.e. $c \to 0$), Detournay & Carbonell (1997) showed that the critical pressure will tends to the following asymptotic expression:

$$P_c\left[\frac{c}{a},f\right]=\frac{1}{1+f}\frac{K_{IC}}{2\sqrt{a}}+\frac{2}{1+f}\frac{\sigma_v+\sigma_H}{2}-\frac{4}{1+f}\frac{\sigma_v-\sigma_H}{2}-\frac{1-f}{1+f}P_p \tag{4.38}$$

Replacing f=0 in the above equation, it reduces to:

$$P_c\left[\frac{c}{a},0\right]=\frac{K_{IC}}{2\sqrt{a}}+3\sigma_H-\sigma_v-P_p \tag{4.39}$$

Comparing this equation with equation 4.14 it is seen that in case of rapid pressurization rate, it recovers the H-W expression.

In case of slow pressurization (f=1), equation 4.38 will reduce to:

$$P_c\left[\frac{c}{a},1\right]=\frac{1}{2}\left[\frac{K_{IC}}{2\sqrt{a}}+3\sigma_H-\sigma_v\right] \tag{4.40}$$

which recovers equation 4.15, i.e. Haimson-Fairhurst (H-F) expression, assuming a dry rock.

Comparing the above equations with equations 4.32 and 4.33 for the case of negligible crack length, it appears that in this model, the critical pressure approaches the value of $\frac{K_{IC}}{2\sqrt{a}}$ whereas in the previous model, it approaches an infinite number (cohesive stress or hydraulic fracture tensile strength of the rock). This may be more representative of field and lab situation as in case of very small crack length, opening the wellbore requires a very high amount of pressure.

Figure 4.12 presents the critical wellbore pressure calculated using equation 4.37. The results are presented for two cases of slow and fast pressurization and assuming isotropic and anisotropic horizontal stresses. Here, for consistency purposes, we use the same input parameters of Table 4.1, however, as the horizontal stress anisotropy is relatively small for Bakken data, in addition to the original values we consider another case where we use the values of σ_H=61.6 MPa and σ_h=30.0 MPa for demonstration purposes. For isotropic case we consider σ_H=σ_h=60MPa.

The results of Figure 4.12 (top) shows that for slow pressurization (f=1), and anisotropic stress case, the crack is unstable for very small crack sizes of less than about 10% of the wellbore radius and then becomes stable until it starts to become unstable again when propagates several radius of the wellbore. In contrary, in isotropic case, the crack is unstable for all crack lengths, i.e. the pressure to propagate crack is reducing as crack length becomes larger. This result was

expected from Figure 4.11 (right) for the case of slow pressurization, where for the isotropic case, in addition to α_4=0, we have α_3=0. As α_2=1 for different crack lengths but α_1 shows a rapid reduction when crack length increases, the combined effect of α_1 and α_2 is expected to always show a declining trend. This means that in this case the rock toughness is the main factor controlling the propagation pressure of the crack and the larger the crack length, the lower the required pressure will be. Also, as expected, the critical borehole pressure to propagate the crack is much larger for isotropic than anisotropic stresses. In this Figure, the two dashed horizontal lines represent the Haimson-Fairhurst (H-F) expressions for the case of very small crack length in presence of isotropic and anisotropic stresses.

Figure 4.12 (bottom) represents the same results for fast pressurization (f=0). It is seen that in this case, for both isotropic and anisotropic stresses, the crack is unstable when its length is less than about 10% of the wellbore radius, and then becomes stable. It is also noted that he critical borehole pressure to open the crack is much larger in case of fast pressurization than that of slow pressurization. Also, the change of pore pressure has no impact on critical pressure in case of fast pressurization.

The above results provide a great knowledge regarding the effect of pressurization rate on fracture propagation pressure and how the flow rate and viscosity in hydraulic fracturing operations may be adjusted to optimize the design parameters. It is important to understand the assumptions integrated in deriving these analytical solutions and therefore their limits of use and shortcomings. In Chapter 5 we present the simulation results and compare with these analytical solutions.

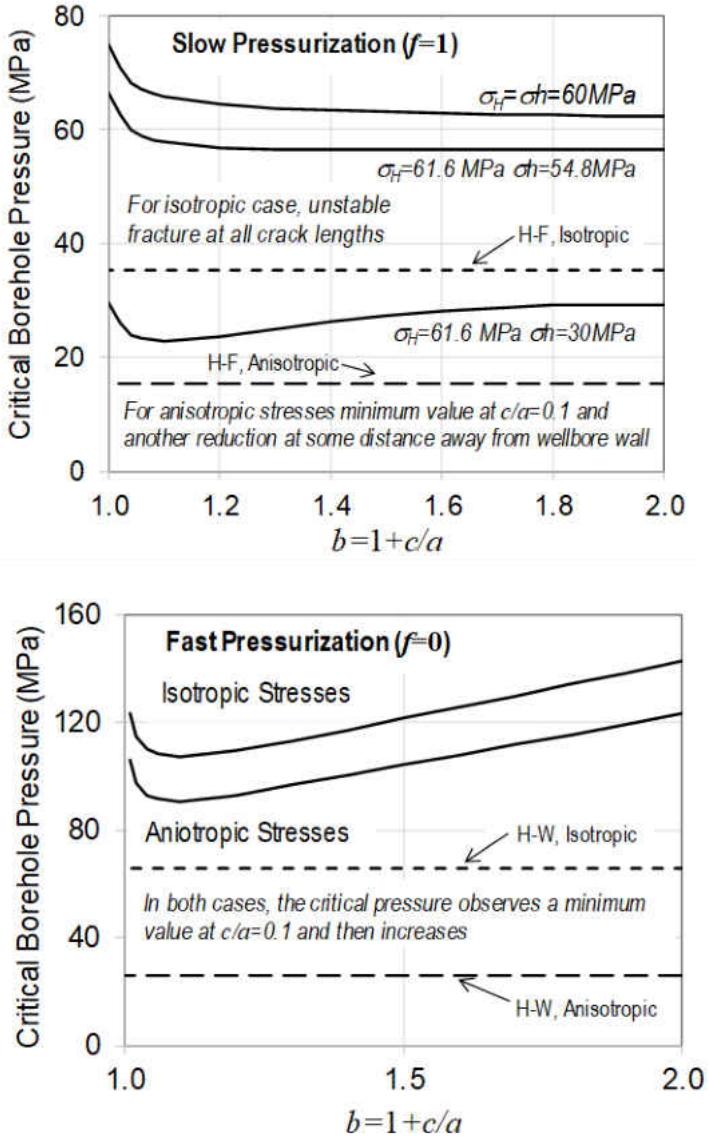

Figure 4.12: Critical borehole pressures calculated for the fast and slow pressurization in case of isotropic and anisotropic horizontal stresses.

4.5 Longitudinal versus Transverse Fractures

In this Section the analytical models of Nilson and Proffer (1984) are presented. In their model, the effect of the notch geometry and type of fracture that is likely to open in a borehole with notch are integrated. The model is presented first for the case of a bi-wing crack and then its extension to multiple crack (also called star crack) is discussed using Bakken data.

4.5.1 Bi-Wing Crack

According to Nilson and Proffer (1984), the strength of the tensile stress singularity at the tip of a fracture emanating from a hole in an infinite elastic medium can be calculated from:

$$K = \frac{2}{\sqrt{\pi}}\sqrt{L}\int_0^L (P-\sigma) f\left(\frac{x}{L},\frac{L}{a}\right)\frac{dx}{\sqrt{L^2-x^2}} \tag{4.41}$$

Also, the width of the fracture (twice the opening displacement) can be estimated as:

$$w(x) = \frac{4}{\pi}\frac{(1-v)}{G}\int_x^L \left(\int_0^a (P-\sigma) f\left(\frac{\xi}{a},\frac{a}{R}\right)\frac{d\xi}{\sqrt{a^2-\xi^2}}\right) f\left(\frac{x}{a},\frac{a}{R}\right)\left(\frac{a+R}{x+R}\right)^n \frac{ada}{\sqrt{a^2-x^2}} \tag{4.42}$$

In the above equation, K is the mode 1 stress intensity factor, L is the length of the fracture, a is the radius of the hole, x is the position variable along the fracture, $P(x)$ is the internal pressure within the fracture, and $\sigma(x)$ is external confining stress acting normal to the fracture plane, therefore, P-$\sigma(x)$ is the net pressure.

It is to be noted that the proposed models here, and also in the previous Sections, are 2D models where, in case of an axial fracture, the base of the fracture (fracture depth), i.e. its length along the wellbore axis (L_a) is consider unit. This represents a plane strain solution. Incorporating the impact of the fracture depth, into these calculations requires development of 3D models, which is not the intention in this work. However, we discuss this in the next Chapter when presenting the numerical simulation results.

The internal pressure $P(x)$ depends on the pressurization type. In case of slow pressurization, where there is enough time for the fluid to penetrate into the crack, the internal crack pressure is equal to the wellbore pressure. However, in case of fast pressurization, as it was mentioned before, the fluid cannot enter the crack, hence the internal pressure is equal to the pore pressure. The discussions presented in this section is with regards to the slow pressurization rate. In case of fast

pressurization limit, the fracture initiation pressure is infinite for the case of transverse fracture and it is higher than slow pressurization limit (up to a factor of two) for axial fracture as noted by Detournay and Carbonell (1997) We present in the next Chapter some simulation results corresponding to these cases for comparison purposes.

The configuration or weight function f is dependent on geometry and can be expressed as a combined effect of radial divergence (f_{rad}) and stress free (uniformly pressurized) notch surface (f_{notch}):

$$f = f_{rad}\, f_{notch} = \left(\frac{x/L+a/L}{1+a/L}\right)^{n}\left[1 + 0.3\left(1-\frac{x}{L}\right)\left(\frac{1}{1+L/a}\right)^{2m}\right] \tag{4.43}$$

In the above equation, m=2 for a cylindrical cavity, which is the geometry of the borehole in this study, and m=3 for spherical cavity. In planar problem, corresponding to an axial fracture in the case of a horizontal wellbore that we analysed earlier (see Figure 4.3), n=0, whereas n=1 in case of axisymmetric problems, corresponding to transverse fracture shown in Figure 4.3.

For transverse fractures (n=1), f_{rad} can be rewritten as a linear function in form of:

$$f_{rad} = \left(\frac{1}{1+a/L}\right)\frac{x}{L} + \left(\frac{a/L}{1+a/L}\right) \tag{4.44}$$

where $\frac{1}{1+a/L}$ is the slope and $\frac{a/L}{1+a/L}$ is the intercept of the linear function, respectively. It is seen that the slope and the intercept of f_{rad} are positive.

Similarly, f_{notch} can be written as a linear function in form of:

$$f_{notch} = -0.3\left(\frac{1}{1+L/a}\right)^{4}\frac{x}{L} + 1 + 0.3\left(\frac{1}{1+L/a}\right)^{4} \tag{4.45}$$

where $-0.3\left(\frac{1}{1+L/a}\right)^{4}$ and $1 + 0.3\left(\frac{1}{1+L/a}\right)^{4}$ are the slope and intercept of the linear function, respectively. The slope and intercept of this function are positive.

Figure 4.13 shows the change of f_{rad}, f_{notch} and the weight function *f* with respect to $\frac{x}{L}$ for axial and transverse cracks, noting that for the axial crack $f_{rad} = 1$ regardless of the crack size and location along the crack. From this Figure and the above equations, the following conclusions can be made:

- When $L/a \ll 1$, i.e. the crack size is very small compared to the borehole radius:

$$f_{rad} \to 1 \tag{4.46}$$

$$f_{notch} \to 1 + 0.3\left(1 - \frac{x}{L}\right) \tag{4.47}$$

In this case, the radial divergence effect is similar for both axial and transverse fracture.

- When $L/a \gg 1$, i.e. the crack length is very large compared to borehole radius:

$$f_{rad} \to \frac{x}{L} \tag{4.48}$$

$$f_{notch} \to 1 \tag{4.49}$$

  In this case, the notch effect is the same for both axial and transverse cracks while the radial convergence effect is dominating the weight function.

- For axial fractures, regardless of the L/a ratio, $f_{rad} = 1$, so $f = f_{notch}$, i.e. the notch effect is only affecting the weight function and this becomes the same when reaching the tip of the crack (*f*=1 when L/a approaches unity). The notch effect is the same for both axial and transverse fracture when the cavity geometry is similar.

- For transverse fractures, f_{rad} is increases for all values of $\frac{x}{L}$. However, as f_{notch} has a decreasing trend for all ratios of $\frac{x}{L}$, therefore the weight function *f* experiences a change of slope at $\frac{L}{a} = 0.164$. It is declining for $\frac{L}{a} < 0.164$ while its trend becomes increasing when $\frac{L}{a} > 0.164$. This value is the change of the slope of the *f* versus x/L plot, which can be expressed mathematically as:

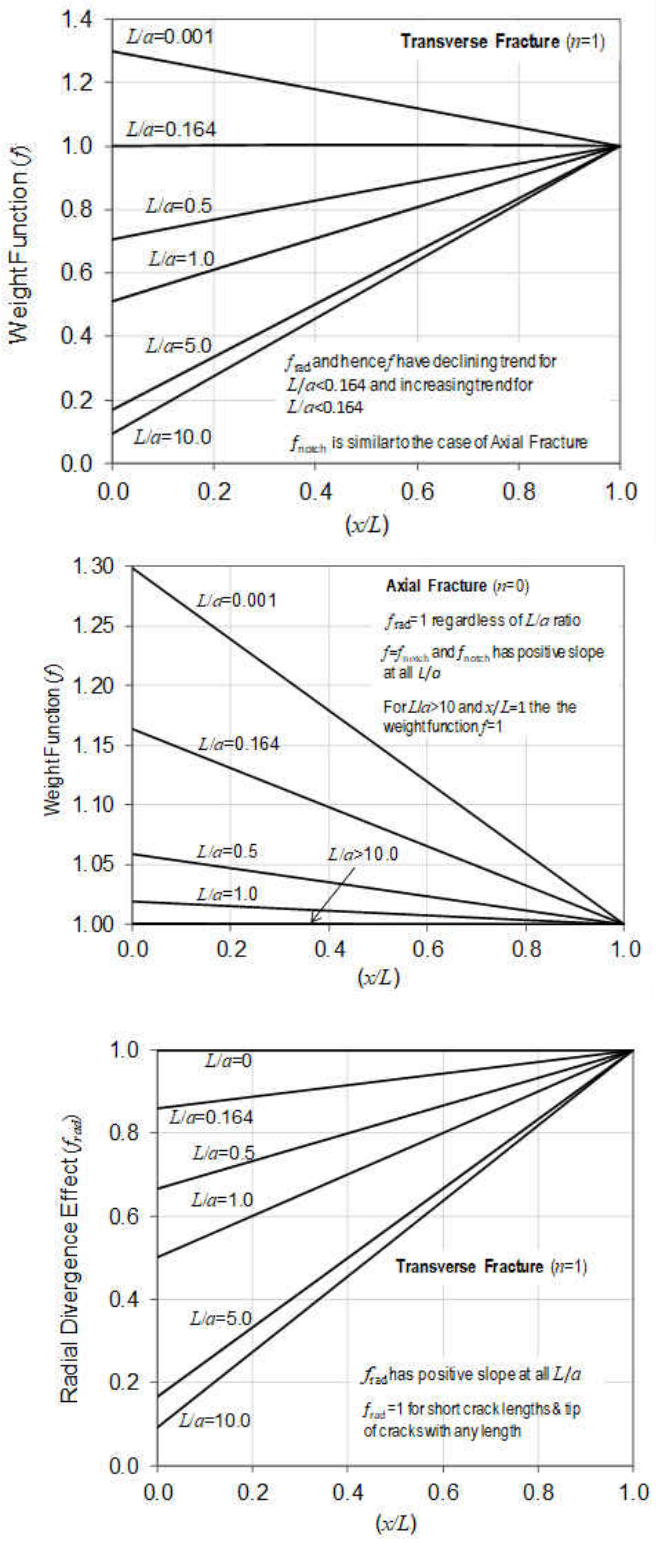

Figure 4.13: Change of the weight function *f* with respect to $\frac{x}{L}$ for axial and transverse cracks.

$$\frac{\partial}{\partial(L/a)}\left[\frac{\partial f}{\partial(x/L)}=0\right]=0 \tag{4.50}$$

The result of the above function is $\frac{L}{a}=0.164$.

We used data from Bakken formation shown in Table 4.1 and calculated the scaled initiation pressure ($\frac{P_f}{P^*}$) for bi-wing notch with different sizes for both axial and transverse fractures along the most favourable directions. The characteristic pressure is defined as (Lecampion et al., 2013):

$$P^*=\frac{\sqrt{32\pi}K_{IC}}{\sqrt{a}} \tag{4.51}$$

where K_{IC} is the mode I of rock fracture toughness. Figure 4.14 shows the results for 4 different cases below:

Case 1: σ_V=68.48 MPa > σ_H=61.58 MPa > σ_h=54.82 MPa

This is the stress values of Bakken formation, a normal stress regime with low horizontal stress anisotropy. The curves corresponding to the transverse and axial fractures cross over at approximately *L/a*=0.2. This means that for cracks or notches larger than this ratio transverse fracture will be dominated and more likely to occur.

Case 2: σ_V= σ_H =60.0MPa > σ_h=54.82 MPa

This is a case at the threshold of normal/strike slip stress regime with isotropic stresses perpendicular to the wellbore direction. The results are the same as Case 1, however, the cross over point has moved to the left indicating that with a notch length of at least 0.1a (i.e. 10% of wellbore radius) the transverse fracture will dominate.

Case 3: σ_V=68.48MPa > σ_H=σ_h=58.21 MPa

This case represents isotropic horizontal stresses with average horizontal stresses considered as the isotropic stress in this case. No cross over is observed in this case meaning that the axial

fracture is always dominant regardless of the crack length. This is a critical situation in practice as transverse fracture is unlikely to initiate.

Case 4: σ_V=68.48 MPa > σ_H=61.58 MPa > σ_h=54.82 MPa

Here, using Bakken data, similar to Case 1, the initiation pressure for axial fractures in three different directions (i.e. perpendicular to σ_H, perpendicular to σ_V, and at 45° with respect to σ_V) are compared with transverse fractures. The results show that the cross over point moves to the right as the axial fracture is further oriented towards its most favourable direction. This means that larger notches are needed to dominate transverse fractures. It is seen that in general, as the stress anisotropy reduces, the cross over points moves to the right, i.e. larger notch length is needed in order to dominate transverse fracture.

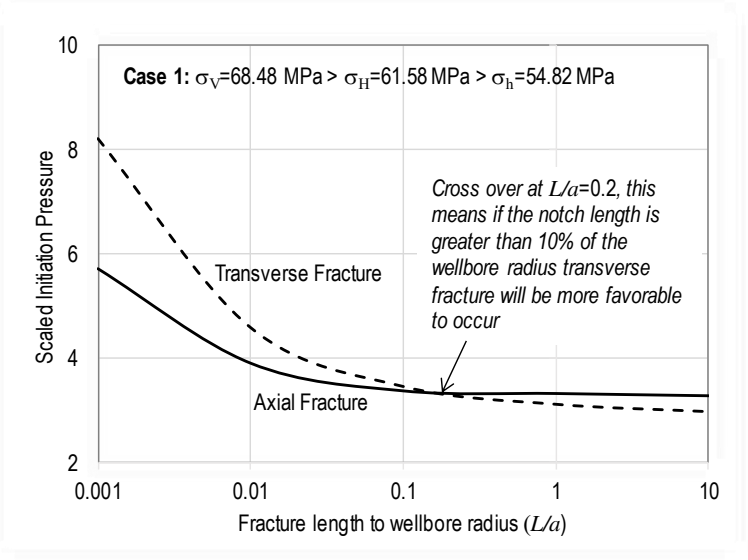

Figure 4.14: Fracture initiation pressures for transverse and axial fractures in presence of different stress regimes.

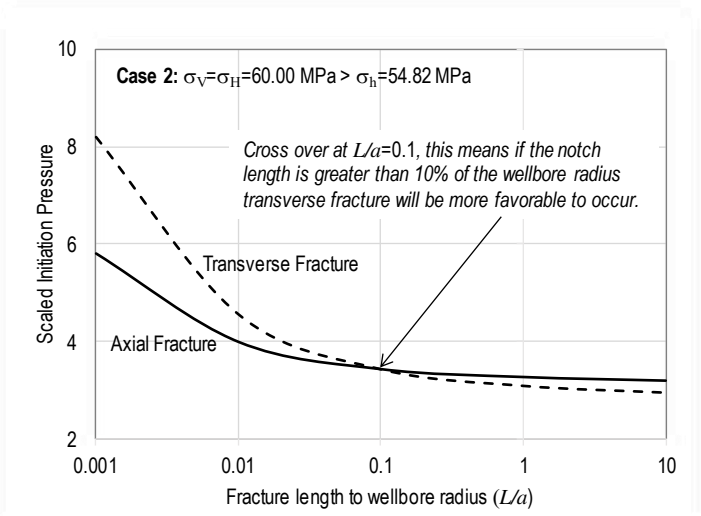

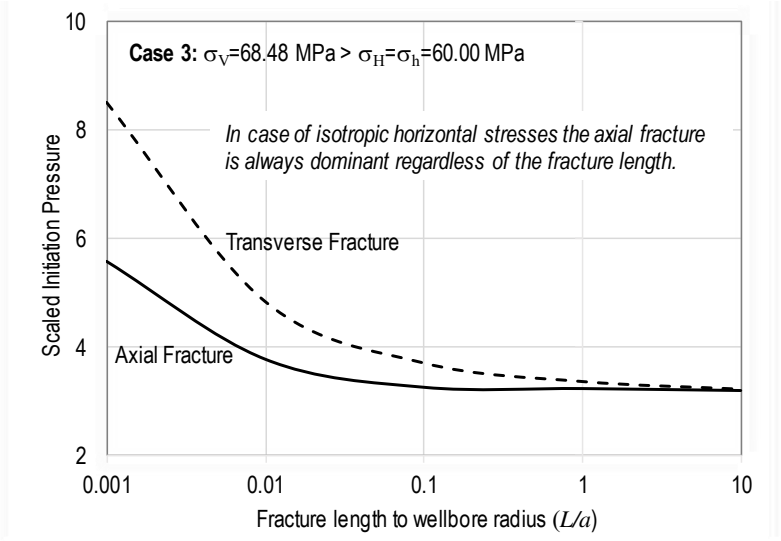

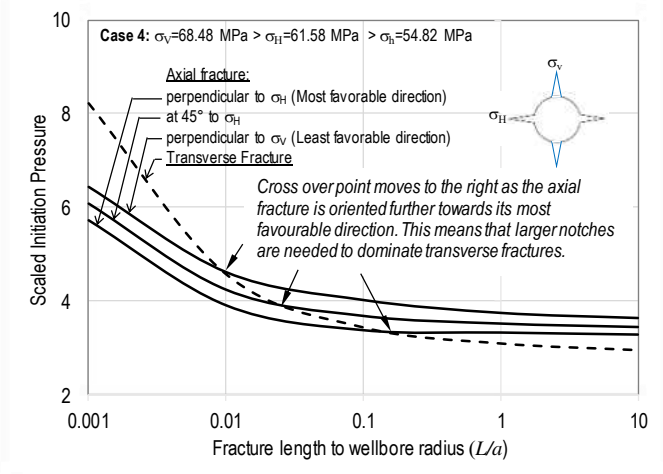

Figure 4.15 (continued): Fracture initiation pressures for transverse and axial fractures in presence of different stress regimes.

4.5.2 Multiple (Star) Crack

Multiple fractures are expected to occur when pressurization rate is fast (i.e. the rise time of the driving pressure pulse is relatively short compared with the time required for stress waves to circle the cavity). This situation is happening more likely in case of axial fracture. For axial multifracture configurations, Nilson and Proffer (1984) extended the geometry function *f* for two wing fracture (see Equation 4.41) by including in the overall weighting function, *f*, an additional multiplier, f_N, in form of (i.e. the *f* function of equation 4.43 is multiplied by f_N for case of more than 2 cracks):

$$f_N = \frac{\left(f_\infty + f_\infty \frac{L}{\pi a/N}\right)}{\left(f_\infty + \frac{L}{\pi a/N}\right)} \tag{4.52}$$

$$f_\infty = 2\frac{\sqrt{N-1}}{N} \tag{4.53}$$

Here, *N* is the number of fractures and $\pi a/N$ is the circumferential distance between fractures. It assumes that cracks have similar distances from each other and the first crack is along the most favourable direction. Figure 4.15 shows the plot of f_∞ versus *N* and f_∞ as a function of $\frac{L}{\pi a/N}$. The results show that the multiplier f_∞ reduces from 1 (for case of bi-wing crack) as the number of cracks increases, corresponding to increase of the crack length to circumferential distance between cracks. This Figure also shows that the multiplier factor becomes flatten as the crack length to circumferential distance increases over 4 to 8 cracks for low to higher number of cracks, respectively.

Figure 4.16 presents the initiation pressures for the case of 6, 15 and 25 axial fractures, respectively. The differences, as seen from this Figure, are minor. In this Figure also the initiation pressure curve corresponding to the transverse fracture is shown. It is seen that as the number of fractures increases, cross over point moves to the left, i.e. less notch length can result in transverse fracture to dominate the axial fracture.

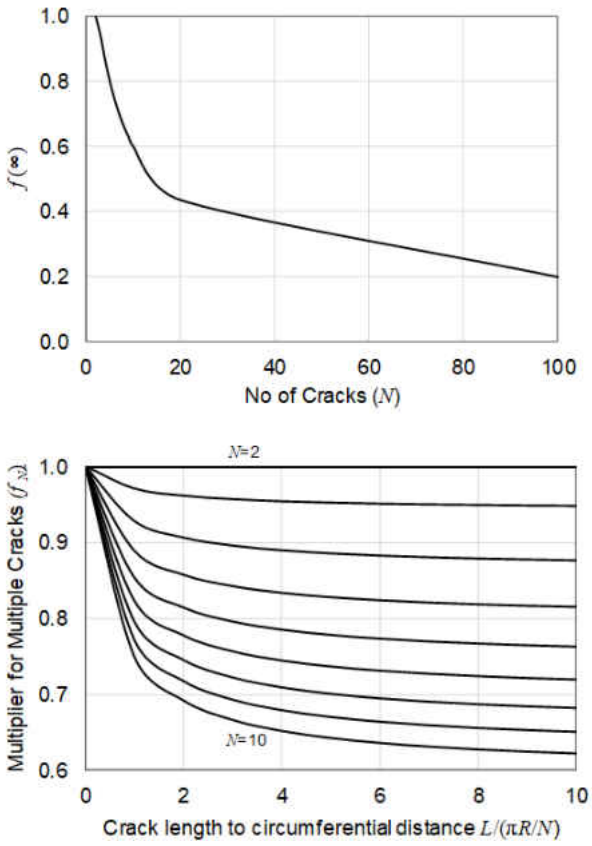

Figure 4.16: Change of the weight function *f* for multiple fractures with respect to the number of fractures and the ratio of crack length to circumferential distance between fractures.

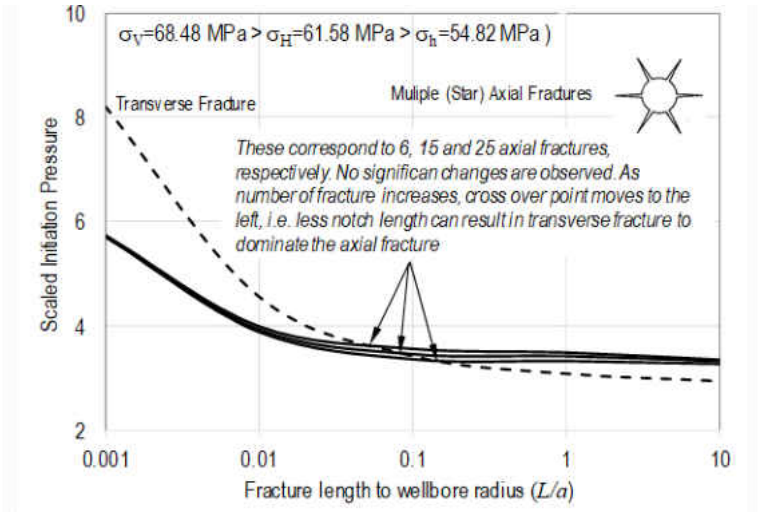

Figure 4.17: Fracture initiation pressures multiple axial fractures.

4.6 Fracture Propagation Regimes and Scaling Law

Fracture propagation is a complex process which is governed by a series of physical mechanisms such as elasticity, fluid flow and leak-off and fracture mechanics (Lecampion et al. 2017). Propagation of a radial hydraulic fracture in the field is expected to be governed at early time, when fracture radius is small, by the dissipation of the viscous flow. This is known as viscosity dominated regime. However, at large time, as the fracture perimeter is increases, the fracture energy, or toughness, to create an increment of fracture surface becomes larger. The fracture propagation in this case is known to be toughness dominated. Here, we ignored the effect of the injection system compliance, which is mostly governed by fluid compressibility and then wellbore deformation. In a small scale laboratory test considering the case of a penny shaped fracture, it is most likely that toughness controls the fracture propagation regime at the final stage of propagation after a period of specific time.

In field scale hydraulic fracturing operations for the purpose of enhanced oil recovery (EOR), the range of injecting fluid viscosity is 0.001-0.1 pa.s (1-100 cp) with the flow rate of 20-30 barrel per minute (0.05-0.08 m^3/s). However, when a lab experiments is performed on very small sample size to represent field scale operations, the fluid viscosity should be increased to as high as on average 100 pa.s with very small flow rate of as low as 1×10^{-9} m^3/s (Sarmadivaleh & Rasouli, 2013). This will ensure that the fracture propagates very slowly within a few centimeters of rock sample size to allow monitoring and recording the pressure versus time data.

In order to propagate the fracture in the same regime (i.e. toughness or viscosity dominated) as occurred in the field, the viscosity and flow rates, as well as the wellbore diameter should be designed accordingly. This is done through the scaling law, which is well known and used for design of a hydraulic fracturing lab experiments (De Pater et al. 1994). For this purpose, a set of

dimensionless groups of physical parameters that describe a specific fracturing process are defined in the way that they become identical using laboratory and field parameters. These dimensionless variables are driven from the fluid flow (mass and momentum conservation laws) and rock behaviour (rock deformation, crack opening and extension) partial differential equations.

The scaling period is valid for the time from initiation until stopping the injection of fluid. To have viscose dominated fracture propagation; following condition should be met during fracture propagation (De Pater et al. 1994):

$$K_{IC} < 2P_n\sqrt{\frac{r_f}{\pi}} \tag{4.54}$$

where r_f is fracture radius and P_n is fracture net pressure.

For viscous dominated propagation regime, the dimensionless toughness parameter of a Penny-Shaped fracture can be calculated as (Detournay 2004):

$$\kappa = K'\left(\frac{t^2}{\mu'^5 Q_o^3 E'^{13}}\right)^{1/18} \tag{4.55}$$

where Q_o is flow rate and t is the experiment time. Other material properties are defined as:

$$K' = \left(\frac{32}{\pi}\right)^{1/2} K_{IC}, \qquad E' = \frac{E}{1-\nu^2}, \qquad \mu' = 12\mu \tag{4.56}$$

Here, μ is fracturing fluid viscosity, E is the rock Young's modulus, and ν is Poisson's ratio. In equation 4.55, the fracture propagation will be viscose dominated if κ is below one whereas it is toughness dominated when dimensionless toughness number exceeds 3.5. In contrast with Equation 4.55, the dimensionless toughness parameter is time dependent: this means that fracture regime may change from one type to another as time evolves. Also the propagation regime was

checked against another criterion proposed by (Bunger et al 2005). In this method the evaluation criterion is based on three characteristic times of leak-off, toughness, and viscosity.

Figure 4.17 (top) plots the changes of dimensionless toughness as a function of pressurization rate for data corresponding to typical lab and field scale HF operations. Average propagation time of 3000s and 100s has een considered as examples, corresponding to field and lab scale testing. In the top Figure, the viscosity is set to a certain value (0.001 pa.s at field scale operation and 100 pa.s for lab experiments) and the pressurization rate is varied by changing the flow rate. As one may expect, larger pressurization rate is expected at field scale HF operation compared with lab experiments. Therefore, in overall, lab experiments HF are more likely to be in viscosity dominated regime. While field scale HF operations starts usually at viscosity dominated regime, it will change into transition and then toughness dominated regimes after long time propagation.

In Figure 4.17 (bottom) the flow rate is set to a constant value (0.08 m^3/s at field scale and 1×10^{-9} m^3/s at lab scale) and the pressurization rate is calculated and plotted against the dimensionless toughness parameter. From this Figure, it is seen that the propagation regime is more sensitive to the changes of viscosity than flow rate, a result which is evident from Equation (4.55).

4.7 Summary

In this Chapter an overview of different analytical models to estimate the fracture initiation pressure through an existing crack emanating from wellbore wall were presented. It was seen that these models are based on some simplified assumptions, so when one using these models, should carefully consider their limits and application ranges. In general, most of these models are based on the concept of superposition law in order to determine the impact of different parameters on fracture initiation pressure. We presented models which consider the effect of in-situ stresses and

wellbore pressure, those which also integrate the impact of pressurization rate and finally models which consider the axial and transverse fracture initiation and propagation.

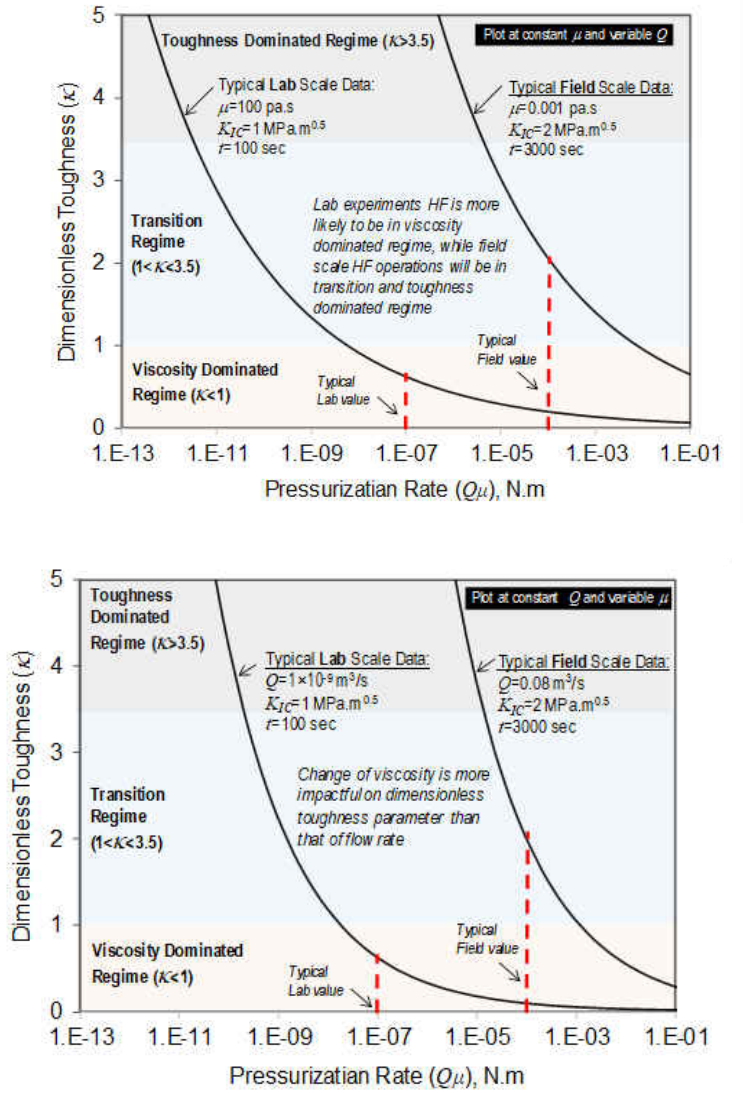

Figure 4.18: Dimension toughness parameter changes as a function of pressurization rate for typical field and lab scale HF operations.

While these models provide great knowledge about the effect of different parameters on crack initiation from an existing notch, they cannot be conveniently used for simulation of real cases where fractures with different geometry and properties are distributed around an OH borehole. Therefore, we introduce the lattice numerical modelling in the next Chapter, which will be used to conduct numerical simulations of some of the cases presented in this Chapter to compare the results

with analytical solutions. We also expand this to more complex cases where analytical solutions do not exist and interpret the results. The results of numerical simulations will be presented in Chapter 5. In the next Chapter we also simulate fracture propagation pressure and discuss the impact of different parameters on competition between axial and transverse fracture propagation.

CHAPTER 5

Numerical Simulations

5.1 Introduction

In this Chapter, the results of lattice numerical simulations of hydraulic fracturing are presented. The effect of both axial and transverse notch geometry on fracture initiation and breakdown as well as propagation pressures will be studied and compared with the analytical models presented in the preceding Chapter. The impact of the flow rate and fluid viscosity together with the pressurization rate on fracture pressure and geometry will be modelled. In addition, the models are presented for different stress regimes and stress anisotropy, as the most important parameter changing the axial to transverse fracture limits. The results will be compared with the analytical models presented in the previous Chapters and conclusions are made.

5.2 Borehole Without Notch

We start the simulations by looking at a horizontal wellbore drilled along the minimum horizontal stress direction in a normal stress regime. It is assumed that no natural fractures or notches present around the wellbore wall. For consistency, we build the model geometry corresponding to the Bakken data presented in Table 4.1, in the previous Chapter.

5.2.1 Model Geometry

As this study focuses initially at the fracture initiation pressure and also fracture propagation near wellbore (i.e. a few times than the wellbore radius), model dimension is considered to be 1.5m×2.5m×2.5m. The model geometry is shown in Figure 5.1, where the stress magnitudes are applied in different directions in such a way that the fracture is expected in the plane of larger model dimension. The horizontal wellbore has a diameter of 0.11m and a length of 8m and is placed in the center of the model. In XSite, there is no direct feature available to keep the external stresses applied to the model constant during the fluid injection and fracture propagation, to mimic real field stresses. Hence, in order to implement the so called servo control stress condition, an outer soft layer with thickness of 0.125m has been placed all around the model. The Young's modulus of this layer is assumed to be much lower than that of the formation Young's modulus (here we assumed 100 times less, to be 0.3 GPa – see Table 4.1) with a large Poisson's ratio (here we considered o.45). This soft boundary will dampen the stresses during the fluid injection time step and keeps the stresses to remain constant on the model.

The model configurations presented in Chapter 3 was used in the simulations of this Chapter. Figure 5.1 shows the model geometry without notch. Because in absence of the notch we expect an axial notch to be initiated and developed, we use the model geometry corresponding to this fracture geometry (see Figure 3.12 in Chapter 3). As discussed in Chapter 3 (see Figure 3.12) two rectangular resolution domains are considered here, the inner domain has an equal length and width of L=W=2.1m and thickness of T=0.3m with a resolution of 2.2m and the outer domain has dimension of L=W=2.3m and thickness of T=0.5m with a resolution of 4.4m. The rest of the model has a resolution of 8.8cm.

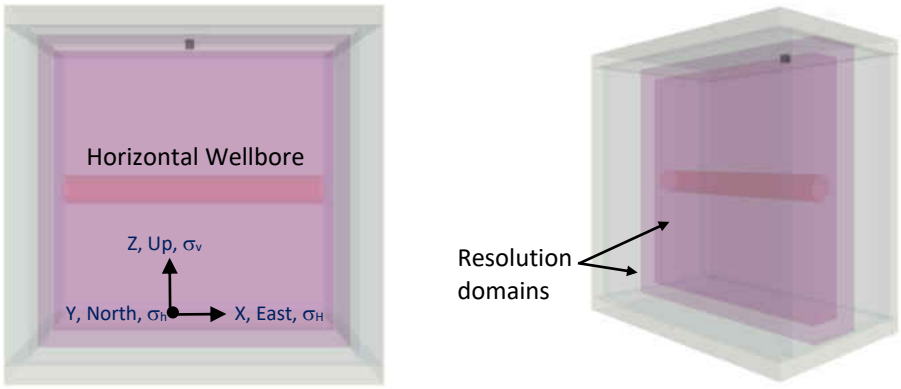

Figure 5.1. Model geometry for a horizontal wellbore along σ_H.

As explained in details in Chapter 3, model construction in XSite includes three steps. Initially, the borehole is excavated. Then, the mechanical step is run, which includes applying the in-situ stresses until the model reaches stability stage. It is to be noted that mechanical stability is achieved when the velocity field data becomes negligible in the entire model. The final step is the fluid step, where the injecting fracturing fluid is applied. This step continues until the fracture initiation and breakdown points are reached and then it propagates to the desired extent. We can monitor several data, including the pressure-time curve, number of initiated fractures before fracture breakdown pressure and after that and fracture aperture contours during model evolution.

The model was run for 0.01s simulation time during mechanical step, and continued for 0.02s during fluid injection step. Figure 5.2 shows the fracture apertures as well as the corresponding pressure-time curve and the number of cracks developed around the wellbore as time evolved for model geometry of Figure 5.1 and the data corresponding to the Bakken formation presented in Table 4.1 in Chapter 4. The results show that in absence of any notch (i.e. natural fractures or any defect at the wellbore wall), several cracks are developed around the wellbore, mostly along the wellbore axis (corresponding to axial fracture). The fracture initiation pressure is approximated at 117MPa which is higher compared to cases where notches exist around the wellbore. This observation is in agreement with the results of the analytical models presented in

Chapter 4 (see Section 4.2). We will see in the next Section, how the presence of a notch facilitated the initiation and propagation of the fracture.

Presence of the peak pressure or breakdown pressure depends on the rock properties and may not be necessarily observed in a HF test. As discussed in Chapter 3, Both initiation and breakdown pressures are functions of the flow rate and viscosity. Therefore, changing these input parameters the pressure values will change.

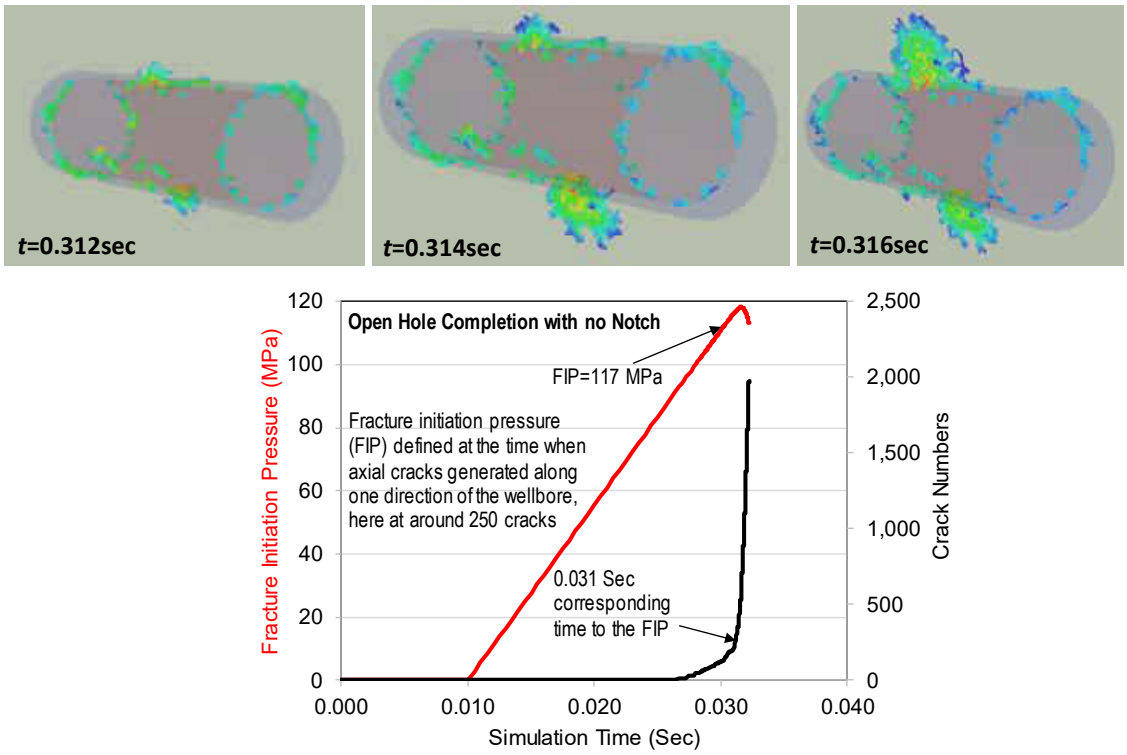

Figure 5.2. Fracture apertures evolution per simulation time from 0.312sec to 0.314sec and 0.316sec, left to right (top), and pressure-time and crack numbers plots (bottom) for an open hole completion with no notch

5.3 Transverse versus Axial Fracture

In this section, the simulation models are presented with both transverse and axial notches to compare the competition between these two types of fracture geometry as a function of the notch dimension, stress anisotropy and stress regimes. The results and discussions are outlined in the

following subsections and include the cases for which analytical analysis was done in Chapter 4 (subsection 4.5.1).

Case 1: σ_V=68.48 MPa > σ_H=61.58 MPa > σ_h=54.82 MPa

This is the case of normal stress regime, corresponding to the Bakken data in Table 4.1 (Chapter 4). Numerical simulations were carried out for transverse fractures with different notch lengths. The initiation pressure for each case was determined corresponding to the time when cracks around the notch perimeter are all open. Similarly, axial fractures were simulated with different notch lengths (L_n) and base length of L_b=1m. Figure 5.3 shows, as examples, the aperture values of the fracture propagated near wellbore for transverse fracture with notch length of L_n =0.011m ($\gamma=L/a$=0.1) at 0.025sec simulation time. In this Figure also the corresponding pressure-time curve and crack numbers are shown. Similar results are shown in Figure 5.4 for the transverse fracture with a notch length of L_n=0.22m (γ=2) at the same simulation time of 0.025sec for the case of transverse fracture with γ=0.1. From Figures 5.3 and 5.4 is it seen that as the notch length increases, the initiation pressure reduces, a conclusion that we expected and discussed based on analytical models in Chapter 4. For small notch size of γ=0.1, it is seen that due to the fact that the notch is not enough long, it is not as effective as it should be and this resulted in the development of some sparse fractures along the wellbore. In this case, the fracture also propagated in one direction more than other directions with an asymmetric geometry.

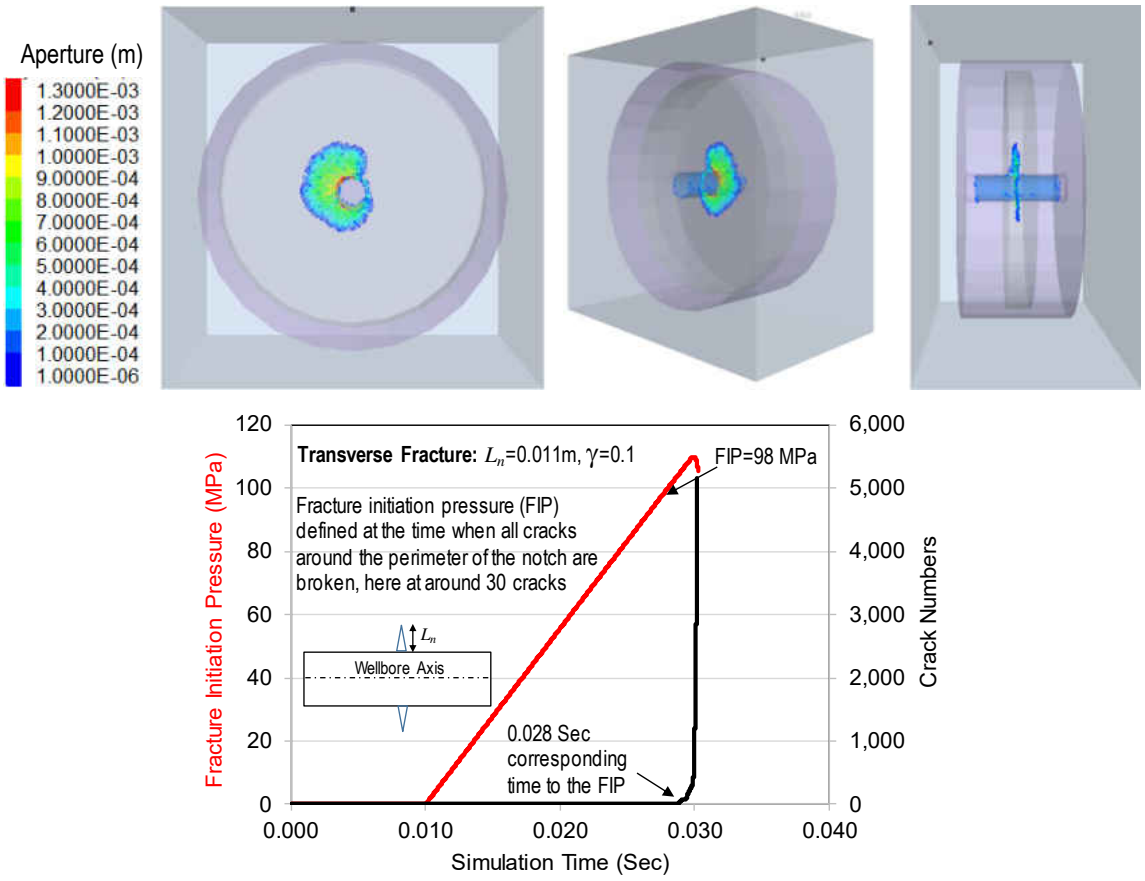

Figure 5.3. Fracture propagation from different views with aperture plots (top) and pressure-time and crack numbers plots (bottom) for transverse fracture with an initial notch length of L_n=0.011m (γ=0.1)

Also, for larger notch sizes, more cracks at the perimeter of the notch are expected to break before reaching the initiation pressure. This is visible from Figure 5.5 where the scaled notch area and perimeter (with respect to wellbore area or perimeter) which shows as the notch length increases the notch area and perimeter increases exponentially. Finally, in general, the larger the notch length, the earlier to reach the fracture initiation point, which is due to the fact that the injecting fluid can more easily penetrate into the crack and also has larger area, hence more power to open and propagate the fracture.

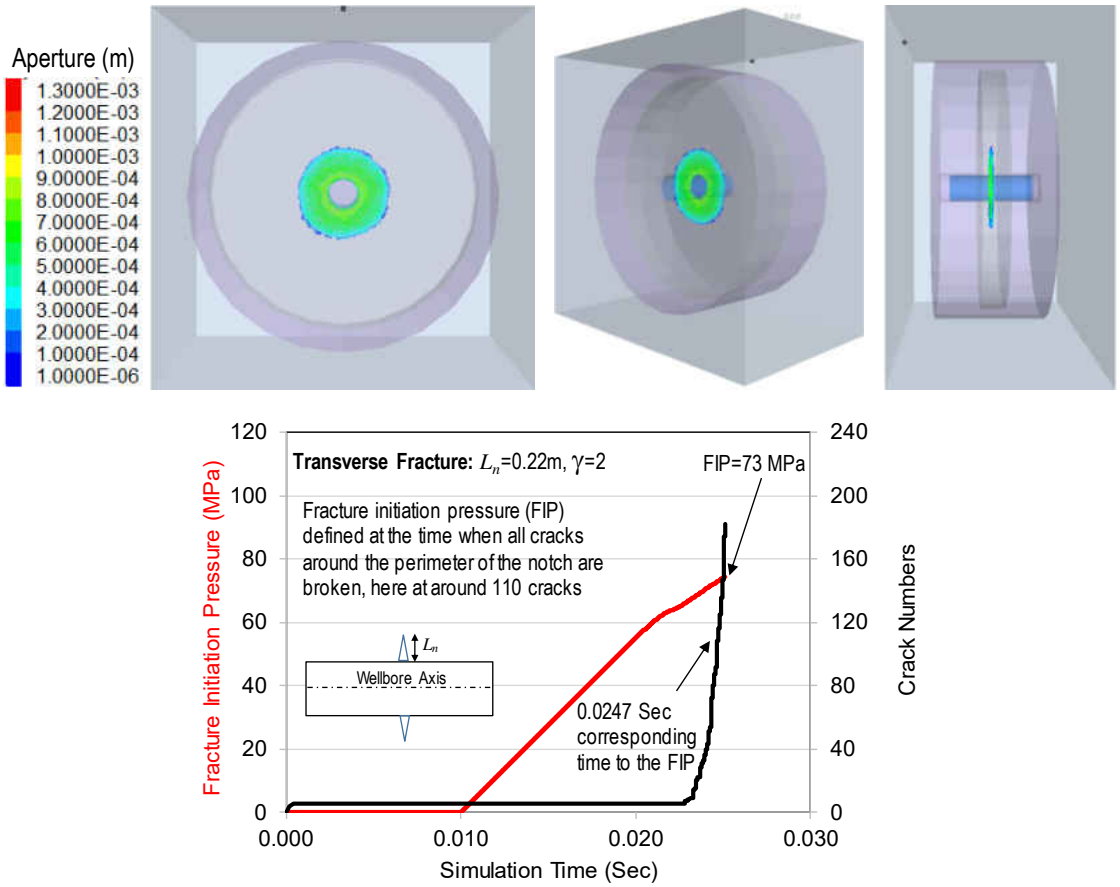

Figure 5.4. Fracture propagation from different views with aperture plots (top) and pressure-time and crack numbers plots (bottom) for transverse fracture with an initial notch length of L_n=0.22m (γ=2) and simulation time of 0.025sec

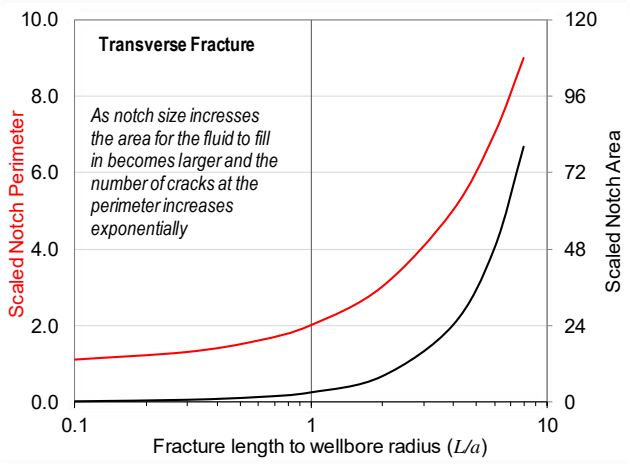

Figure 5.5. Scaled area and perimeter of transverse notch as a function of Fracture size

In Figures 5.6 and 5.7, similar results to Figures 5.3 and 5.4 are presented for axial fractures with notch length of L_n=0.011m (γ=0.1) and L_n=0.22m (γ=0.2), respectively and base length of

L_b=1m for a simulation time of 0.045sec. Similar conclusions drawn for the case of transverse fracture are observed here. It is seen that the fracture has opened larger in case of larger notch length of γ=2 (higher aperture values) comparing to γ=0.1. Also, comparing the same notch lengths, axial fractures result in higher apertures than transverse fractures (see Figures 5.3 and 4.5) which is due to their larger area open to the fluid flow.

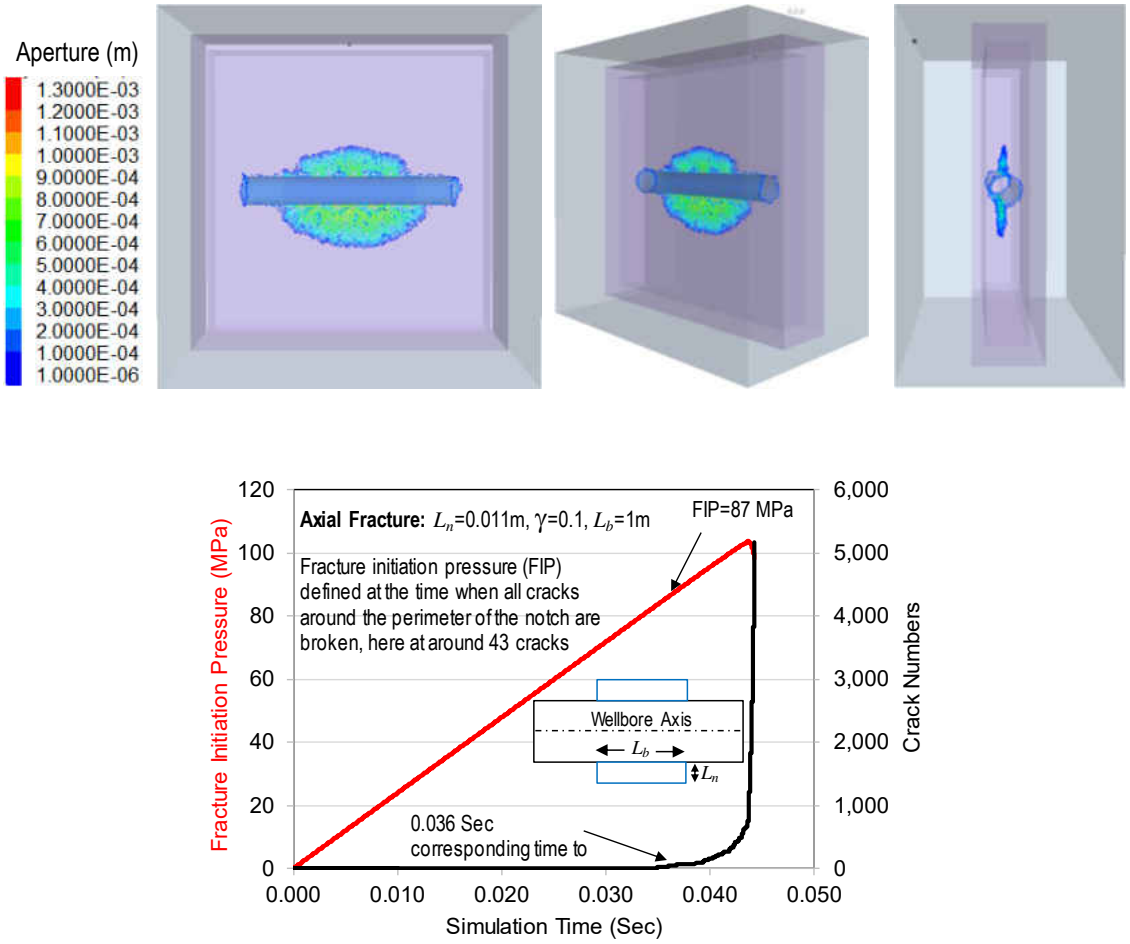

Figure 5.6. Fracture propagation with aperture plots from different views (top) and pressure-time and crack numbers plots (bottom) for axial fracture with an initial notch length of L_n=0.011m (γ=0.1) and based length of L_b=1m and simulation time of 0.045sec

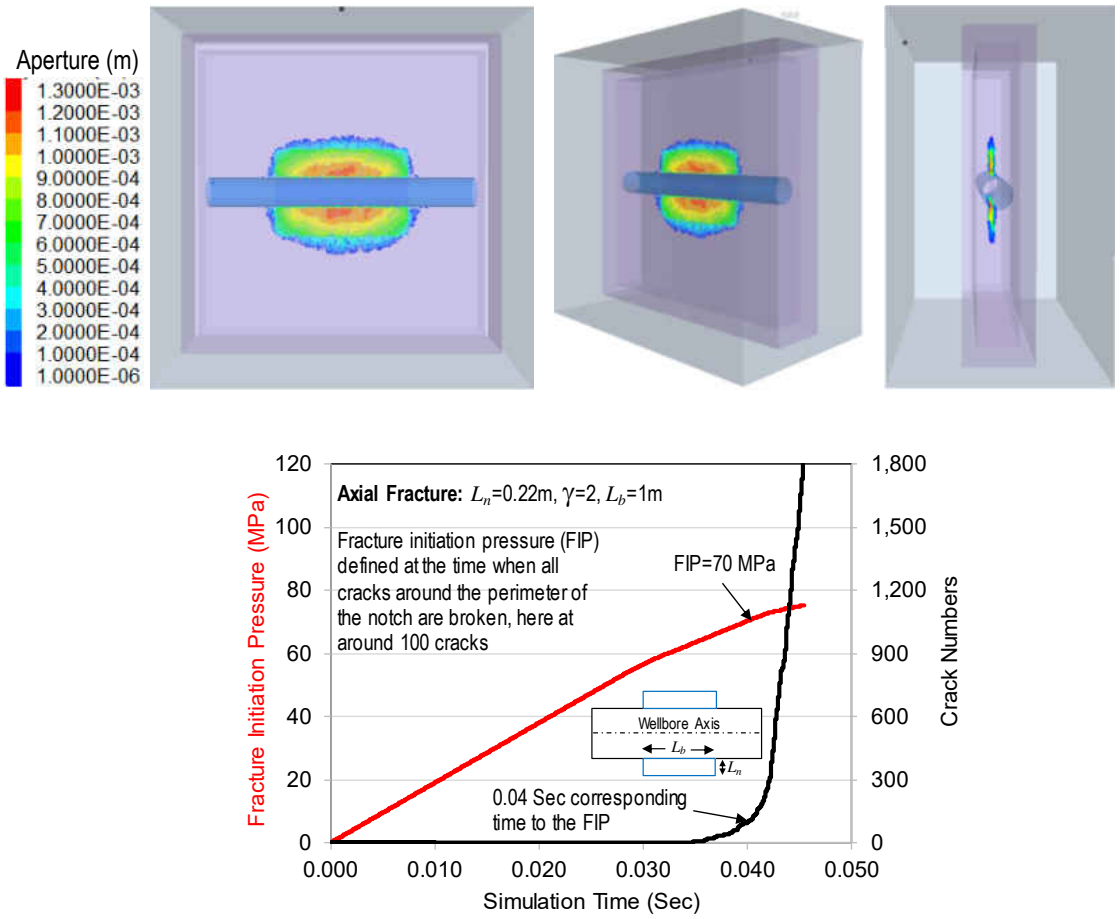

Figure 5.7. Fracture propagation with aperture plots from different views (top) and pressure-time plot (bottom) and crack numbers for axial fracture with an initial notch length of L_n=0.22m (γ=2) and base length of L_b=1m and simulation time of 0.045sec

Correct comparison of the results of axial notch with the transverse notch requires careful consideration of the base length L_b. To explain this, in Figure 5.8 the results of scaled notch area and perimeter of the transverse fracture (Figure 5.5) are compared with two axial notches with base lengths of L_b=1m and L_b=0.5m. from this Figure it is seen that in case of L_b=1m (top plot in Figure 5.8) the area and perimeter of axial notch are larger than transverse fracture but this does change after a certain notch length. However, for base length of L_b=0.5m or smaller, the axial notch has always larger area and perimeter than that of transverse notch. This indicates that depending on the notch base length the time to reach the FIP and the number of corresponding cracks at the perimeter of the notch may how different trends.

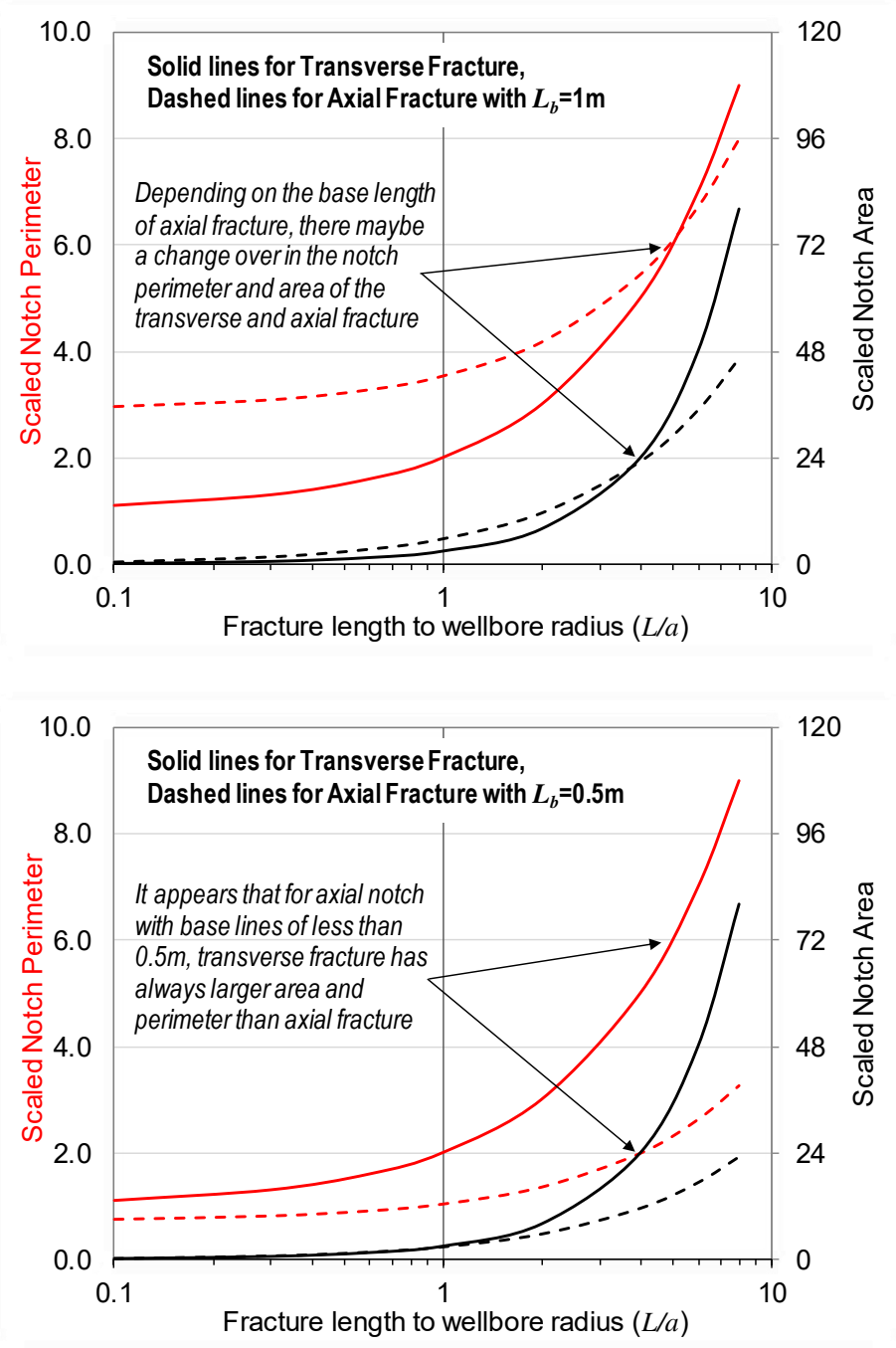

Figure 5.8. Scaled area and perimeter of axial notch with base length L_b=1m (top) and L_b=0.5m (bottom) as a function of Fracture size compared with transverse notch

However, from practical point of view, as the base length of the axial fracture reduces, the chance for the fluid to enter the crack becomes less, resulting the notch to be ineffective to act as the starting point for fracture initiation regardless of its length. This is visible from Figure 5.9

where the fracture geometries are shown for three axial notches with base length of L_b=0.5m, γ=0.1m (top), L_b=0.2m, γ=0.1m (middle) and L_b=0.2m, γ=8 (bottom) and the same simulation time of 0.045sec for the case of L_b=1m. From this Figure (top and middle), it is seen that the fracture initiated from the axial notch appears to be irregular and also a number of other fractures starting to grow along the axis of the wellbore. Also it is seen that the fracture did not propagate as much as it did in the case of axial fracture with a base length of L_b=1m, which shows that the notch base length is not adequate to present a good path for the fluid to flow easily and open the fracture. It is to be noted that the fractures developed at both ends of the wellbore are due to the boundary effect and should not be considered for interpretation purposes in the context of this study. From Figure 5.9 (bottom) it is observed that even that the notch length is very long, as the base length is small, the fracture starts to propagate to the sides and not from the end of the notch lengths. If the simulation time continues further propagation of axial notches are expected in this case. One should also note that these conclusions are valid for the geometry of the notches used in these simulations and if the notch geometry is change, for example, a rectangular geometry for transverse notch or radial geometry for axial notch are considered the analysis should be repeated. The last point to add is that the XSite simulations do not consider the effect of compressibility of the system including the wellbore or drillstring, while this effect cannot be neglected (Lecampion, 2013). This effect should be considered in the future simulations.

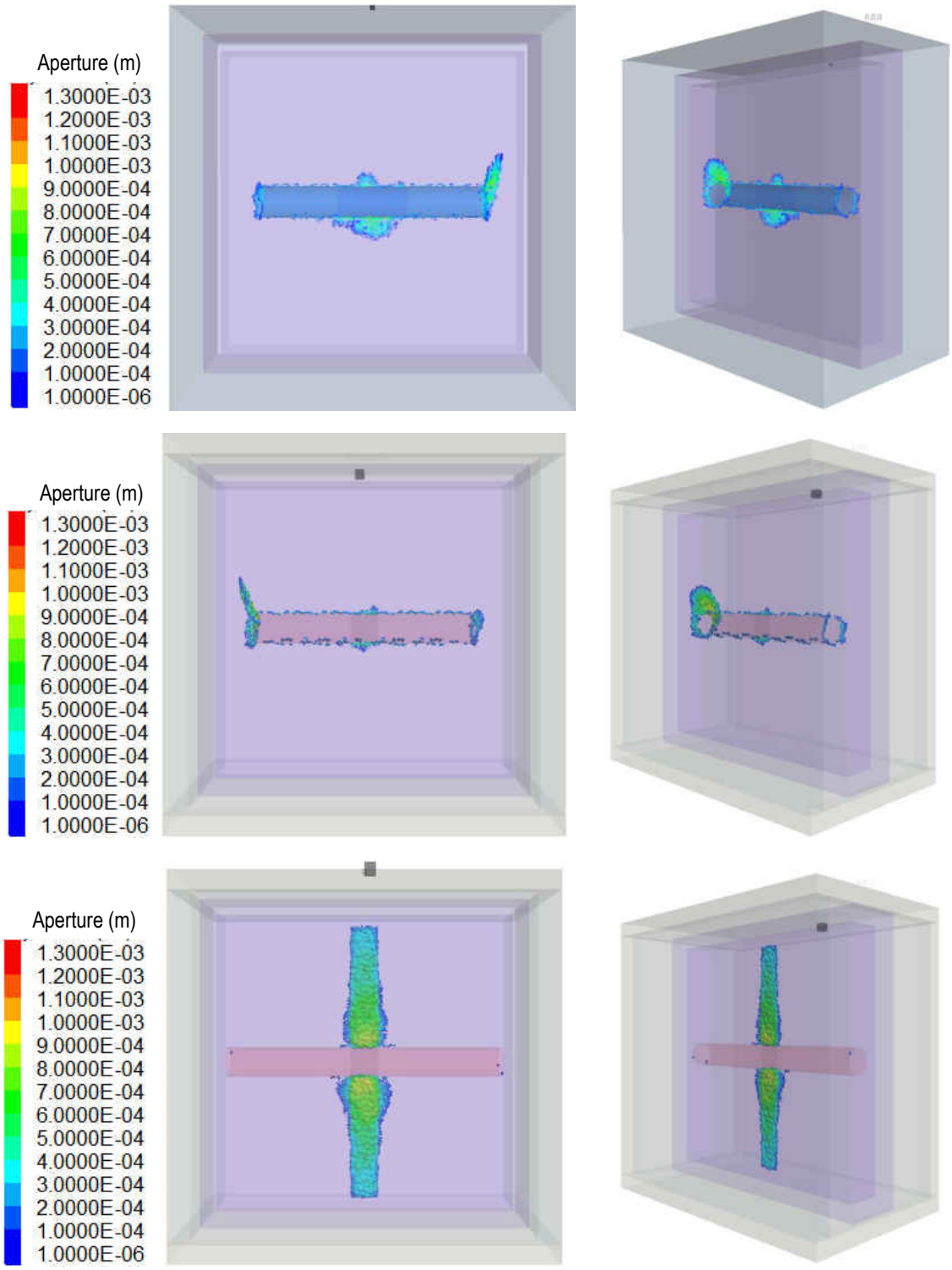

Figure 5.9. Fracture propagation and aperture plots from different views for axial fracture with base length L_b=0.5m, L_n=0.011m (γ=0.1) (top); L_b=0.2m, L_n=0.011m (γ=0.1) (middle) and L_b=0.2m, L_n=1.98m (γ=8) (bottom) and simulation time of 0.045sec

The initiation pressures for transverse and axial fractures with different notch sizes are presented in Figure 5.10. Also, in this Figure the results of analytical models presented in Chapter 4 are shown in this Figure. A number of observations are made from results of Figure 5.4. Firstly, it is seen that regardless of fracture geometry, the simulation results show higher initiation pressure than analytical models. This is a reasonable observation as the analytical models do not consider several parameters such as the fracture tortuosity and frictional pressure drop resulting in underestimation of the initiation pressure. Secondly, the cross over from axial to transverse fracture is found to be at L/a=4 compared to L/a=0.2 which resulted from analytical solution. This suggests that in real cases larger notch lengths are needed to dominate transverse fracture over the axial fracture. Finally, it is to be noted that simulations with notch lengths of $L/a < 0.1$ resulted in no transverse fracture but unstable fracture growth mostly in form of axial fracture and similar to the case of no notch case, presented in the previous Section. Therefore, no data are reported for this part of the plot in Figure 5.10.

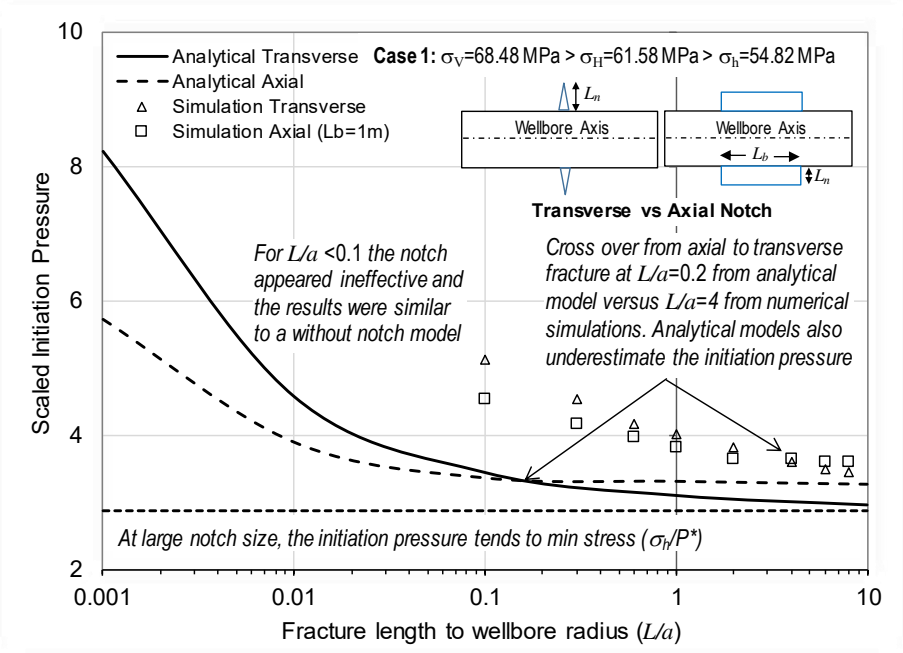

Figure 5.10. Scaled initiation pressures for transverse and axial fractures with different notch lengths. The axial notch has a base length of L_b=1m

The above results are based on the assumption of a base length of L_b=1m for the axial fracture. In order to investigate the impact of the base length on the cross over point, simulations of axial fracture were repeated with a smaller base length of L_b=0.5m. Figure 5.11 shows the result as addition of the new data to Figure 5.10. From this Figure, it is seen that with reducing the base length, as expected, the fracture initiation pressure increases, but more importantly, the cross over point moved to the left at L/a=0.6 and becomes closer to the analytical model of L/a=0.2. Also, at this base length, the results of axial fracture initiation are very close to the transverse fractures. This result shows the importance of the base length on determining initiation pressure for the case of axial fractures. From practical point of view, when detecting the natural fractures around the wellbore from the image logs, it is important to also note their mark length on the wellbore wall, in specific, when it is aligned in the wellbore axis. This will assist to make a more reasonable estimation of impact of these natural fractures as potentials for the starting point of fracture initiation.

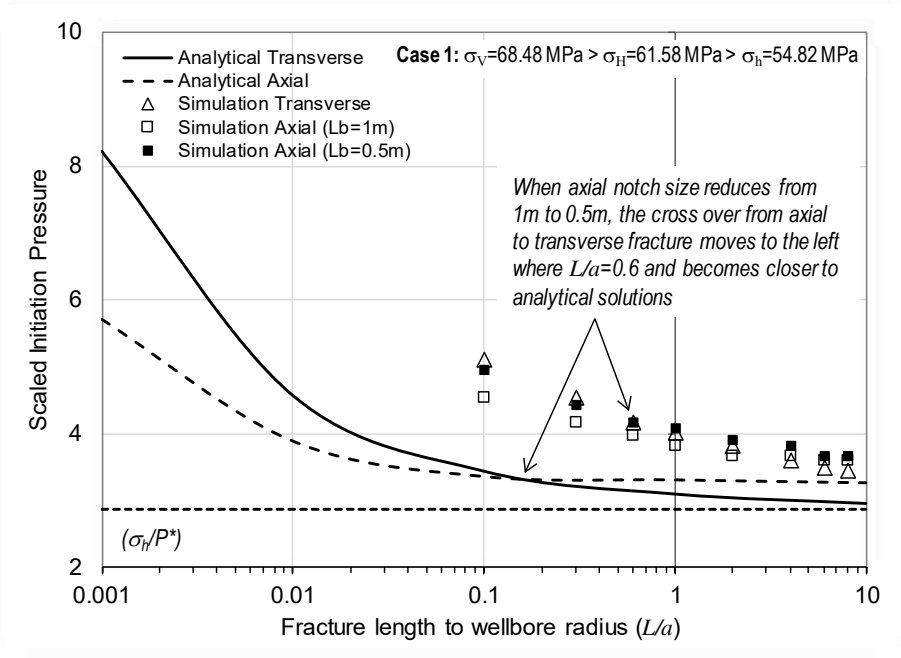

Figure 5.11. Scaled initiation pressures for transverse and axial fractures in a normal stress regime

Case 2: $\sigma_V = \sigma_H = 60.0\text{MPa} > \sigma_h = 54.82\ \text{MPa}$

In this case, the stress regime is in transition between normal to the strike slip. With the results observed from Case 1, here and for the rest of simulations in this Chapter, for the axial fracture, we only present the simulations for a notch base length of L_b=0.5m. Figure 5.12 presents the results of scaled initiation pressure versus scaled notch length for this stress regime. The results of analytical models for both transverse and axial fractures are shown in this Figure. The simulation results for the case of transverse fracture is similar to Case 1 (see Figure 5.11). This is due to the fact that the transverse fracture opens against σ_h, which is identical in both cases. The simulation results for the case of axial notch with base length of L_b=0.5m is also presented in Figure 5.12. The cross over point, in this case, is L/a=0.02 from analytical model and is $0.1 < L/a < 0.2$ from simulations. It is seen that, for both analytical and simulation results, the cross over point has shifted to the left, compared to Case 1, as expected. This indicates the dominant effect of stress regime on the initiation pressure and the design of proper notch size if transverse fracture is preferred to be created.

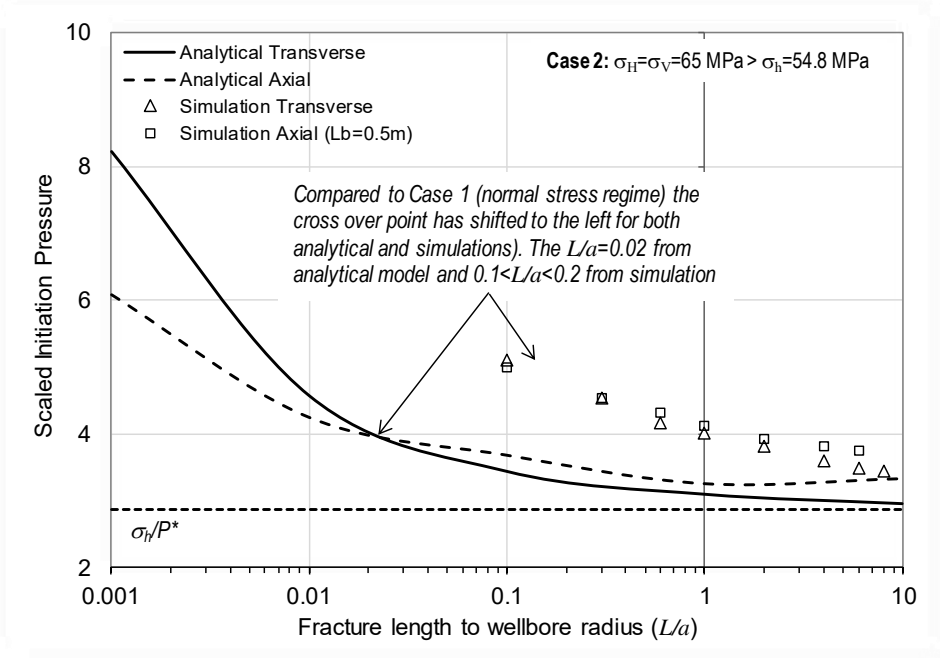

Figure 5.12. Scaled initiation pressures for transverse and axial fractures in a transition from normal to strike slip stress regime

Case 3: σ_V=68.48MPa > σ_H=σ_h=58.21MPa

This case represents isotropic stresses, where the horizontal stresses considered as the average of σ_H and σ_h in Bakken. The analytical solution indicates that regardless of the notch size, always axial fracture is dominant. This result was discussed in Chapter 4. The simulation results presented in Figure 5.13, show the same conclusion, while higher initiation pressures observed comparing to analytical models as explained earlier on. The results shown in this Figure correspond to an axial notch with a base length of L_b=0.5m. Shortening the base length will increase the initiation pressure as the chance for the fluid to penetrate into the notch will be less. This could potentially result in cross over of the transverse and axial notch curves, however, as explained in detail in Case 1, from practical point of view the fracture does not tend to propagate symmetrically and penetrate into the formation effectively. Therefore, in case of isotropic field stresses, creation of transverse fractures will be challenging.

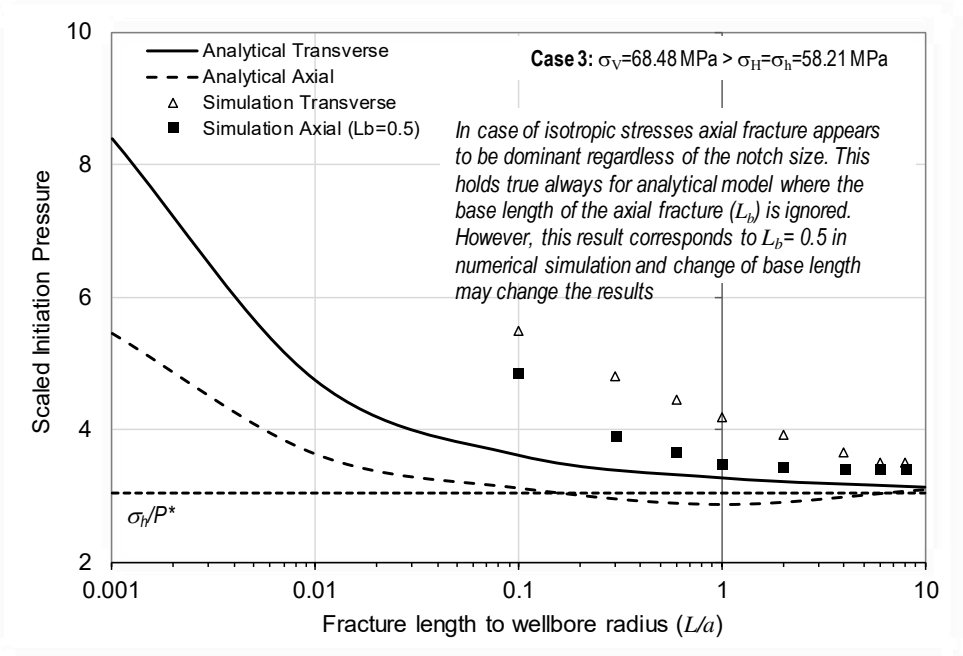

Figure 5.13. Scaled initiation pressures for transverse and axial fractures with different notch lengths for isotropic stresses

5.4 Axial Fractures with Different Orientations

In the previous Section, the results of HF simulations for axial fractures were presented for the cases where the axial notch was created perpendicular to the minimum stress. In case of normal stress regime, this is perpendicular to the maximum horizontal stress, σ_H. This is the most favourable orientation for an axial fracture to initiate and propagate near wellbore. The results presented for notches with different lengths and two base lengths of 0.5m and 1.0m. in this Section, for comparison purposes, axial notches with similar base length of 1m are simulated in the same normal stress regime as in the previous Section, but in two different orientations of ξ=45° and ξ =90° with respect to the most favourable orientation. The simulations will be done for three notch lengths corresponding to γ=0.1, 0.3 and 0.6.

Figures 5.14 to 5.16 show, correspondingly, the evolution of fracture propagation for an axial notch at 90° with respect to the preferred direction (ξ =90°) with three notch lengths of γ=0.1,

γ=0.3 and γ=0.6 with base length of L_b=1m at two different time steps of t=0.051sec (top) and t=0.055sec (bottom). From Figure 5.14 it is seen that, as the notch size is small, the fracture did not propagate from the notch, but instead cracks started to initiate along the axis of the wellbore at ξ=0°, i.e. the preferred propagation plane. This means that when the notch length is not adequate, it is not effective and the fracture initiation is similar to a wellbore without notch (see Figure 5.2). From this Figure it is also observed that as the time evolves, the fracture starts to propagate from the ends of the wellbore, here, mostly from the left end, instead of along the preferred propagation plane. This is due to the model geometry and the short length of the wellbore simulated here and should not misinterpreted incorrectly.

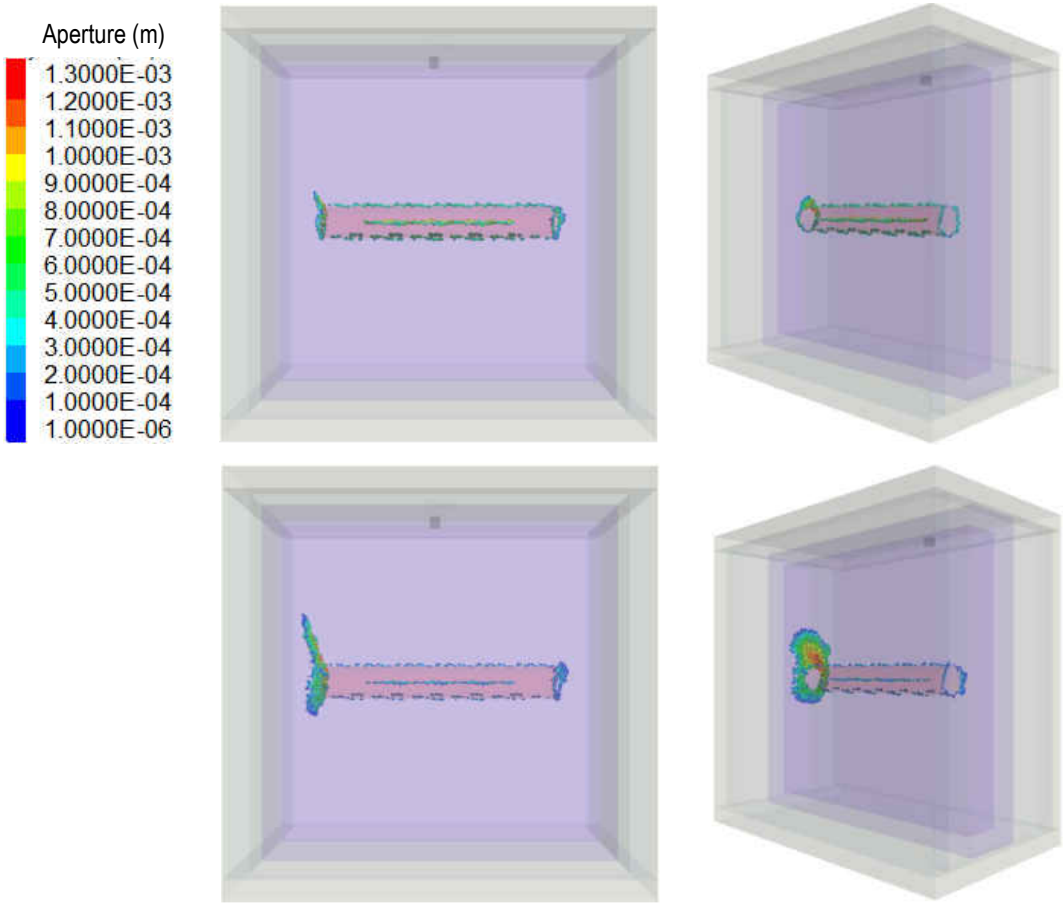

Figure 5.14. Fracture propagation for an axial notch at 90° with respect to the preferred direction. L_b=1m, L_n=0.011m (γ=0.1) at simulation time of t=0.051sec (top) and t=0.055sec (bottom)

In Figure 5.15 similar results to Figure 5.14 are shown but the notch length has increased to γ=0.3. It is seen that in this case, the fracture initiation begins from the notch, yet some dispersed cracks start to grow along the wellbore axis, perpendicular to the notch plane, but less than the case of γ=0.1. This observation becomes more manifest when the notch size increases to γ=0.6 (see Figure 5.16): the fracture initiates more favourably from the notch comparing to smaller notch sizes, with less cracks growing outside the notch plane. In all cases, if the fracture propagates further away from the wellbore wall, it is expected that it will reorient itself to become perpendicular to the preferred propagation direction, i.e. orthogonal to σ_H plane (i.e. when ξ=0°). While this is not clearly visible from Figure 5.16, due to the very long running time of the high resolution model, we observed this behaviour in models with lower resolutions.

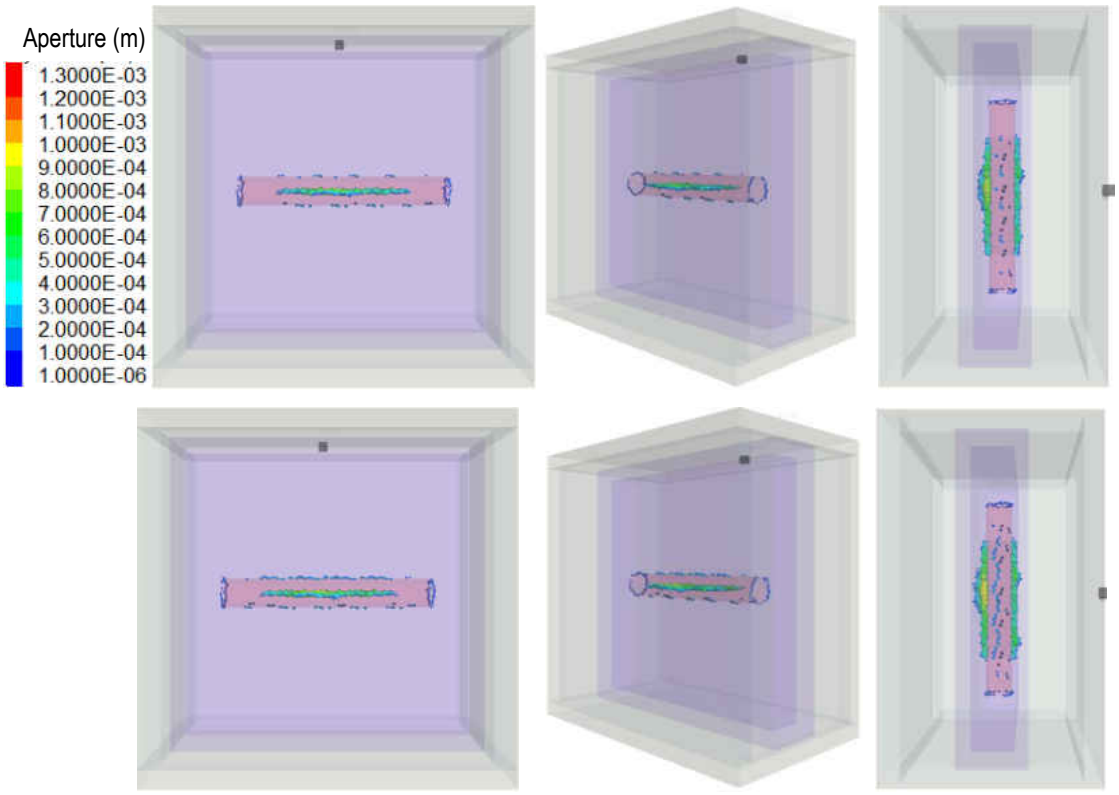

Figure 5.15. Fracture propagation for an axial notch at 90° with respect to the preferred direction. L_b=1m, L_n=0.033m (γ=0.3) at simulation time of t=0.051sec (top) and t=0.055sec (bottom)

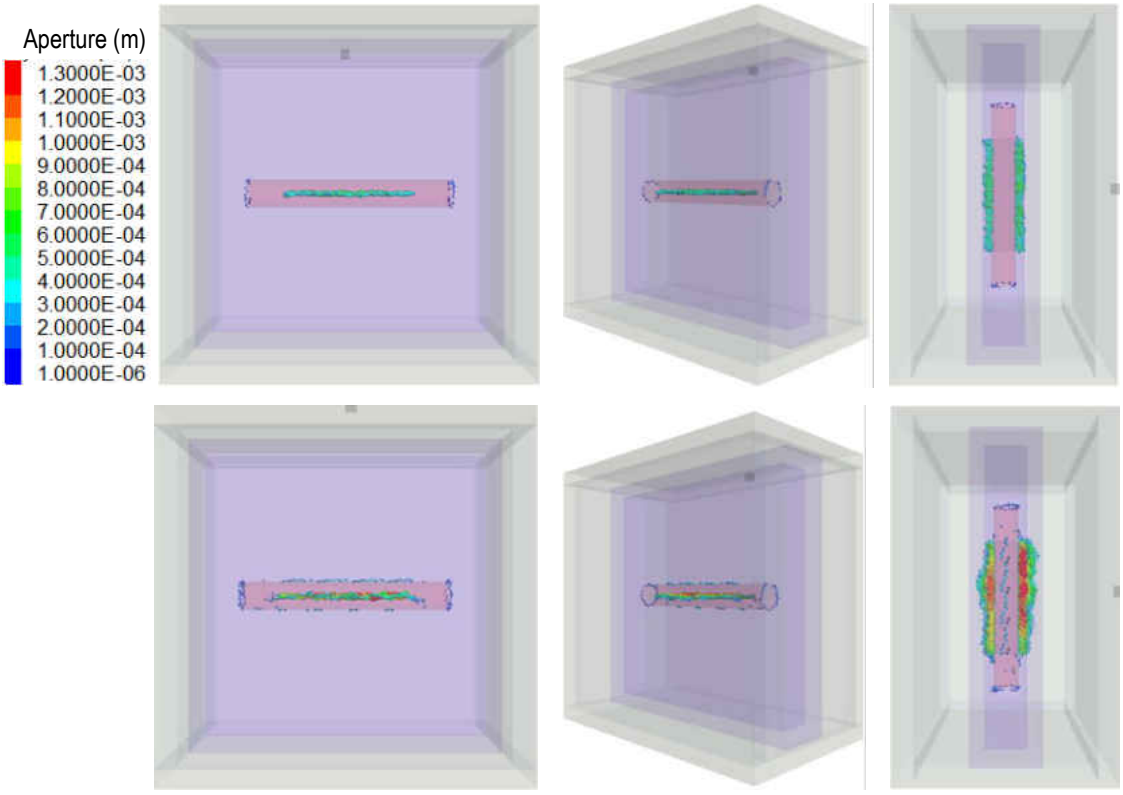

Figure 5.16. Fracture propagation for an axial notch at 90° with respect to the preferred direction. L_b=1m, L_n=0.066m (γ=0.6) at simulation time of t=0.051sec (top) and t=0.055sec (bottom)

For the case of the axial fracture at ξ=45° the simulation results for γ=0.1 showed that the fracture did not initiate from the notch plane, instead cracks started to grow along the preferred propagation plane, similar to the previous case. For γ=0.3 the crack initiated from the notch but did not propagate much. Figure 5.17 shows the results for the case of γ=0.6. from this Figure, it is seen that the fracture has initiated and propagated from the notch. It is interesting to see that in this case, the fracture intends to propagate to the downside of the wellbore rather than upper side, resulting in an asymmetric geometry. As we did not activate the gravitational effect in the simulation, this observation is due to the slippage effect that is maximized at 45° degree inclined fracture surface. At this orientation, the shear component of the fluid injection pressure is higher than that of the normal component. This also, as can be seen from Figure 5.17 compared to Figure 5.16, resulted in less fracture aperture. Finally, while it is not very much visible from Figure 5.17,

after some distance from the wellbore, the fracture plane started to reorient itself along ξ=0°, i.e. the preferred propagation plane.

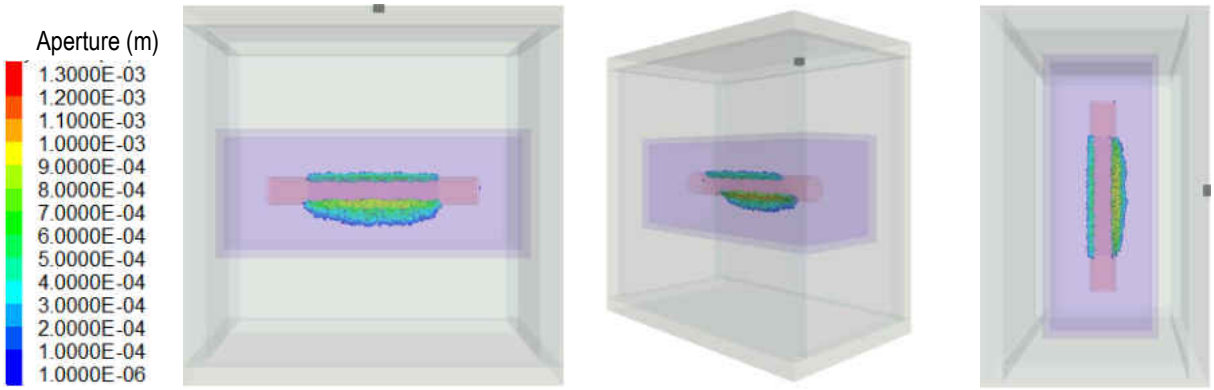

Figure 5.17. Fracture propagation for an axial notch at 45° with respect to the preferred direction. L_b=1m, L_n=0.066m (γ=0.6) at simulation time of t=0.046sec

Figure 5.18 shows the results of fracture initiation pressures for axial notches with different lengths and orientations. The results show as deviating from the most favourable propagation direction, the initiation pressure increases. Also, the larger the notch length the lower the initiation pressure. While these results were expected, these simulations provide quantitative measures of the change of initiation pressure as a function of notch geometry.

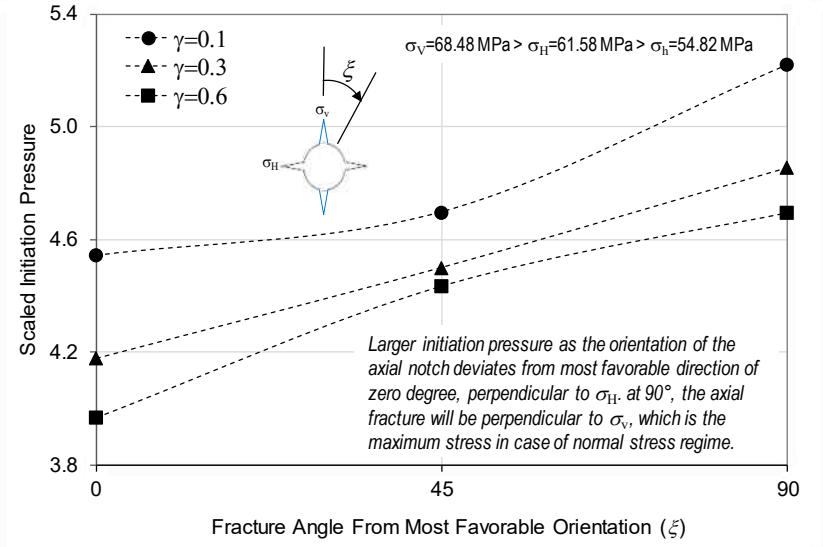

Figure 5.18. Fracture initiation for axial notches with different lengths and orientations with respect to the preferred propagation direction. The base length is L_b=1m

5.5 Multiple Fractures

In real field OH cases, there are multiple natural fractures intersecting the wellbore at different orientations with different lengths and geometry. The induced fracture tends to initiate initially from the weakest notch, based on the detailed discussions presented in the previous sections and also in the previous Chapter. Understanding the location of the weakest notches along the OH section is of paramount importance in terms of design of the multistage fracturing and determining if there will be need to create a weaker notch that existing natural fractures along a given OH section to dominate the existing cracks and act as the initiation point for induced fracture.

5.5.1 Axial Star Fractures

The case of multiple axial (star cracks) is perhaps one of the simplest type of multiple fractures that one can consider for simulations. This is similar to the geometry for which the analytical models were presented in Subsection 4.5.2, in the preceding Chapter. Figure 5.19 presents the geometry of the model with 8 cracks of equal distance around the wellbore. Notch length of L_n=0.066m (γ=0.6) with a base length of L_b=1m was used for simulation purposes. All fractures have similar initial aperture of 1×10^{-5}m. Figure 5.20 shows the aperture plots around the wellbore and fracture pressure and crack numbers versus time as well as the after 0.05sec simulation time. From this Figure it is seen that the initiation started initially from the notch oriented at ξ=0°, i.e. the direction perpendicular to σ_H (least stress in this geometry) with larger aperture comparing to other cracks.

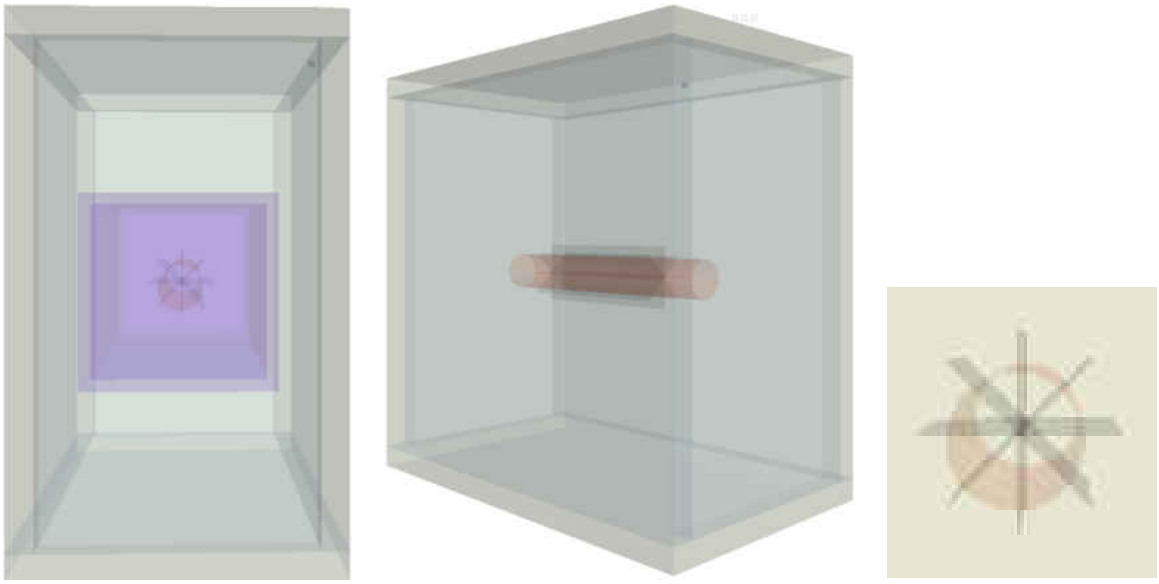

Figure 5.19. Geometry of 8 axial (star) cracks with L_n=0.066m (γ=0.6) and L_b=1m, different views

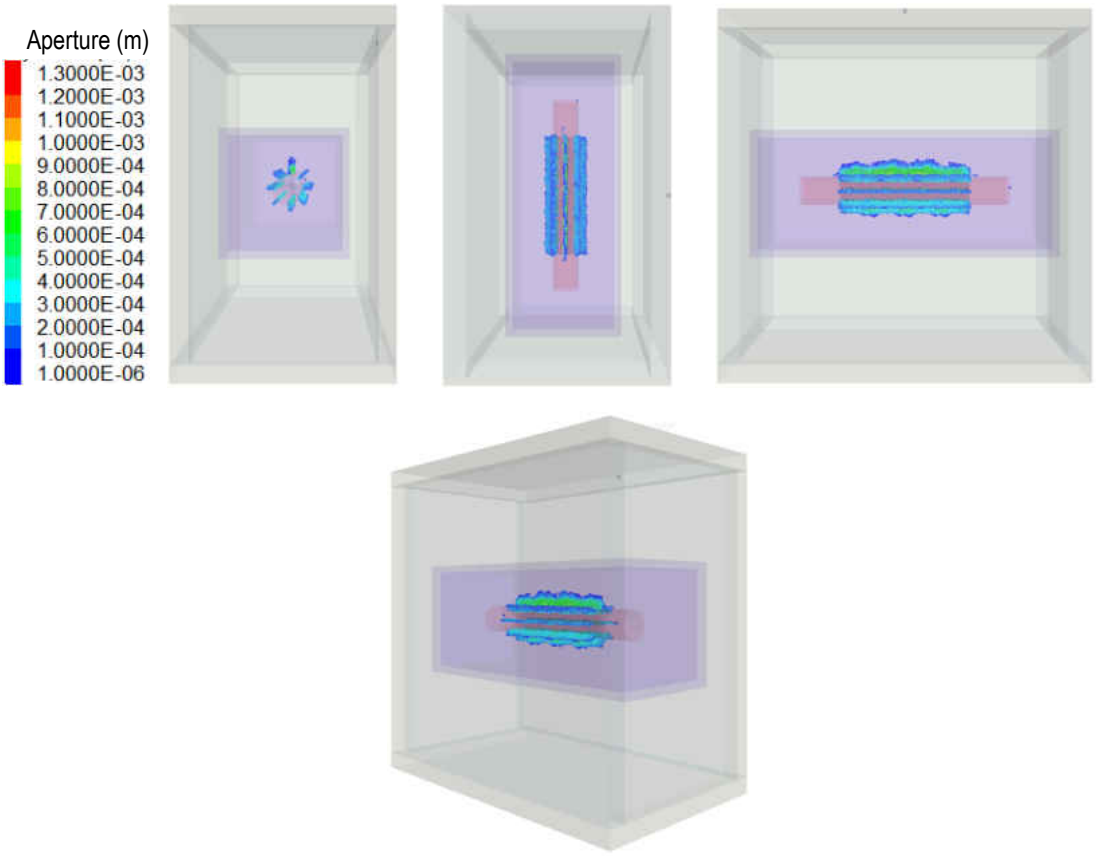

Figure 5.20. Fracture propagation with aperture plots from different views for multiple (star) axial fracture with an initial notch length of L_n=0.066m (γ=0.6) and based length of L_b=1m and simulation time of 0.05sec

Figure 5.21 shows the pressure and crack numbers versus time plot for the 8 cracks model. The fracture initiation pressure is approximately 78MPa, which is slightly larger than its corresponding bi-wing case of 74MPa (see Figure 5.11). From analytical models presented in subsection 4.5.2 of Chapter 4, it is found that the shape coefficient (F_n) for the case of 8 cracks with L_n=0.066 is F_n=0.765 (Equation 4.52). Multiplying this coefficient by the weight factor *f* of equation 4.43, and doing the calculations using equation 4.41, the initiation pressure is estimated to be 64.3MPa, which is less than what was seen from the numerical simulations. This underestimation could be due to the ignorance of pressure drop due to the friction and flow convergence effect around the wellbore that is ignored in the analytical models.

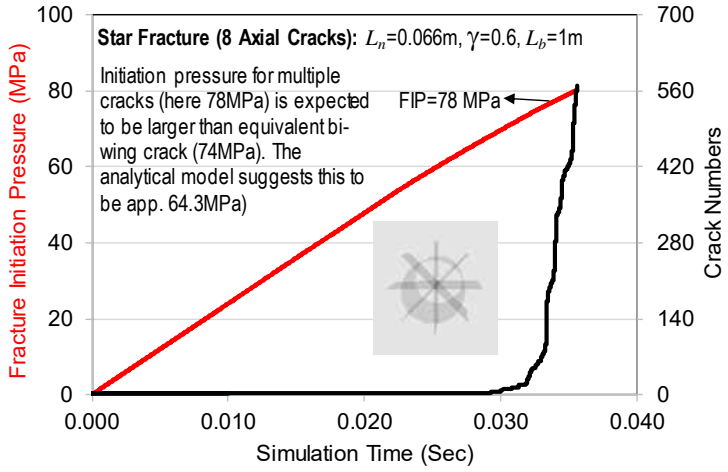

Figure 5.21. Fracture pressure and crack numbers versus time plot for 8 axial fracture model geometry

5.5.2 Multiple Transverse Fractures

The first example in this Section represents simulation of three vertical transverse fractures as shown in Figure 5.22. From right to left, the fractures are perpendicular, parallel and at 45° with respect to σ_h, or wellbore axis. The fracture parallel to the wellbore axis is indeed an axial fracture with a circular geometry. The model contains two resolution domains and used the same data as previous models for comparison purposes. The fracture apertures are illustrated in Figure 5.23. As

one expects, the fracture perpendicular to σ_h (the rightest fracture in this Figure) is the fracture which took the fluid first and has the largest opening and propagation. As the notch size is adequately large, we expect to be on the right side of the cross over point, hence the axial transverse fracture dominates over the axial one.

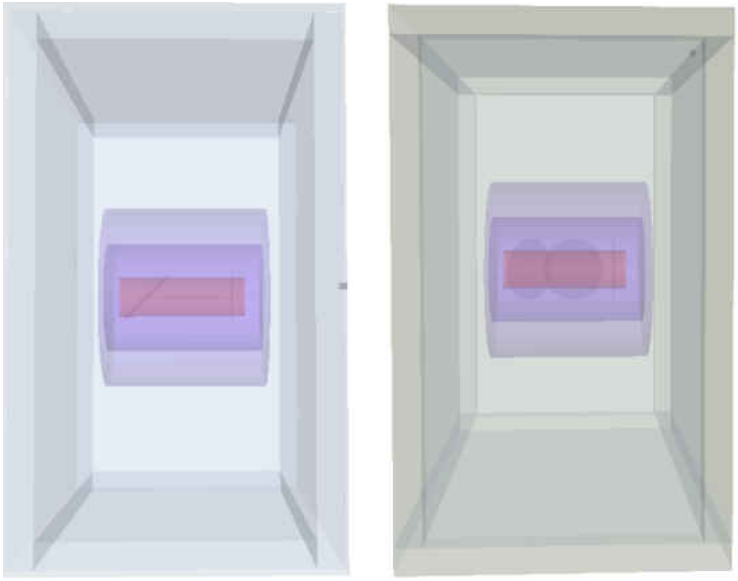

Figure 5.22. Model geometry of three transverse fractures perpendicular, parallel and at 45° with respect to wellbore axis. View from the top (left) and front (right)

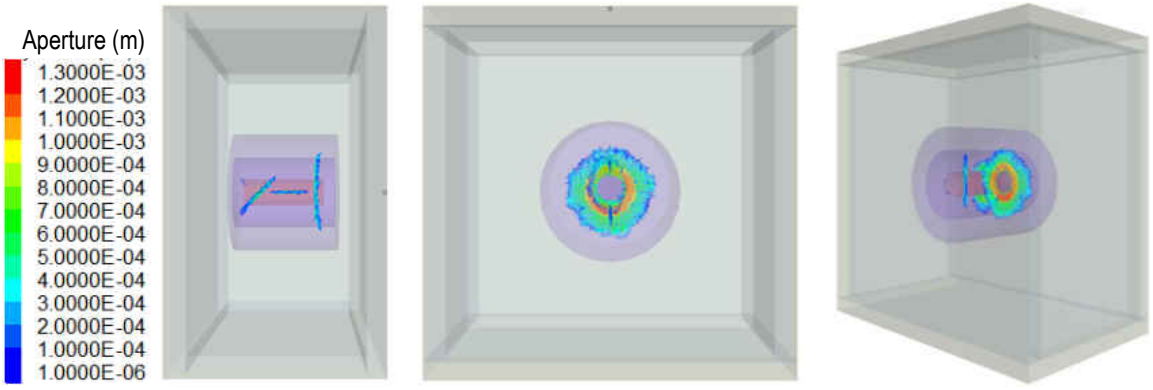

Figure 5.23. Fracture apertures (different views) for the model with three transverse fracture with different orientations

As a second example, similar to the axial star fractures transverse fractures with different orientations were modelled to examine how they compete in receiving the fluid and acting as the main fracture initiation point. Figure 5.24 shows the geometry of 8 wings transverse fractures

equivalent to γ=0.6. two cylindrical resolution domains of 2.2cm and 4.4cm have been considered around the wellbore with the remaining part of the model having resolution of 8.8cm. The wellbore ais long σ_h, so the fracture perpendicular to the wellbore axis is the most favourable one to open. Figure 5.25 confirms this as it shows that the apertures of this fracture after a simulation time of 0.028sec are larger than other fractures. It is interesting to see that the fracture parallel to the wellbore axis, which in fact is an axial fracture, has initiated slightly and the other two fracture sets with orientation of 45° and 135° with respect to the most favourable propagation plane have relatively similar openings, as expected. The results of this simulation also show the effect of fracture geometry and orientation and field stresses on the effectiveness of notches to act as the initiation point.

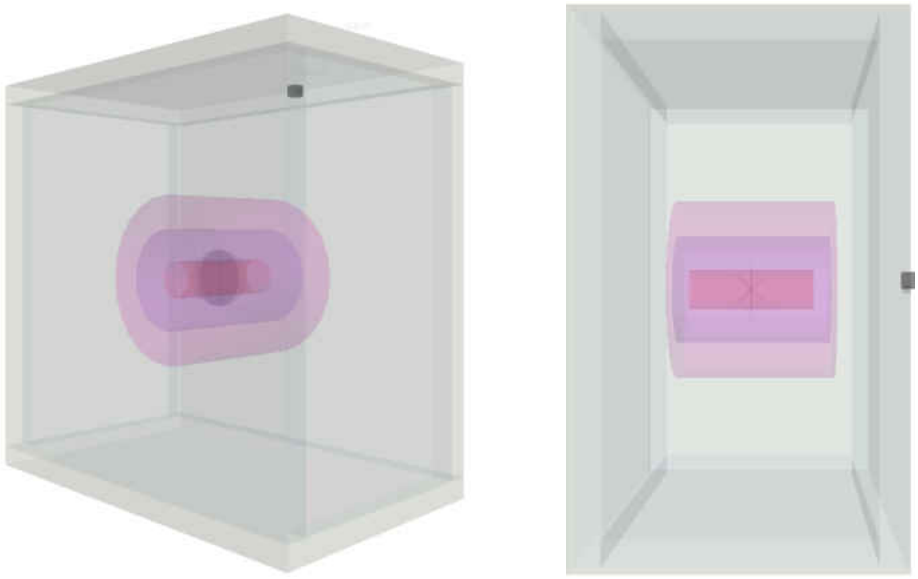

Figure 5.24. Geometry of 8 wings transverse fractures used for HF simulations. Perspective view (left) and plan view (right). All cracks have similar scaled length of γ=0.6

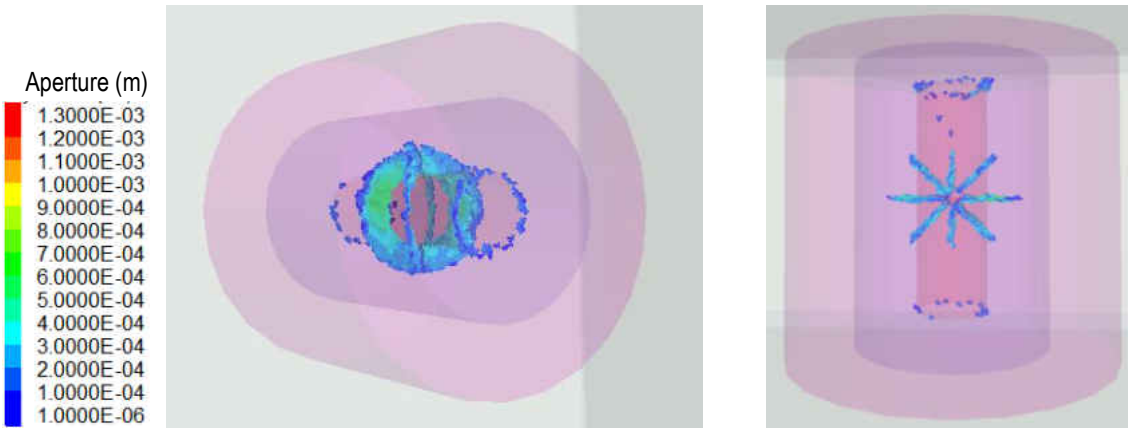

Figure 5.25. Fracture apertures after simulation time of t=0.028sec. Perspective view (left) and from above (right)

5.5.3 Random Fractures

In real cases, the distribution of natural fractures is random and based on the analysis of image logs it may follow a Gaussian distribution. Here, the objective is not to simulate complex real examples of natural fractures around the wellbore, however, to explain the application of the knowledge gained from this study to determine which of the natural fractures may act as the seed point to initiate the hydraulic fracture, as an example, 6 natural fractures with different orientations and lengths were considered for simulation purposes. Figure 5.26 shows the geometry of the fractures from above (top) and front (bottom) views. The most left and right fractures (#1 and 6) represent transverse notches with radius of 0.2m and 0.14m, respectively. The second and third fractures from left (#2 and 3) represent two axial notches, first one oriented horizontally along the least favorable direction (i.e. ξ=90°) with L_n=0.18m and L_b=0.5m, the second one vertically oriented along the most favorable direction (i.e. ξ=0°) with L_n=0.28m and L_b=0.4m (note that L_n is the length of one side of the notch from the wellbore wall). Two fractures are also considered with dip and dip directions of 45°/30° and 135°/60°, respectively (#4 and 5) with the length and width along the fracture plane of 0.4m and 0.5m for the first and 0.7m and 0.286m for the second notch. All fractures have similar initial aperture of 1×10^{-5}m.

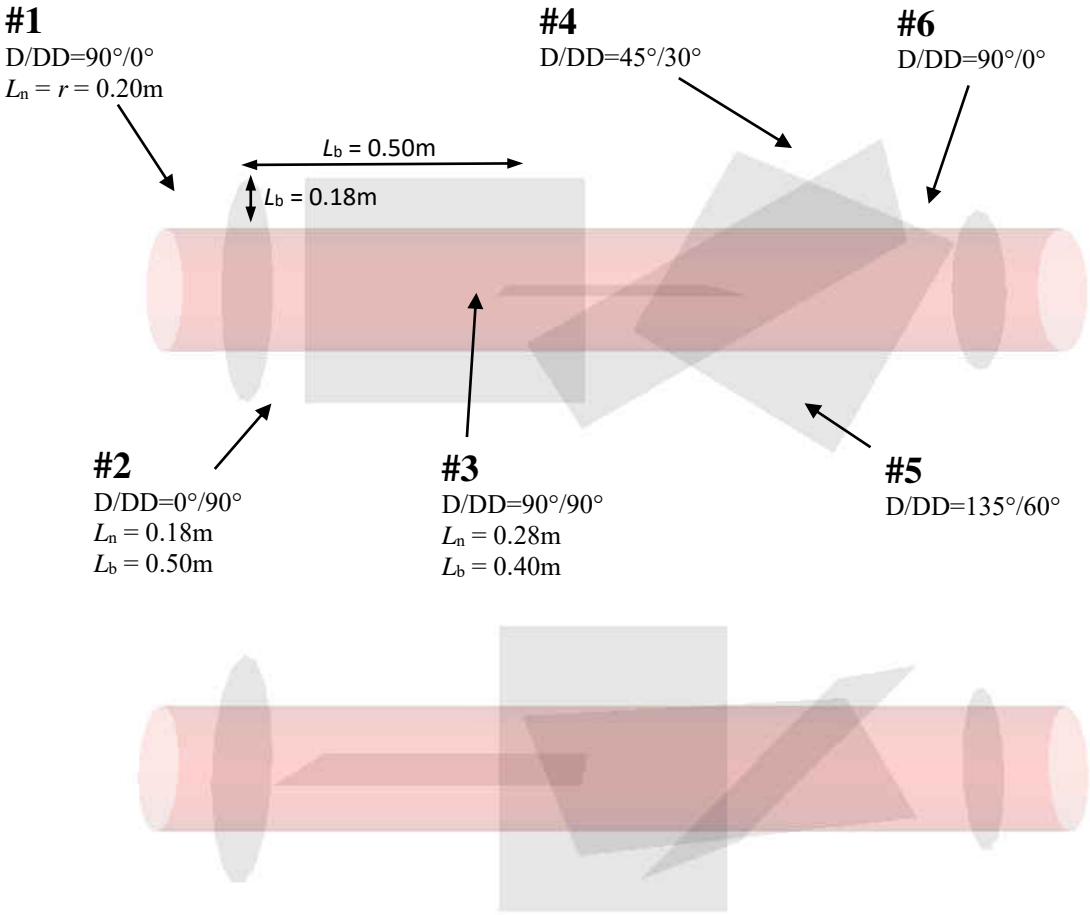

Figure 5.26. Six notches with random orientations and sizes used to simulate fracture initiation. Views from the top (top) and front (bottom)

Figure 5.27 and 5.28 show the fracture apertures after simulation time of t=0.0475sec and t=0.488sec, respectively. from these Figures, it is seen that the apertures in vertical axial fracture (#3) started to open before other fractures and continued to propagate longer with higher apertures than other fractures. Comparing to axial fracture #2, this notch is weaker and more prone to open as it is oriented along the most favourable orientation and its length (L_n=0.28m) is larger than fracture #2, even though its base length is slightly smaller. Comparing to transverse fractures, while the length of this fracture is slightly less than fracture #1 (L_n=0.2m), it appears that it is still less than the minimum length of the cross over point, so the axial fracture is dominant. The two

oriented notches #4 and #5 compete in taking the fluid to this time of simulation but look to be more competent than both transverse fractures.

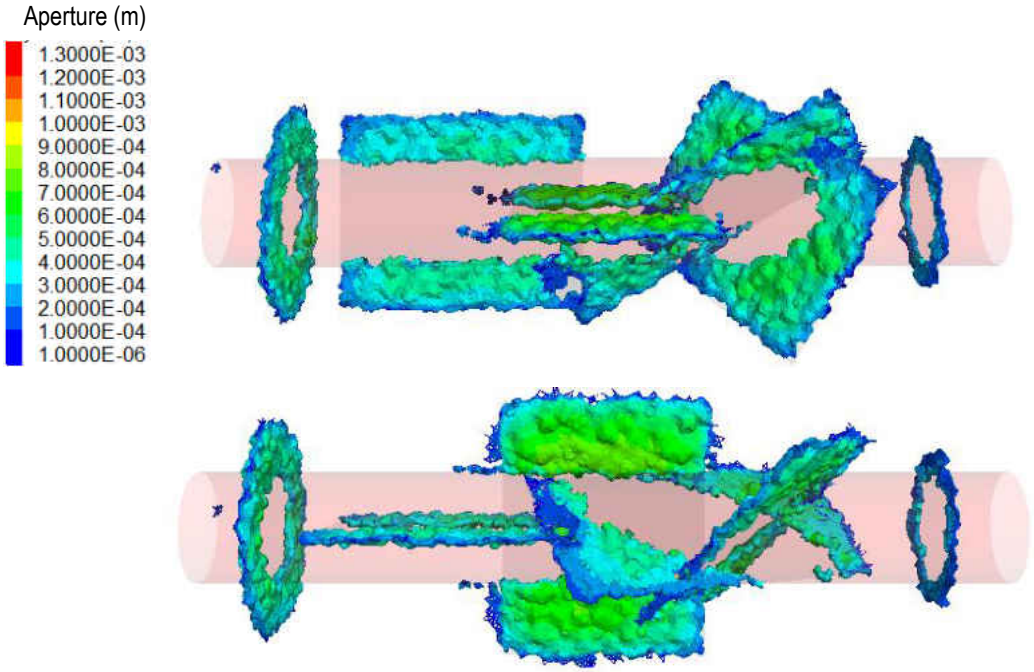

Figure 5.27. Fracture apertures after t=0.0475sec simulation time. Views from the top (top) and front (bottom)

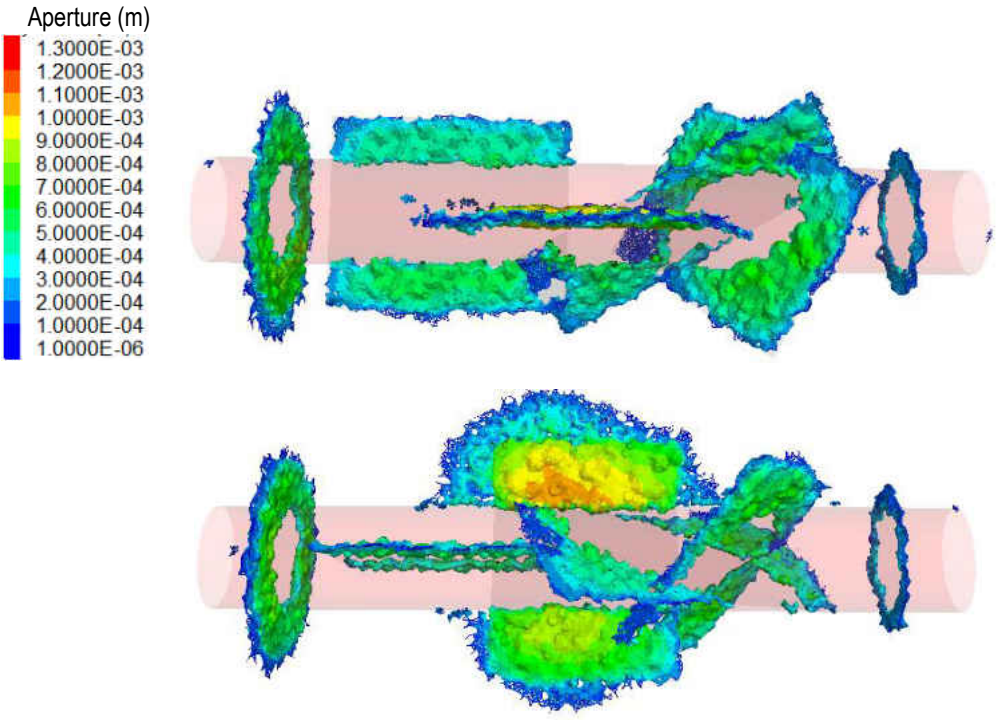

Figure 5.28. Fracture apertures after t=0.488sec simulation time. Views from the top (top) and front (bottom)

In real field cases, in order to design the notch geometry in order to confine the location of the fracture initiation, the FMI and other image logs may be utilized to extract the geometry of natural fractures around the wellbore. With currently available advanced commercial software packages this is straightforward to do. Figure 5.29 shows an example of natural fractures dip events picked, categorized, and displayed by using the Schlumberger's Techlog wellbore software platform with data from the FMI-HD microimager. Natural fractures 3D geometry is presented in the second track and the last track shows the dip and dip direction analysis. Extracting the geometry of natural fractures in each HF stage and conducting similar analysis presented in this study using simulations and analytical models will help to identify the most likelihood fractures which will be the initiation point of an induced fracture and if necessary notches can be designed and created to control the location of the fracture initiation. While from the image logs the type of fractures (e.g. open, close, semi-close, conductive), orientation and aperture can be defined, estimation of the fracture length (i.e. the penetration into the formation) may not be easily calculated. This is a topic that needs further studies to establish a specific algorithm to extract the fracture data with their use in this type of study from the image logs and other tools, including sonic scanner.

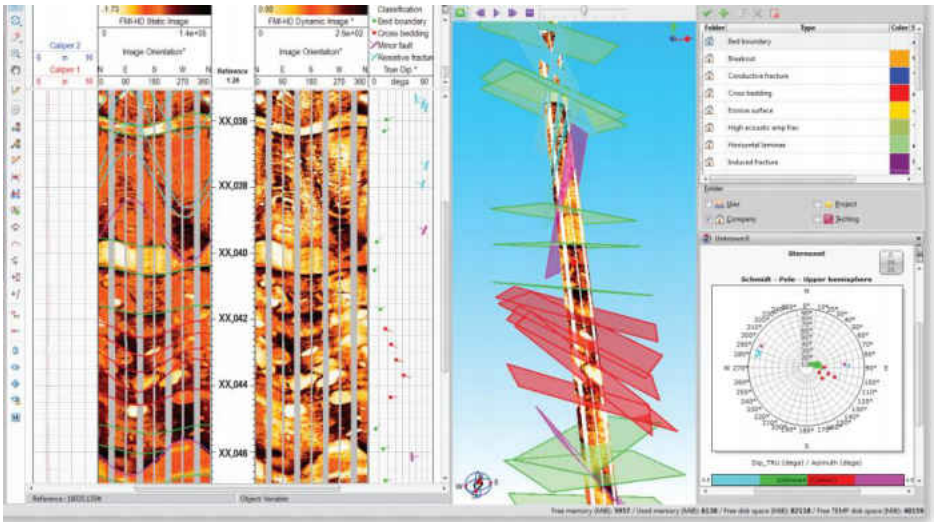

Figure 5.29. Natural fractures dip event extracted from the FMI-HD microimager using the Techlog platform (image is courtesy of Schlumberger)

5.6 Summary

In this Chapter the results of XSite numerical simulations of hydraulic fracturing with pre-existing transverse and axial notches were presented. The effect of notch size on fracture initiation pressure and geometry of the propagated fracture near wellbore were discussed. It was seen that the stress anisotropy is the dominant parameter in competition between transverse and axial notch creation. The larger the stress anisotropy the easier for transverse fracture to initiate at smaller notch length. For isotropic stress fields, it was seen that creation of transverse fracture, even with a very large notch size is challenging. For the case of axial fracture, it was observed that the base length plays an important role in initiation of fracture. The smaller the notch base length the less opportunity for the fluid to flow into the fracture and even with large fracture length, the fracture cannot propagate symmetrically and penetrate into the formation. The results of simulations presented were compared with analytical models of the previous Chapter and it was seen that the analytical models, due to their simplified assumptions, underestimate initiation pressure and also may not consider realistically the geometry of the fractures, especially in case of axial fracture. Extension of the simulations to the multiple fractures including star cracks showed the competition between different notches in initiating the fracture, depending on their size, geometry and orientation. These findings will help to analyze the natural fractures along an OH section of the wellbore from the image logs before HF operation to predict the likelihood location of the fracture initiation and creating notches as required to dictate the location of fracture initiation.

CHAPTER 6

Conclusions and Recommendations

The effect of transverse and axial pre-existing cracks (notch) on fracture initiation pressure was studies in details as part of this research project. The first Section of this Chapter lists the main conclusions made from this work and the second Section presents some of the future work that is recommended as continuation of this study.

6.1 Conclusions

From this study the following conclusions are drawn:

- OH completion is more favorable over CH completion due to larger production and less costs and operational complexity. Creating properly designed pre-existing cracks (notches) along the OH section of each stage of a multi-stage HF can dictate the point of fracture opening and avoid unfavorable single or multiple fracture growth around the wellbore which is one of the issues in OH HF operation.
- The design of proper notch geometry in an OH section of a horizontal wellbore can dominate the fracture initiation to start from this point instead of existing natural fractures and defects along the lateral at unfavorable locations. It also reduces the fracture initiation pressure and mitigates the near wellbore damage and tortuosity.

- The only controllable parameters during fracturing operation are the injection rate and fluid viscosity. These parameters individually and their combined effect, i.e. pressurization rate, have great influences on the type of fractures initiating in an OH HF operation.
- Analytical models are of great use to obtain preliminary information about the impact of the notch on fracture initiation pressure and how different parameters influence it. However, each of them have simplified assumptions which result in deviating from the real cases. Therefore, conducting numerical simulations, before field trial is of great importance.
- The superposition law is an effective analytical method to estimate the influence of different parameters on fracture initiation pressure.
- The results of analytical models indicated that for slow pressurization, and anisotropic stress case, the crack is unstable for very small crack sizes of less than about 10% of the wellbore radius and then becomes stable until it starts to become unstable again when propagates several radius of the wellbore. In contrary, in isotropic case, the crack is unstable for all crack lengths, i.e. the pressure to propagate crack is reducing as crack length becomes larger.
- The results of analytical models showed that for fast pressurization, for both isotropic and anisotropic stresses, the crack is unstable when its length is less than about 10% of the wellbore radius, and then becomes stable. It is also noted that he critical borehole pressure to open the crack is much larger in case of fast pressurization than that of slow pressurization. Also, the change of pore pressure has no impact on critical pressure in case of fast pressurization.
- From practical point of view, generation of transverse fractures are more favorable than axial (longitudinal) fractures. Among other parameters, design of proper notch geometry can facilitate generation of the transverse over axial fractures in some cases.

- Among other parameters, it is evident that stress anisotropy has a dominant effect on whether transverse or axial fracture will initiate from an OH lateral.
- Theoretically, in absence of any pre-existing notch, or ineffective notches (e.g. inadequate length) axial fractures dominate and initiate from multiple section of the wellbore. In this case, the fracture initiation pressure becomes very large.
- Analytical models showed that minimum initiation pressure to open a fracture reduces as the notch size increases. However, for notches less than a certain length the axial notch is dominant, whereas, exceeding this limit, the transverse fracture is more favorable to open. The notch length at which this change of behavior is observed is mostly affected by the stress anisotropy. As the stress anisotropy increased this cross over point shifts to the left, i.e. transverse fractures can open with smaller notch size. For fully isotropic stresses it was observed that the axial fracture is always dominant.
- Assuming a horizontal wellbores drilled along minimum stress direction, in case of axial fractures, in different directions it was seen that the cross over point moves to the right as the axial fracture is further oriented towards its most favorable direction. This means that larger notches are needed to dominate transverse fractures.
- Multiple fractures are expected to occur when pressurization rate is fast (i.e. the rise time of the driving pressure pulse is relatively short compared with the time required for stress waves to circle the cavity). This situation is happening more likely in case of axial fracture. The results of analytical models showed that in this case, as the number of fractures increases, cross over point moves to the left, i.e. less notch length can result in transverse fracture to dominate the axial fracture.

- XSite software, which is a lattice based DEM numerical simulator, and works based on the analysis of particles forces and displacement, showed great capabilities to simulate near wellbore hydraulic fracturing and takes into consideration the effect of notch in OH completion.
- The coupled mechanical and fluid model implemented in XSite can simulate real geometry of the fracture depending on stress regime and rock inhomogeneity. It was seen that using correct resolution in modelling is perhaps the most important key factor to generate realistic results. The use of resolution domains helps to reduces the running time.
- In 3D numerical simulations, as opposed to the 2D analytical models, for the case of axial fracture, in addition to the notch length, the length of the notch along the wellbore axis is a secondary parameter to be considered in model geometry. It was seen that this base length has a great impact on the initiation and propagation of fractures.
- The results of numerical simulations when compared with analytical models, showed that, in general, analytical models underestimate the initiation pressure, which is due to several simplified assumptions that are used to develop them.
- The fracture geometry looks more symmetric and circular during the viscosity dominated propagation regime, which is usually during the early time, and asymmetric and non-circular in late time, when the propagation becomes toughness dominated.
- It was observed that the initiation pressure is a function of the injection rate and fluid viscosity and as these two parameters are increasing the initiation pressure becomes larger.
- The initiation point in XSite models can be determined at the time when the entire cracks around the notch perimeter are broken.

- The simulation results for both axial and transverse fractures showed that the cross over point is at larger notch length compared to the analytical models. This means that in real cases, larger notch sizes should be made to dominate initiation of transverse fracture. However, as the axial fracture base length is reduced, the cross over point shifts to the left.
- As the base length of the axial fracture becomes less, the fluid cannot flow easily into the crack, which results in higher initiation pressures, less effectiveness of the notch and more axial fractures being developed around the wellbore axis.
- As the notch length increases the notch area and perimeter increases exponentially. This results in more cracks to be broken to reach the fracture initiation point. Also, the larger the notch length, the earlier to reach the fracture initiation point, which is due to the fact that the injecting fluid can more easily penetrate into the crack and also has larger area, hence more power to open and propagate the fracture.
- In general, comparing the same notch lengths, axial fractures result in higher apertures than transverse fractures due to their larger area open to the fluid flow.
- Depending on the geometry of the notch, the initiation pressure and the effectiveness of the notch may be different.

6.2 Recommendations

Several ideas and potential applications of notched driven OH HF were mentioned throughout this study, which require further investigations. Here, some of these ideas are recommended as continuation of this study:

- Expanding the analytical models in 3D will be a great expansion of this work to compare their results with the simulations.

- Developing the 2D and 3D analytical models to determine the stress intensity factor and notch geometry effects on HF initiation pressure in transverse isotropic (TI) formations representing shales will carry great applications as shale plays require HF treatment for enhanced production.
- XSite simulations do not consider the effect of compressibility of the system including the wellbore or drillstring, while this effect cannot be neglected. This effect should be considered in the future simulations and the possibility of adding this feature to XSite will be beneficial for future research.
- Using the anisotropic rock properties features in XSite to simulate notch driven HF in OH completion is an application to further study. The existing feature in XSite allows to consider two Young's Modulus and permeabilities for the rock in two orthogonal directions replicating shales.
- While in this study we considered a radial notch in case of transverse fracture and a rectangular notch geometry for axial fracture, due to their closeness to real fracture geometry that are expected to be propagated, one may simulate the impact of other type of notch geometry (e.g. pyramid) to see the extend of the changes in the result. If any specific geometry will favor the initiation of transverse fracture, that may be considered for possible field implications.
- While the FMI and other image logs can be used to determine the type of natural fractures (e.g. open, close, conductive) and their aperture and length marked on the wellbore wall, determining the length of these fractures penetrating into the formation (i.e. depth) is not straight forward. Investigation of the use of the image logs in combination with sonic scanner or the use of any other methods to estimate the depth of natural fractures will be important in order to design proper notch geometry in a section of OH.

- A few field scale notch makers have been proposed in OH HF. The operation of these tools are mechanical or hydraulic. There is a big demand of studies in this area to propose a deployable tool in order to make the required notch geometry and in specific orientation as fast as possible with less inconvenience.

REFERENCE

Abass, H. H., Soliman, M.Y., Tahini, A.M., Surjaatmadja. J.B., Meadows. D.L., and Sierra.L., 2009. Oriented Fracturing: A New Technique to Hydraulically Fracture Openhole Horizontal Well. Proceedings - SPE Annual Technical Conference and Exhibition:124483.

Aidagulov, G., Alekseenko, O., Chang, F.F., Bartko, K., Cherny, S., Esipov, D., Kuranakov, D., and Lapin, V., 2015. Model of hydraulic fracture initiation from the notched open hole. SPE178027-MS.

Al-Naimi, K.M,. Lee, B.O., Bartko, K.M., Kelkar, S.K., Shaheen, M and Johnston, B., 2008. Application of a Novel Open Hole Horizontal Well Completion in Saudi Arabia. SPE Indian Oil and Gas Technical Conference and Exhibition:113553.

Bagci, S., Castro, L., and Flores, J., 2017. Optimization of Hydraulic Fracturing and Production Enhancement: Case Studies for US Shale Plays and Tight Sand Reservoirs. Society of Petroleum Engineers - SPE Europec Featured at 79th EAGE Conference and Exhibition (June):1057–81.

Bellarby, J., 2009. Well Completion Design.Developments in Petroleum Science.

Belyadi, H., Fathi, E., and Belyadi, F., 2019. Hydraulic Fracturing in Unconventional Reservoirs, Theories, Operations, and Economic Analysis. 2nd edition. p 632

Bueckner, H.F., 1970. A novel principle for the computation of stress intensity factors. Z. angew. Math. Mech. 50, 529-546.

Bunger, Andrew P., Emmanuel Detournay, and Dmitry I. Garagash. 2005. Toughness-Dominated Hydraulic Fracture with Leak-Off. International Journal of Fracture 134(2):175–90.

Chang, F. F., Bartko, K., Dyer, S., Aidagulov, G., Suarez-Rivera, R., & Lund. J., 2014. Multiple fracture initiation in openhole without mechanical isolation: First step to fulfill an ambition. SPE Hydraulic Fracturing Technology Conference

Charlez, Ph.A. 1997, Rock Mechanics: Vol. 2 – Petroleum Applications, Editions Technip, Paris, 661 pp

Chen, Y., Meng, Q., and Zhang, J., 2018. Effects of the Notch Angle, Notch Length and Injection Rate on Hydraulic Fracturing under True Triaxial Stress: An Experimental Study. Water 2018, Vol. 10, 801.

Cundall, P. A. 2011. Lattice method for modeling brittle , jointed rock. C Continuum and Distinct Element Numerical Modeling in Geomechanics

Damjanac. B., Detournay. C., Cundall. P., Puvance. M., Hazzard. J. 2011. XSite Description of Formulation Revision I

Damjanac, Branko., Detournay. C and Cundall. P.A. 2016. Application of Particle and Lattice Codes to Simulation of Hydraulic Fracturing. Computational Particle Mechanics 3(2):249–61

De Pater, C.J., Cleary, M.P., Quinn, T.S., Barr, D.T., Johnson, D.E., and Weijers, L., 1994. Experimental verification of dimensional analysis for hydraulic fracturing. SPE Prod Facil Vol 9(4), p.p 230–238.

Detournay, E. 2004. Propagation Regimes of Fluid-Driven Fractures in Impermeable Rocks. International Journal of Geomechanics 4(1):35–45.

Detournay, E., and Carbonell, R., 1997. Fracture-mechanics analysis of the breakdown process in minifracture or leakoff test. SPE production and facilities. p.p 195-199.

Dunn, M.L., and Suwito, W., 1997. Fracture initiation at sharp notches: correlation using critical stress Intensities. Int. J. Solids Structures Vol. 34, No. 29, p.p. 3873~3883.

Economides, M.J., Nolte, K.G., 2000. Reservoir stimulation, 3rd edition. Wiley, New York

Ellis, P. D., Kniffin, G. M and Harkrider, J. D., 2007. Application of Hydraulic Fractures in Openhole Horizontal Wells. SPE/Petroleum Society of CIM 65464

Fallahzadeh, S. H., James Cornwell, A., Rasouli, V and Hossain, M .,2015. The Impacts of Fracturing

Fluid Viscosity and Injection Rate on the near Wellbore Hydraulic Fracture Propagation in Cased Perforated Wellbores. 49th US Rock Mechanics / Geomechanics Symposium 2015. 2:984–1001.

Fallahzadeh, S.H., Hossain,M., Cornwell, AJ and Rasouli,V., 2017. Near Wellbore Hydraulic Fracture Propagation from Perforations in Tight Rocks: The Roles of Fracturing Fluid Viscosity and Injection Rate. Energies V10. Issue(3).

Gandossi, L., 2013. An Overview of Hydraulic Fracturing and Other Formation Stimulation Technologies for Shale Gas Production.

Glinka, G., 1996. Development of weight functions and computer integration procedures for calculating stress intensity factors around cracks subjected to complex stress fields. A report prepared for Analytical Services& Materials, Inc.

Gottschling, J. C., 2005. Openhole vs Cased-Hole Hydraulic Fracturing. SPE 97172.

Haimson.. B and C. Fairhurst. Initiation and extension of hydraulic fractures in rocks. SPEJ, Dec., 310-318, 1967

Huitt, J. L., 1960. Hydraulic Fracturing with the Single-Point Entry Technique. Journal of Petroleum Technology 12(03):11–13.

Hussain, M.K and Murthy, K.S.R.K., 2019. Evaluation of mixed mode (I/II) notch stress intensity factors of sharp V-notches using point substitution displacement technique. Vol. 48 pp. 599-610.

Jeffrey, RG., Zhang, X., 2010. Mechanics of Hydraulic Fracture Growth from a Borehole. CSUG/SPE 137393. Pages 1112-1121

Kirsch, G., 1898, Die Theorie der Elastizitat und die Bediirfnisse der Festigkeitslehre: Zeitschr. Ver. Deutsch. Ingenieure, v. 42, p. 797

Lecampion, B., Abbas, S., Prioul, R., 2013. Competition between transverse and axial hydraulic fractures in horizontal wells. SPE163848.

Lecampion, B., Desroches, J., Jeffrey, R.G., and Bunger, A.P., 2017. Experiments versus theory for the initiation and propagation of radial hydraulic fractures in low-permeability materials. J. Geophys. Res. Solid Earth, 122, p.p 1239–1263

Lhomme, T.P.Y, 2005. Initiation of hydraulic fractures in natural sandstones. Master Thesis in Geomechanics, University of Minnesota

Leguillon, D., and Yosibash, Z., 2003. Crack onset at a v-notch. Influence of the notch tip radius. International Journal of Fracture 122: 1–21.

Martinez, E.R., Farias, M.M., and Junior, F.E., 2019. Investigation of the notch angle in hydraulic fracturing using XFEM. Journal of the Brazilian Society of Mechanical Sciences and Engineering.

Nakagawa, S., Rutqvist, J., Kneafsey, T., Kim, K., Birkholzer, J., and Prieto, H., 2016. Laboratory and Numerical Investigation of Hydraulic Fracture Propagation and Permeability Evolution in Heterogeneous and Anisotropic Shale. Lawrence Berkeley National Laboratory.

Nilson, R.H., and Proffer, W.J., 1984. Engineering formulas for fractures emanating from cylindrical and spherical holes. J. Appl. Mech. 51:929-933

Patutin, A., and Serdyukov, S., 2017. Transverse Hydraulic Fracture Initiation by Indentation in an Uncased Borehole. Procedia Engineering 191, pp. 287 – 290

Potyondy, D.O.., Cundall, P.A., 2004. Abbonded particle model for rock. International Journal of Rock Mechanics and Mining Sciences.p.p 1329-1364

Qiu. D., Rasouli .V., Damjanac.B., and Wan.X., 2019. Narrow versus Wide Fairway Fracture Geometry.53rd U.S. Rock Mechanics/Geomechanics Symposium.

Rasouli, V., Zacharia, J., and Elike, M., 2011. The influence of perturbed stresses near faults on drilling strategy: A case study in Blacktip field, North Australia. Journal of Petroleum Science & Engineering. 76: 37-50.

Renpu, W., 2011. Advanced Well Completion Engineering.Third edition. p.p 256-293

Rice, J.R., 1972. Some remarks on elastic crack-tip stress fields. Int. J. Solids Structures. Vol. 8, pp. 751-758.

Rummel, F. (1987). Fracture Mechanics Approach to Hydraulic Fracturing Stress Measurements. In: Fracture mechanics of rock. Ed. by Atkinson, B. K. Academic Press geology series. London: Academic Press, pp. 217–239.
Schwartzkopff, A.K. 2017. Breakdown pressure and propagation surface of a hydraulically pressurized circular notch within a rock material. Ph.D. Dissertation, University of Adelaide.
Song, H., and Rahman, S., 2018. An extended J-integral for evaluating fluid-driven cracks in hydraulic Fracturing. Journal of Rock Mechanics and Geotechnical Engineering Vol. 10, pp. 832-843.
Vahid , S. and Ghassemi, A. 2011. Hydraulic Fracture Initiation from a Wellbore in Transversely Isotropic Rock. 45th US Rock Mechanics / Geomechanics Symposium.
Weijers, L., De Pater, C.J., Owens, K.A., and Kogsboll, H.H., 1994. Geometry of hydraulic fractures induced from horizontal wellbores. SPE production and facilities.
Williams, M. L. (1952) Stress singularities resulting from various boundary conditions in angular corners of plates in extension. Journal 0/ Applied Mechanics 74, 526-528.